AFCRL-65-692 ASE-1056

THE ENERGETIC CHARGED PARTICLE ENVIRONMENT OF THE EARTH

HITCH-HIKER I DATA ANALYSIS

F. R. PAOLINI
G. C. THEODORIDIS
M. BATE

AS&E
AMERICAN SCIENCE AND ENGINEERING, INC.
11 Carleton Street, Cambridge, Massachusetts 02142

CONTRACT NO. AF 19 (628)-4207
PROJECT NO. 0000
TASK NO. 000024

FINAL REPORT

Period Covered: 15 May 1964 - 14 August 1965

13 SEPTEMBER 1965

This research was supported by the Air Force In-house Laboratory Independent Research Fund

PREPARED FOR

AIR FORCE CAMBRIDGE RESEARCH LABORATORIES
OFFICE OF AEROSPACE RESEARCH
UNITED STATES AIR FORCE
BEDFORD, MASSACHUSETTS

AFCRL-65-692 ASE-1056

THE ENERGETIC CHARGED PARTICLE ENVIRONMENT OF THE EARTH (HITCH-HIKER I DATA ANALYSIS)

F. R. Paolini, G. C. Theodoridis, M. Bate

American Science and Engineering, Inc.
11 Carleton Street
Cambridge, Massachusetts 02142

Contract No. AF 19 (628) - 4207

Project No. 0000
Task No. 000024

FINAL REPORT

Period Covered: 15 May 1964 - 14 August 1965

13 September 1965

This research was supported by the Air Force
In-house Laboratory Independent Research Fund

Prepared for

AIR FORCE CAMBRIDGE RESEARCH LABORATORIES
OFFICE OF AEROSPACE RESEARCH
UNITED STATES AIR FORCE
BEDFORD, MASSACHUSETTS

ABSTRACT

The results of the reduction and analysis of data obtained from instrumentation flown on the Air Force Satellite Hitch-hiker I (1963-25B) are presented. The instrumentation included two electrostatic analyzers (one for electrons, 15 to 100 kev, the other for protons, 15 to 100 kev); a scintillation spectrometer (for electrons, 0.7 to 4.0 Mev); a phoswich scintillation spectrometer (for protons 1. to 5. Mev and 7.5 to 120 Mev); and a Geiger counter (electrons greater than 4. Mev, protons greater than 40. Mev). Detailed data on integral energy spectra, pitch angle distributions, and perpendicular unidirectional intensities, as functions of B, L (or λ, L) and time are given in five papers appended to this report. No substantial intensities of protons, 15 to 100 kev, were observed. Electrons, 15 to 100 kev, were observed with intensities as great as $2 \times 10^5/cm^2$-sec-ster-kev at 40 kev, but the anomalous angular distributions obtained cast doubt on the credibility of these data. Peak inner belt intensities for electrons above 1 Mev were about 5×10^6 electrons/cm^2sec ster at $L \approx 1.6$. Spectra were of the shape $\exp(-E/E_o)$, with $0.7 \leq E_o \leq 1.2$ Mev. Outer belt intensities fluctuated substantially, with severe depletions at times of magnetic and solar activity, and subsequent recoveries in periods of a few to several days. Maximum observed intensities of electrons above 1 Mev at the horns of the outer belt at $L \approx 4.5$ were about 10^5 electrons/cm^2sec ster. Loss of outer belt electrons through dumping at high latitudes in the Anomaly was detected at rates up to 2×10^{11} ergs/sec. Outer belt spectra between 0.7 and 4 Mev were also approximately exponential, with $E_o = 0.4 \pm 0.1$ Mev. No drastic spectral shape changes were seen accompanying the observed

intensity variations. The protons defined two belts, with hearts at L ~ 1.6 and L ~ 4.5, and a slot at L ~ 3.0. The integral spectra observed were all similar in shape, with approximately an exponential energy dependence. The spectra tended to be much steeper than electron spectra in the same energy range in the inner belt. Typical measured omnidirectional intensities for energy E > 2 Mev were $10^8/cm^2$ sec at $(L, \lambda) \approx (1.6, 8^\circ)$ and $2 \times 10^6/cm^2$ sec at $(L, \lambda) \approx (4.5, 55^\circ)$, higher than values of other observers, for reasons which appear to be instrumental. All electron and proton pitch angle distributions observed with the scintillation spectrometers were peaked at 90° and had cutoffs consistent with theory. Data on electrons 0.7 to 4. Mev and protons 1.5 to 4. Mev are summarized in the main body as iso-intensity contours of perpendicular unidirectional intensities on rectangular B, L plots.

ACKNOWLEDGEMENTS

The authors wish to acknowledge their gratitude to Professors Bruno Rossi, William Kraushaar, Stanislaw Olbert, and to Doctors Herbert Bridge and Gordon Garmire, all of Massachusetts Institute of Technology; to Doctors Martin Annis, Riccardo Giacconi, Jack Carpenter, and Oscar Manley of American Science and Engineering, Inc.; and to Ludwig Katz, Don Smart, and George Kuch of AFCRL; for many interesting hours of discussion of the data obtained. We thank them also for the many valuable suggestions they made concerning specific lines of investigation into the profusion of data obtained.

TABLE OF CONTENTS

1.	INTRODUCTION	1
	1.1 Launch and Orbital Information	1
	1.2 Instrumentation	1
	1.3 Methods of Data Analysis	2
	1.4 Pertinent Documentation	5
	1.5 Organization of the Report	7
2	DISCUSSION	9
	2.1 Electron Electrostatic Analyzer	9
	2.2 Proton Electrostatic Analyzer	22
	2.3 Electron Scintillation Spectrometer	28
	2.4 Proton Scintillation Spectrometer - Low Energy Channel	28
	2.5 Proton Scintillation Spectrometer - High Energy Channel	39
	2.6 Geiger Counter	40
3.	SUMMARY OF DATA	43
4.	REFERENCES	50
	APPENDICES	
A.	" A Study of Energetic Electrons in the Radiation Belts with Hitch-hiker I" (ASE-992, August 1965) Paper presented to the Advanced Study Institute at the Christian Michelson Institute in Bergen, Norway, on 16 August - 3 September 1965.	51
B.	"Measurements on 1.5 to 4. Mev Protons in the Radiation Belts". Paper presented at the Forty-Sixth Annual Meeting of the American Geophysical Union at Washington, D. C., on 19 - 22 April 1965.	83

TABLE OF CONTENTS (Con'd.)

C. "Measurements on 0.7 to 4. Mev Electrons in the Radiation Belts from Hitch-hiker I." Paper presented at the Forty-Sixth Annual Meeting of the American Geophysical Union at Washington, D. C. on 19 - 22 April 1965. 95

D. "Effect of a Solar Flare on the Outer Radiation Belt." Paper presented at the Forty-Sixth Annual Meeting of the American Geophysical Union at Washington, D. C. on 19 - 22 April 1965 and at the 1965 Annual Meeting of the American Physical Society at New York, on 27 - 30 January 1965. 109

E. "Measurements on Differential Energy Spectra of Electrons (15 to 100 Kev) in the Magnetosphere" (ASE-646, October 1964). 121

LIST OF FIGURES

1.	Aspect Geometry	4
2.	40 kev Electrons, ϕ 25	10
3.	Low Energy Electrons, ϕ 25	11
4.	Low Energy Electrons, ϕ 25	14
5.	Low Energy Electrons, ϕ 26	15
6.	Low Energy Electrons, ϕ 25	16
7.	Low Energy Electrons, $\phi 323_D$	17
8.	Low Energy Electrons, $\phi 96_D$	18
9.	Low Energy Electrons, $\phi 26_D$	20
10.	70 - 90 kev Electrons, ϕ 431	21
11.	Low Energy Electrons, ϕ 25	23
12.	40 kev Protons, ϕ 431	24
13.	Low Energy Proton Spectra, ϕ 431	26
14.	70 - 90 kev Protons, 431	27
15.	Electrons Stopped in Aluminum	29
16.	Electron- Proton Scintillation Light Equivalents in Anthracene	31
17a.	Protons, >2 Mev, Inner Belt (Unidirectional Intensities at 90°)	32
17b.	Unidirectional Intensities of Electrons (>1 Mev) at 90° for Comparison	33
18a.	Protons, >2 Mev, Outer Belt (Unidirectional Intensities at 90°)	34
18b.	Electrons, >1 Mev, Outer Belt (Undiriectional Intensities at 90°)	35
19a.	Protons, 1 - 4 Mev, Outer Zone Energy Spectrum	36
19b.	Protons, 1 - 4 Mev, Outer Zone Energy Spectrum for Comparison	37

LIST OF FIGURES (Con'd)

20a. Iso-Intensity (j_1) Contours of Electrons > 1 Mev (Typical) 44

20b. Iso-Intensity (j_1) Contours of Electrons > 1 Mev Maximum, ϕ 25 45

21a. Iso-Intensity (j_1) Contours of Protons > 2 Mev Typical 46

21b. Iso-Intensity (j_1) Contours of Protons > 2 Mev Maximum, ϕ 25 47

LIST OF TABLES

I. ELECTRON ENERGY SPECTRA (0.7 to 4 Mev) 49

II. PROTON ENERGY SPECTRA (1.5 to 4 Mev) 49

1. INTRODUCTION

1.1 Launch and Orbital Information

The Air Force sub-satellite Hitch-hiker I (1963-25B) was launched on 1 July 1963 into a near polar orbit of 82.14° inclination with perigee at 326 km and apogee at 4150 km. The angle between the ascending node of the orbit and the Earth-Sun line was initially about 63°, and regressed at a rate of approximately (-1 1/2°) per day. The orbital period was 133 minutes. The sub-satellite was spin-stabilized at 68 rpm with its axis of rotation at an angle of about 25° to the axis of the Earth.

The satellite orbit covered a substantial portion of the inner belt, from $R \approx 1.0$ near perigee to $R \approx 1.7$ at apogee. The satellite also penetrated the horns of the outer belt. Since the apogee of the orbit was on the sunlit side of the Earth, the deepest penetration into the outer belt (and therefore most of the data) corresponded to local daytime.

1.2 Instrumentation

Detailed descriptions of the instruments on board Hitch-hiker I are included in document AFCRL-64-435, listed in Section 1.4. There we will merely enumerate the instruments and give some of their chief characteristics.

(1) Electron Electrostatic Analyzer: angular aperture about $8.5° \times 8.0°$ and geometrical factor $A\Omega \approx 0.2$ cm^2 ster; this instrument gives differential energy spectra of electrons between 15 and 100 kev, with an energy resolution of about 15% and a dynamic range from 2×10^5 to 5×10^{10} kev/cm^{2}sec ster.

(2) Proton Electrostatic Analyzer: detects 15 to 100 kev protons; other characteristics same as previous instrument.

(3) Electron Scintillation Spectrometer: angular aperture approximately 25° cone (FWHM) and $A\Omega \approx 0.12$ cm^2 ster. The "count rate channel" gives integral energy spectra of electrons between 0.7 Mev and 4 Mev, with a dynamic range from 8 x 10 to 10^6 electrons/cm^2 sec ster. The "rate of energy deposition channel" measures the rate of energy deposition by electrons above approximately 0.15 Mev, with a dynamic range from 8 x 10^2 to 8 x 10^8 Mev/cm^2 sec ster.

(4) Proton Scintillation Spectrometer: angular aperture approximately an 8° cone and $A\Omega \approx 8.4 \times 10^{-4}$ cm^2 ster. The "low energy channel" gives integral energy spectra of protons between about 1.5 and 4 Mev, with a dynamic range from 1.2 x 10^4 to 2 x 10^8 protons/ cm^2 sec ster. The "high energy channel" gives integral energy spectra of protons between 7.5 and 120 Mev, with a dynamic range from 0 to 4 x 10^5 protons/cm^2 sec ster.

(5) Geiger Counter: geometrical factor $A\Omega \approx 1$ cm^2 ster. This instrument detects electrons of energies above approximately 4 Mev and protons above 40 Mev, with a dynamic range from 10 to 2 x 10^4 particles/cm^2 sec ster.

(6) Two three-axis flux gate magnetometers used for aspect determination. Ranges: -600 to +600 milligauss and -200 to +200 milligauss.

1.3 Methods of Data Analysis

The data obtained from about 50 orbits in July and August 1964 were analyzed with the help of the computer program discussed in detail in the report ASE-909 listed in Section 1.4.

Besides extracting and presenting the data from a desired instrument for any specific times, in the pertinent absolute units, the program also calculated the satellite aspect, and determined the pitch angle corresponding to each datum from the magnetometer readings and timing data. The pitch angle θ corresponding to a rotating vector $\bar{a}$ (perpendicular to the spin axis $\bar{J}$) can be determined uniquely by knowing the angle γ between $\bar{J}$ and the local magnetic field $\bar{B}$, and the angle ϕ (a function of time) between $\bar{a}$ and the intersection of the plane normal to J with the plane of $\bar{B}$ and J. (See Figure 1).

The angle γ was calculated using the measured components of $\bar{B}$; a flux gate magnetometer of each set had its axis parallel to the satellite spin axis. The magnitude of the field expected from the satellite ephemeris served as a check on the magnetometer accuracies. The time of minimum pitch angle, and the angle $\omega(t - t_o)$ were determined by fitting the readings of the two magnetometers of each set whose axes were perpendicular to the spin axis (and to each other) to the functional form expected from the rotation of the satellite. The accuracy of the least squares fits used, as estimated comparing aspects obtained from the two magnetometer sets independently, was within a few degrees. The angle γ was known with an uncertainty of about 10^o, judging from the scatter of the obtained values. The uncertainties in the calculated pitch angles therefore range from a few degrees around 90^o pitch angle to about 10^o at 0^o or 180^o. Detailed information on the computational methods employed in the computer program, including, for example, noise rejection standards, are contained in the report ASE-909.

Data could be obtained from the computer in various formats, suitable for different purposes. For example, a condensed format giving instrument outputs at a selected energy and at 90^o pitch angle for the scintillation spectrometers, or at maxima and minima of the electrostatic analyzers outputs,

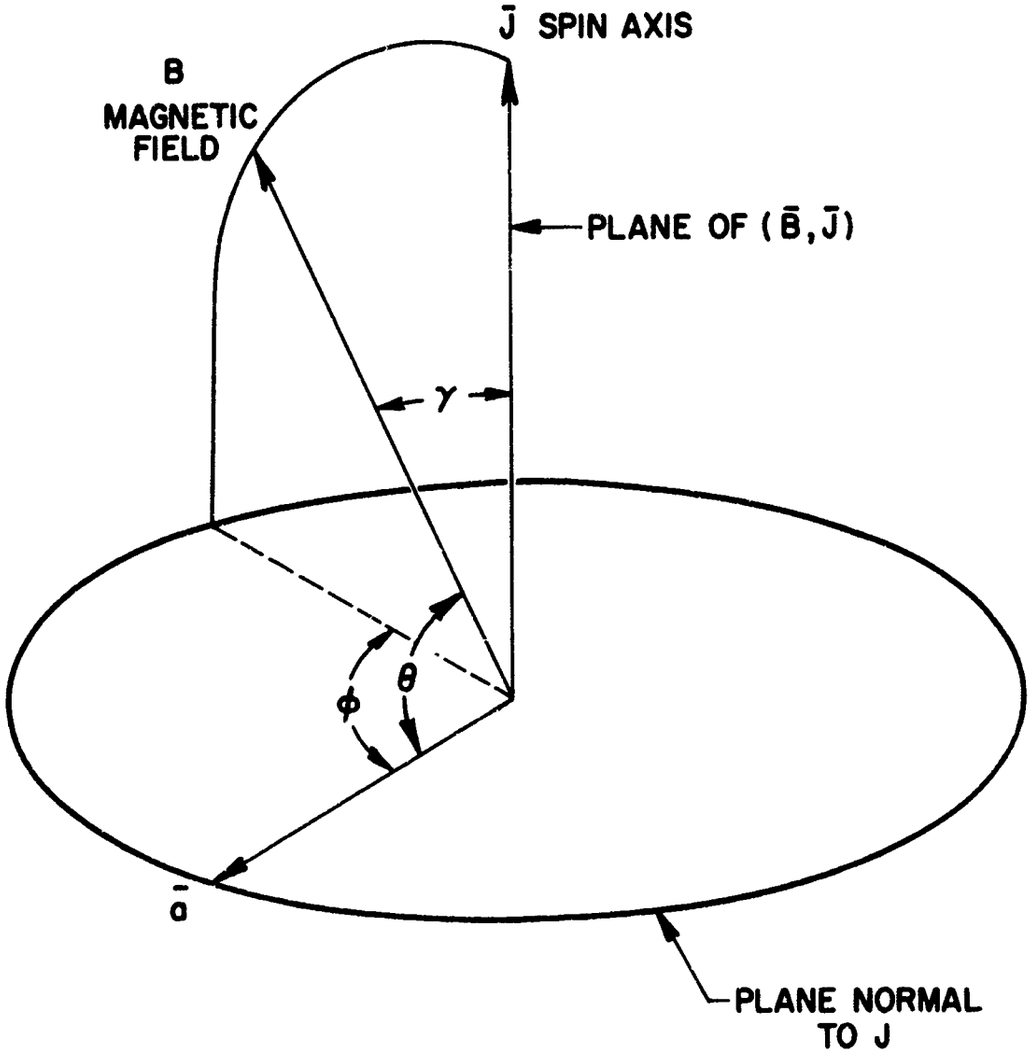

Fig. 1 Aspect Geometry

was very useful in surveying the data in a concise form. Such printouts have been obtained and compiled into books for all the instruments and all available orbits. Detailed printouts giving all the data, with energy and pitch angle information, were obtained for specific time periods of interest, where energy spectra and pitch angle distributions were desired.

1.4 Pertinent Documentation

The following documents were generated under Contract AF 19 (628) - 2392, which concerned primarily the design, development, and fabrication of the instruments:

(1) F. R. Paolini, J. Waters; ASE-503, 24 January 1964 "Preliminary Analysis of Data Obtained from Air Force Satellite 1963-25B."

(2) F. R. Paolini, R. Giacconi, J. R. Waters, T. G. Quinn; ASE-546, AFCRL-64-435, 27 May 1964, "A Research Program To Investigate the Charged Particle Flux in the Near-Earth Magnetosphere From A P-11 Sub-Satellite " (Final Report).

(3) F. R. Paolini, R. Giacconi, J. R. Waters, L. Katz, D. Smart; Space Research V, 466 (1965), Proceedings of the Fifth International Space Science Symposium, Florence, May 8 - 20, 1964.

(4) M. Bate; ASE-470, 29 November 1963; "IBM 7090 Program to Process Digitized Data Tapes from Satellite 1963-25B".

25 copies of documents (1), (2) and (4) were submitted to AFCRL. The following documents were generated under this current contract, AF 19 (628) - 4207.

(1) F. R. Paolini, R. Giacconi, J. R. Waters, L. Katz, D. Smart; ASE-646, October 1964, "Measurements on Differential Energy Spectra of Electrons (15 to 100 kev) in the Magnetosphere."

(2) L. Katz, G. C. Theodoridis, F. R. Paolini, "Effect of a Solar Flare on the Outer Radiation Belt." Paper presented at the Forty-sixth Annual Meeting of the American Geophysical Union at Washington, D. C. on 19 - 22 April 1965, and abstracted in Transactions, AGU, Vol. 46 p. 137 (1965).

An earlier version of this paper appeared as:

F. R. Paolini, G. C. Theodoridis, "Effect of a Solar Flare on Electrons in the Outer Radiation Belt." Paper presented at the 1965 Annual Meeting of the American Physical Society, New York, 27 - 30 January 1965, and abstracted in Bulletin of the American Physical Society, Series II, Vol. 10 p. 14 (1965).

(3) F. R. Paolini, G. C. Theodoridis, "Measurements on 0.7 to 4 Mev Electrons in the Radiation Belts from Hitch-hiker I." Paper presented at the Forty-sixth Annual Meeting of the American Geophysical Union, Washington, 19 - 22 April 1965, and abstracted in Transactions, AGU, Vol. 46 p. 136 (1965).

(4) G. C. Theodoridis, F. R. Paolini, "Measurements on 1 to 4 Mev Protons in the Radiation Belts." Paper presented at Forty-sixth Annual Meeting of the American Geophysical Union at Washington, D. C. on 19 - 22 April 1965, and abstracted in Transactions, AGU, Vol. 46 p. 136 (1965).

(5) G. C. Theodoridis, F. R. Paolini, L. Katz, D. Smart; ASE-992, August 1965; "A Study of Energetic Electrons in the Radiation Belts with Hitch-hiker I" Paper presented to the Advanced Study Institute ("Radiation Trapped in the Earth's Magnetic Field") at the Christian Michelsen Institute in Bergen, Norway, on 16 August - 3 September 1965.

(6) M. Bate; ASE-909, 15 May 1965 "Computer Program (For IBM 7090) to Aid in the Analysis of Results from Hitch-hiker I (1963-25B).

Documents (1) through (5) listed above are appended to this report. 25 copies of document (6) were submitted to AFCRL

1.5 Organization of the Report

This report contains, as appendices A through E, five papers written during the analysis of Hitch-hiker I data. In the subsequent section 2., which is a discussion of the results of data analysis, material contained in the appendices will not therefore be repeated. However, new interpretations of some of the previous results are included in the discussion, and references to the pertinent papers in the appendices are given. A general summary of results is given at the end of this report.

BLANK PAGE

2. DISCUSSION

2.1 Electron Electrostatic Analyzer

Electron data obtained from the electrostatic analyzer yield reasonable intensity levels and differential energy spectra for the energy range 15 to 100 kev. A preliminary discussion on these data is given in Appendix E. Major difficulties arise however in the interpretation of the pitch angle distributions obtained. The observed angular distributions in certain instances do not present the azimuthal symmetry expected for charged particles in a magnetic field. The data nevertheless exhibit systematic patterns with a high degree of reproducibility.

Figure 2 gives a summary of the recorded unidirectional intensities at an energy level of 40 $\pm$ 5 kev over one orbit on 3 July 1963. Curves a and b give the maximum and minimum intensities recorded during the satellite rotation. Also included in the figure are the values of the geomagnetic coordinates L and λ, the geographic latitude, the satellite altitude, and the angle γ between the satellite spin axis and the local magnetic field. The shaded bar indicates the dark portion of the orbit. The counting rate of the Geiger counter is also given as a measure of the penetrating radiation present.

Several regions with rather distinct spectra and pitch angle distribution patterns can be distinguished in any one orbit. During the apogee crossing through the heart of the inner belt (UT around 63000 sec and 71000 sec in Figure 2) large minimum and maximum intensities are recorded. The pitch angle distributions in these regions are rather flat as illustrated in Figure 3a. This suggests that the high intensities recorded at the heart of the inner belt may be due to energy deposition by

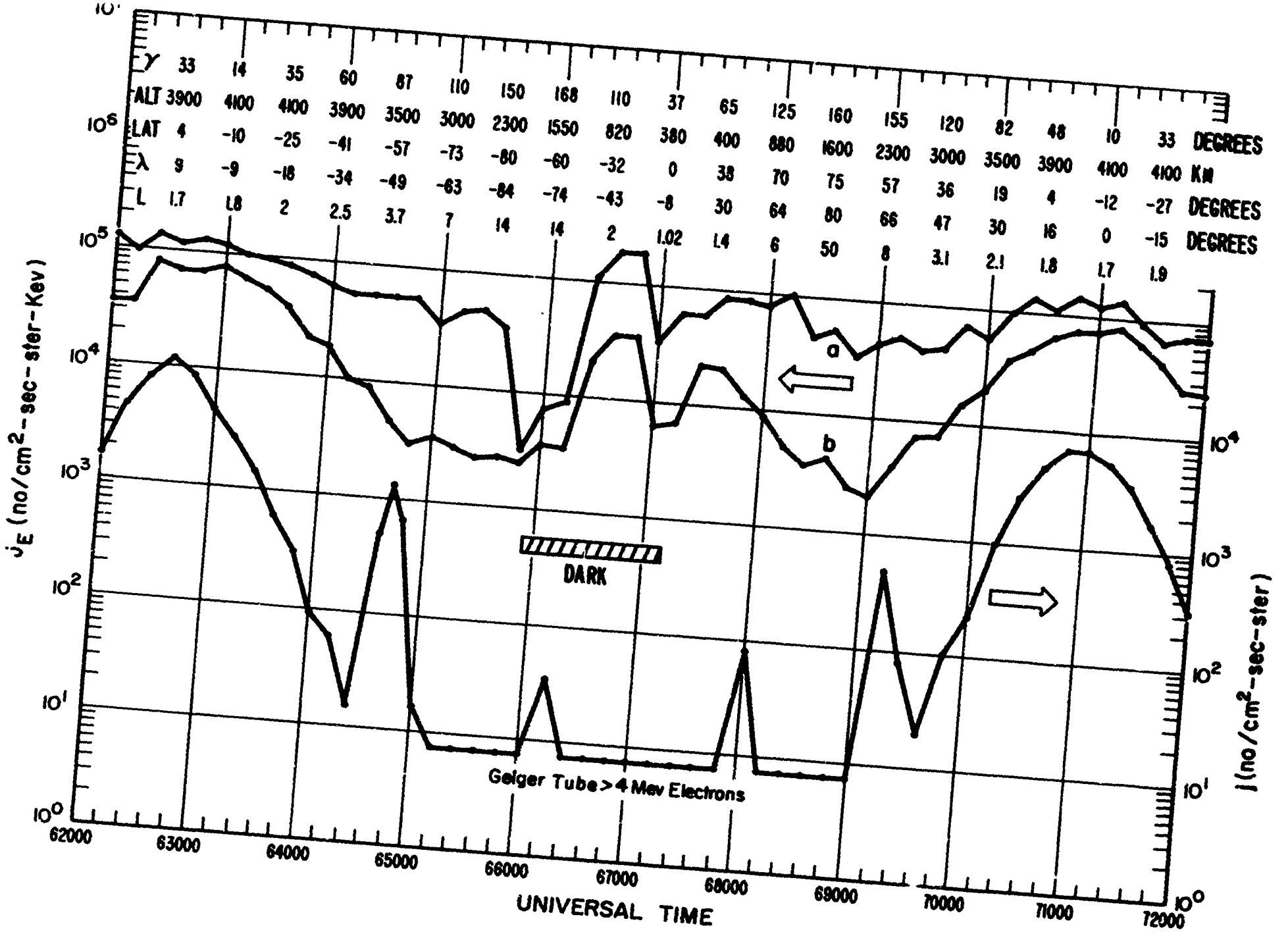

Fig. 2 40 kev Electrons, ϕ 25

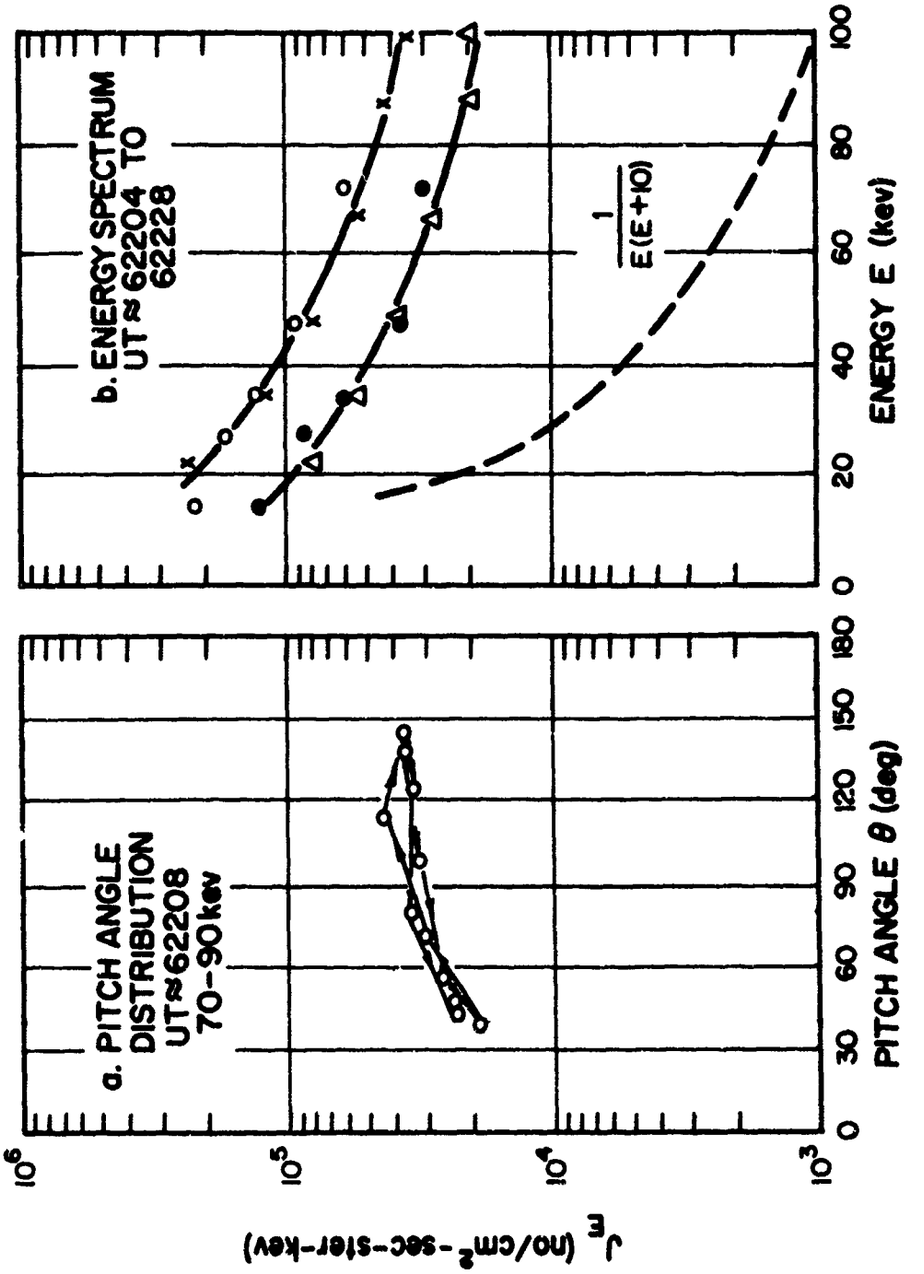

Fig. 3 Low Energy Electrons, ϕ 25

energetic particles which penetrate the shielding of the electrostatic analyzer. Minimum shielding was about 5g/cm^2 equivalent to the range of about 10 Mev electrons and 65 Mev protons) over approximately 2 cm^2-ster of this instrument, compared to the geometrical factor of $A\Omega \approx 0.2$ cm^{2}ster. The observed peak intensities at the heart of the inner belt can be approximately accounted for by the high energy protons present in the inner belt, which probably make the main contribution in energy deposition in the 0.1 g/cm^2 plastic scintillator.

Figure 3b gives the energy spectra of the maximum and minimum intensities from the electron ESA near the heart of the inner belt. For a rate of energy input independent of the plate sweep voltage, such as a contribution from penetrating particles, the apparent energy spectrum would be proportional to $1/E(E + 10)$ (this is the energy dependent part of the factor by which measured energy deposition rates in the scintillator are multiplied to be translated into intensities of particles per unit energy.) The spectra derived at the heart of the inner belt (Figure 3b) present a monotonically decreasing pattern but often they are somewhat flatter than $1/E(E + 10)$ (dotted curve in Figure 3b). This indicates contributions besides those from high energy penetrating particles.

High Geiger tube counting rates are not always accompanied by high ESA intensities with little pitch angle modulation. This is not surprising since the composition of the penetrating component may be different at various locations and consequently the response of the two detectors can also be different. The ESA readings usually indicate no significant penetration through the shielding in regions of high Geiger tube counting rates in the outer belt (where the trapped radiation is predominantly electrons). This therefore suggests that the main contribution in rate of energy deposited by penetrating particles at apogee passes through the inner belt is due to high energy inner belt protons.

In the polar portions of the orbits (UT 65000 - 66000 sec and 68000 - 69000 sec in Figure 2) the typical pattern consists of low minimum intensities (close to the lowest limit of sensitivity imposed by the photomultiplier dark current) and high maximum intensities in the sunlit portions, dropping

abruptly to about the level of the minimum intensity at the transition to darkness (For example, at UT ≈ 65800 sec in Figure 2). The pitch angle distributions in these regions are rather flat except for a sharp peak corresponding approximately to the direction of the Sun; Figure 4a illustrates this. The energy spectra, as shown in Figure 4b, have about the form to be expected for a constant rate of energy input, independent of the plate voltage (i.e., a 1/E(E + 10) shape). It therefore appears that in the polar regions the electron ESA does not measure anything significantly above its lowest limit of sensitivity, apart from an apparent constant rate of energy input when looking in the direction of the Sun. This is consistent with the ESA's detector being slightly light sensitive.

In the portion between the heart of the inner belt and the polar region (around UT ~ 64000 sec and 69000 sec in Figure 2) the electron ESA intensity decreases while the pitch angle distributions remain relatively flat; (see Figure 5a). The energy spectra as given in Figure 5b (maximum and minimum curves) are flat and quite divergent from the 1/E(E + 10) form. This indicates that the detector readings are due to an input sensitive to the plate voltage. The smooth transition from the spectral shape of Figure 5a to that if Figure 3a which is closer, but still flatter than 1/E(E + 10), shows that the electron ESA readings in the inner belt cannot be fully accounted for by penetrating energetic particles alone.

The most puzzling pattern of the ESA results is observed in a region centered around the dark portion of each orbit (about UT 66000 - 67000 in Figure 2). A marked increase in the maximum and minimum intensities occurs in this region. Pitch angle distributions indicate a pronounced azimuthal asymmetry by their shapes (an ellipse, as in Figures 6a and 8a; or an ellipse plus a sharp peak as in Figure 7a). The direction corresponding roughly to the major axis of the ellipse is about 40° to the East of the zenith vector, while the direction of the sharp peak, whenever it is present (Figure 7a) is toward the sky.

Energy spectra in this region are invariably inconsistent with a constant rate of energy input curve (1/E(E + 10). Sometimes both the maximum and minimum intensity curves are rather flat with a broad maximum

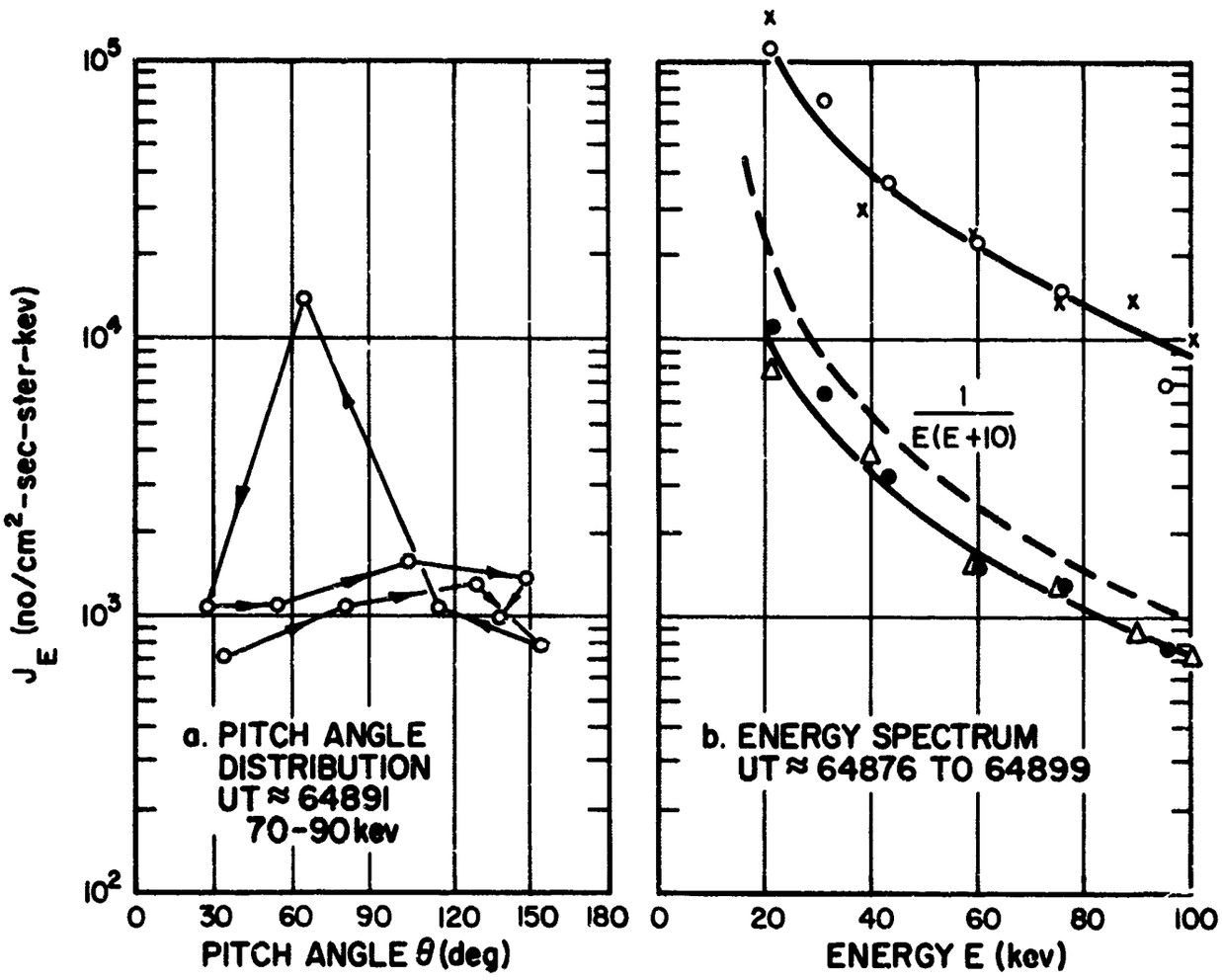

Fig. 4 Low Energy Electrons, ϕ 25

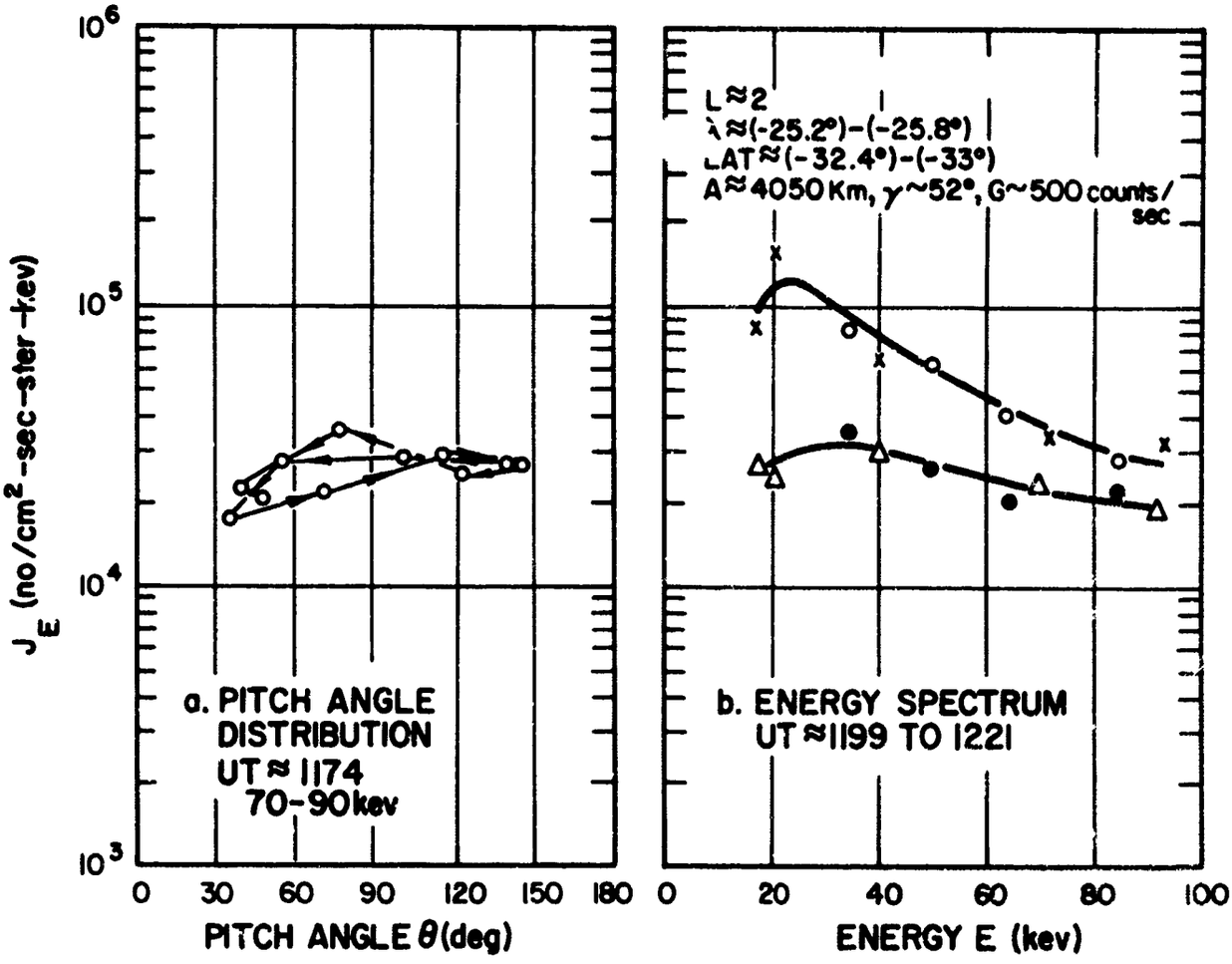

Fig. 5 Low Energy Electrons, ϕ 26

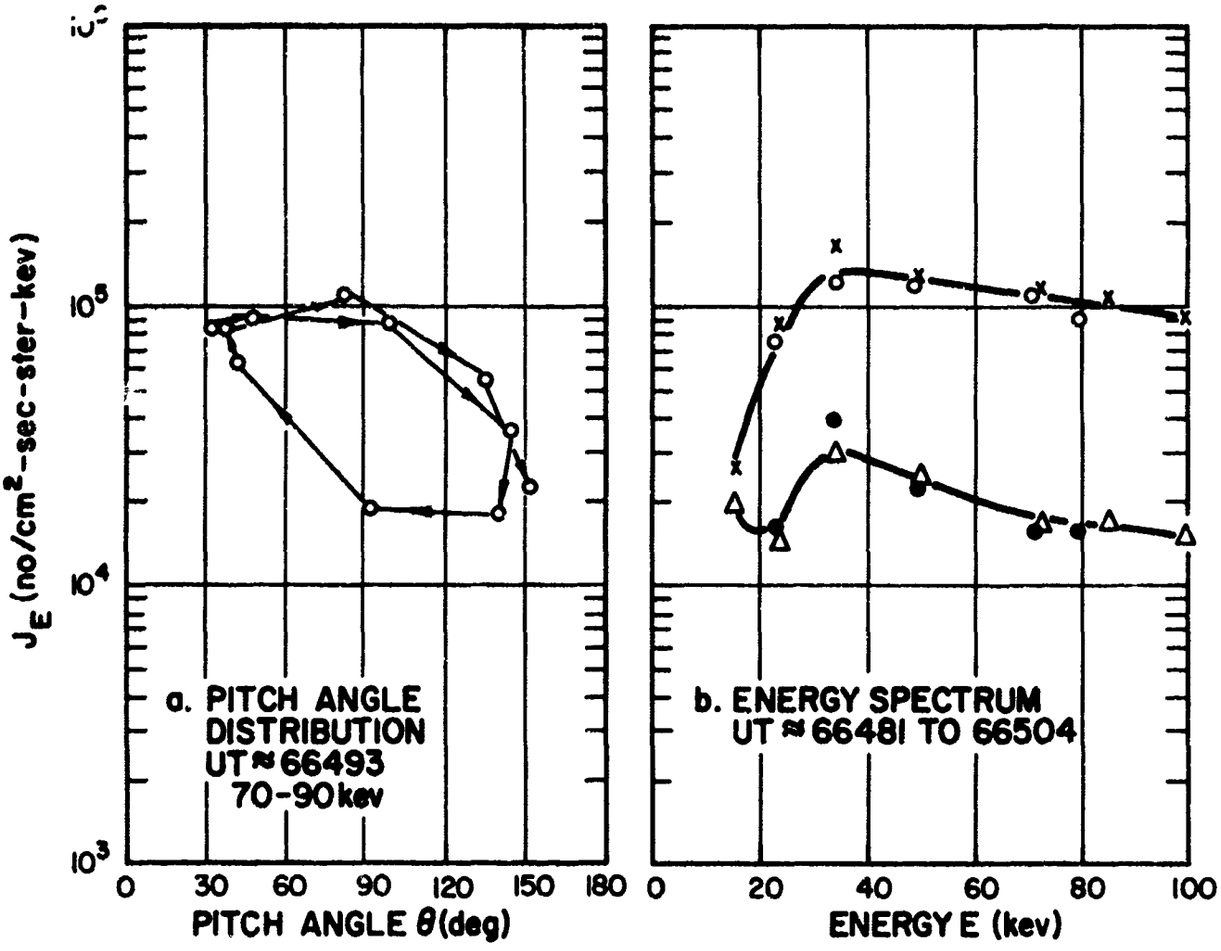

Fig. 6 Low Energy Electrons, ϕ 25

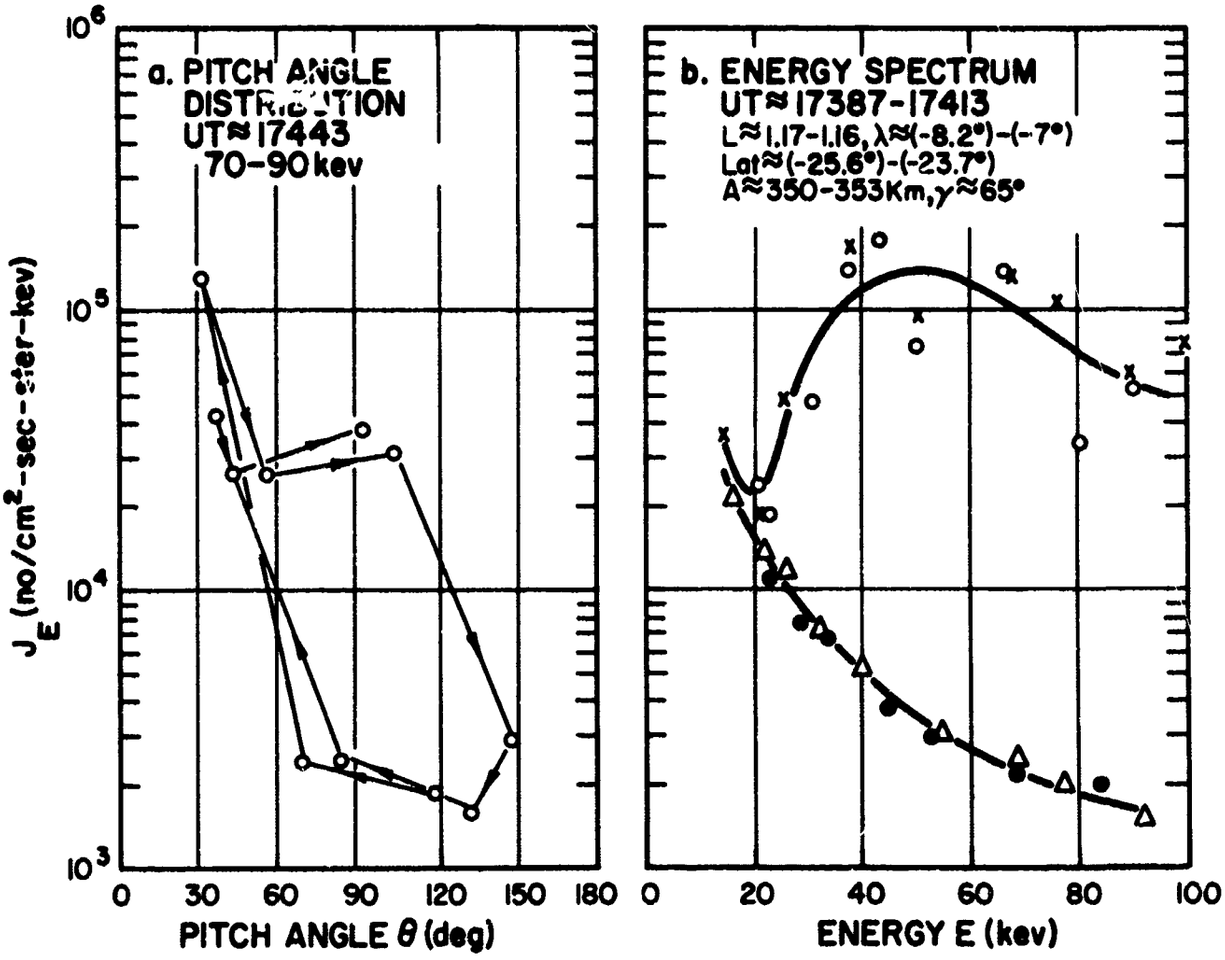

Fig. 7 Low Energy Electrons, $\phi 323_D$

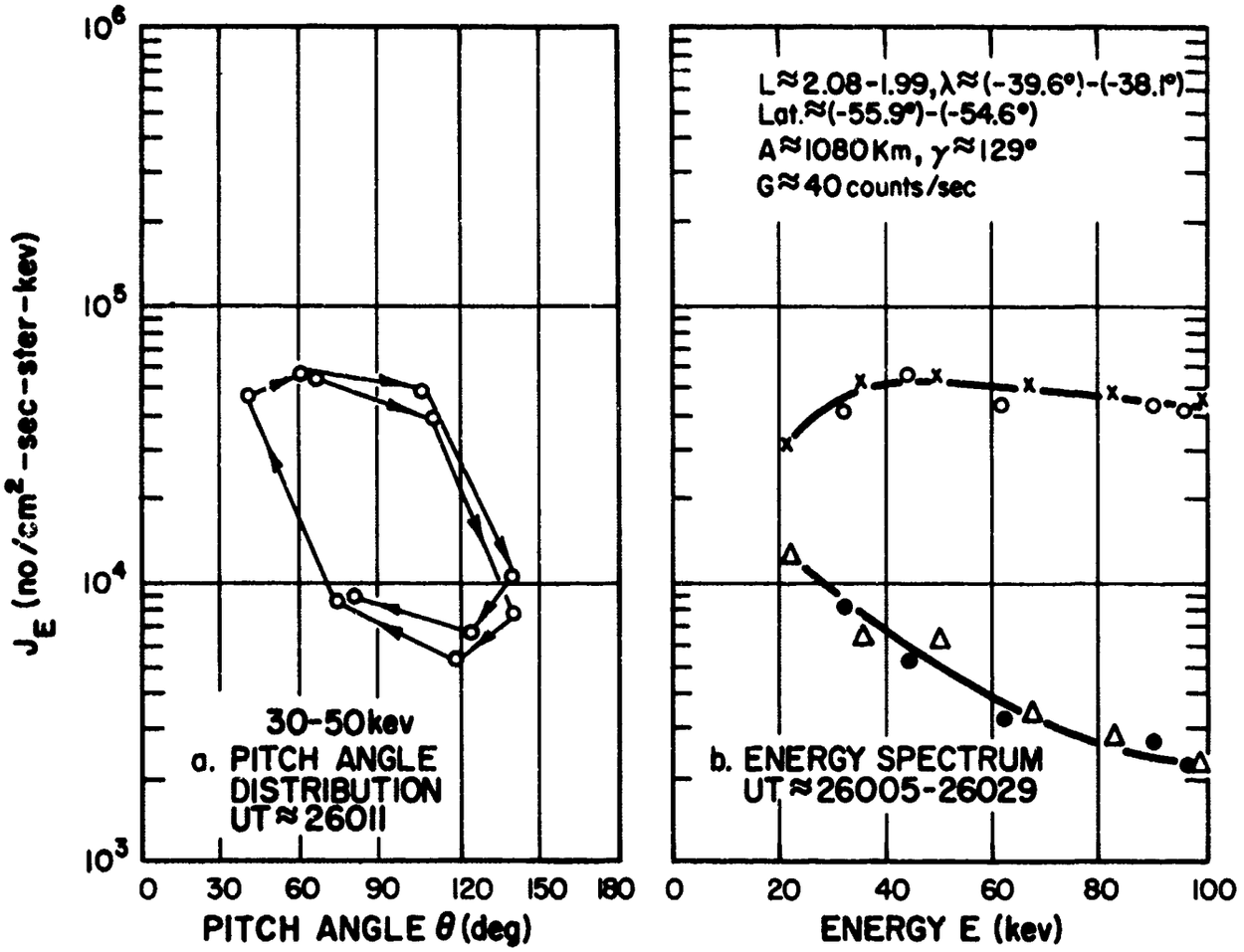

Fig. 8 Low Energy Electrons, $\phi 96_D$

around 40 kev falling off at lower energies (e.g., see Figure 6b), while at other times the maximum curve has this shape and the minimum curve is approximately $1/E(E + 10)$, consistent with a minimum due to the photomultiplier dark current (e.g., see Figures 7b and 8b).

The region where the behavior described is observed is around the perigee crossing of the inner belt, although its extent cannot be determined in terms of the usual geomagnetic coordinates. It is approximately centered around the dark portion of the orbit, beginning about 100 to 500 sec after the onset of darkness, and ending about 500 sec before, to 200 sec after, the onset of light.

The extent of the pitch angle modulation does not depend on the angle γ of the spin axis of the satellite to the local magnetic field. In Figure 9 we have the pitch angle distribution and the energy spectrum in a situation when the pitch angles scanned by the axis of the field of view differ among themselves far less than the opening of the instrument. A large angular modulation is nonetheless observed.

The possibility that the aspect determination might be at fault is ruled out by the behavior of the outputs of other instruments on board. In Figure 10 the highly modulated output of the electron ESA (Figure 10a) is contrasted to the simultaneous readings of the electron scintillation spectrometer (Figure 10b). The spectrometer readings are seen to be consistent with the small value of γ, yielding only the top portion of the sharply peaked pitch angle distribution shown complete for a different point on the same orbit in Figure 10c. It should be noted here that the spectrometer field of view is much narrower than that of the ESA, which means that on simultaneous readings at small γ the ESA should be expected to produce less angular modulation than the scintillator.

We therefore conclude that in the dark portion of the orbit we observe angular modulation in the electron ESA readings which cannot be accounted for by charged particles in the magnetic field. On the other hand, some

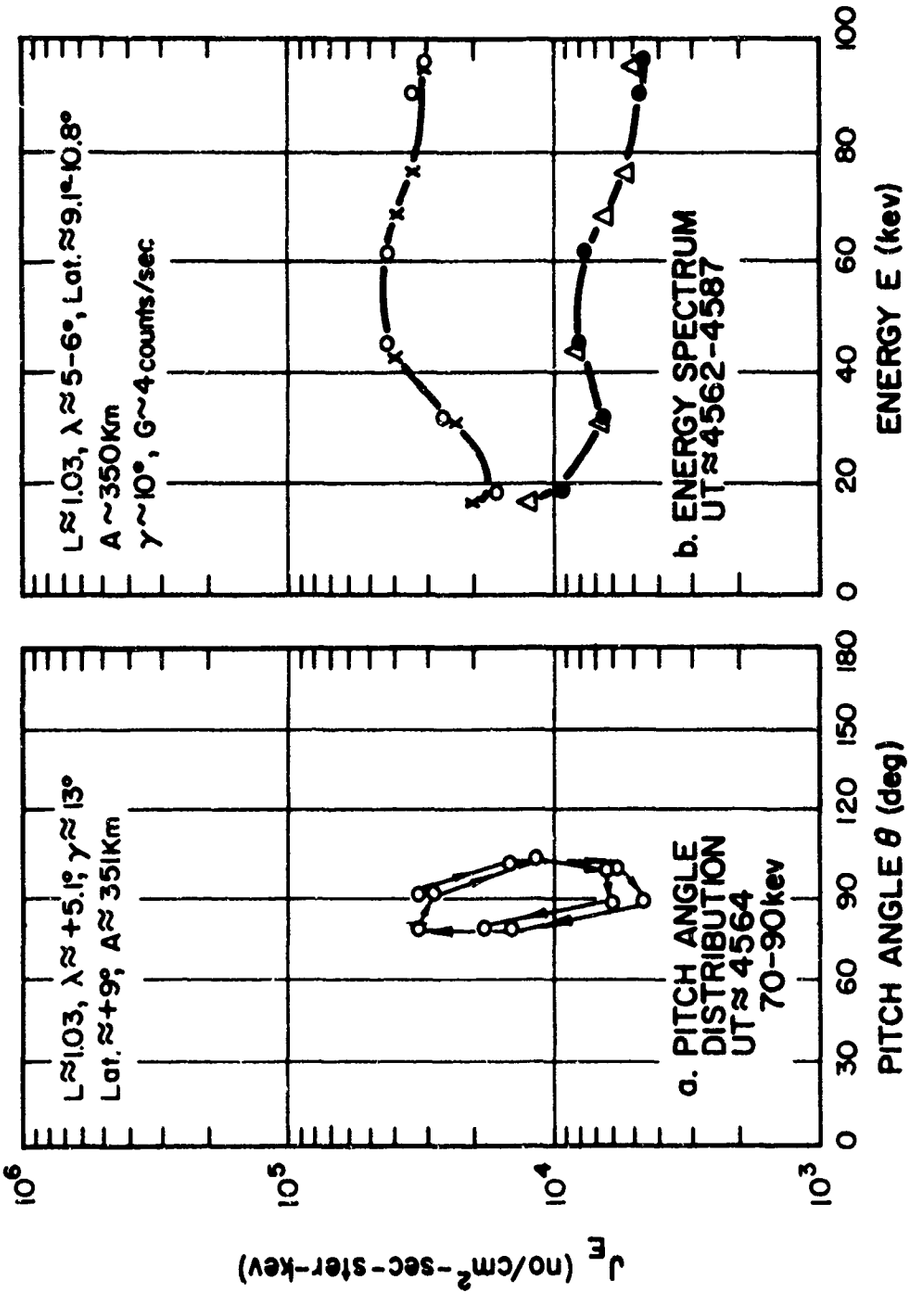

Fig. 9 Low Energy Electrons, $\phi 26_D$

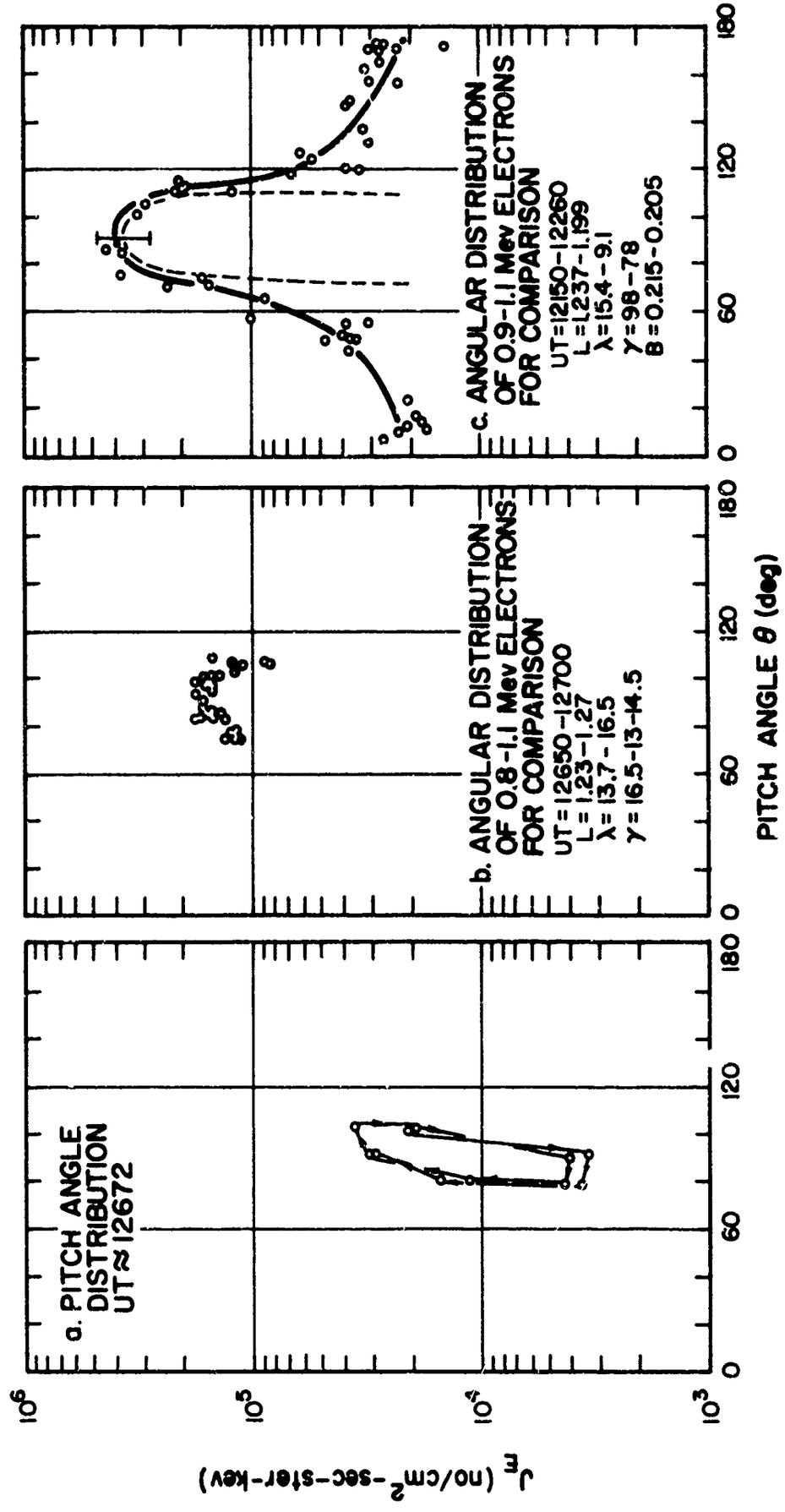

Fig. 10 70 - 90 kev Electrons, ϕ 431

spectra (Figures 5b through 8b inclusive) are definitely not of the form expected for a constant rate of energy input, indicating that the instrument responds to something sensitive to the plate sweep voltage.

Immediately following the dark portion of the orbit there is usually another period of rather high maximum and minimum intensities. (e.g., U.T. ~ 67600 sec in Figure 2). Spectra in this region are flat with a broad maximum around 40 kev (Figure 11b). The pitch angle distributions (Figure 11a) do not present the elliptical patterns observed in the dark portion of the orbit.

2.2 Proton Electrostatic Analyzer

For the data obtained from the proton ESA, the maximum and minimum intensities recorded during a satellite spin had an energy dependence consistent with a constant rate of energy input independent of the plate sweep voltage (i.e., spectral form $1/E^2$). It appears that the output of this instrument can be accounted for by energy deposited in the scintillator by light entering the aperture and to some extent, by high energy particles which penetrate the shielding.

Figure 12 is a summary of recorded unidirectional intensities at 40 ± 5 kev. Curves a and b give the maximum and minimum intensities measured during the satellite rotation. Also included are the values of the geomagnetic coordinates L and λ. The shaded bar marks the dark portion of the orbit. The counting rate of the Geiger counter is given also as a measure of the penetrating radiation present.

The maximum intensities in the sunlit portion of the orbit are clearly attributable to sunlight which continuously saturates the instrument (Figure 12, curve a). The minimum intensity (curve b) presents a peak in the regions of high Geiger tube counting rates as the apogee pass

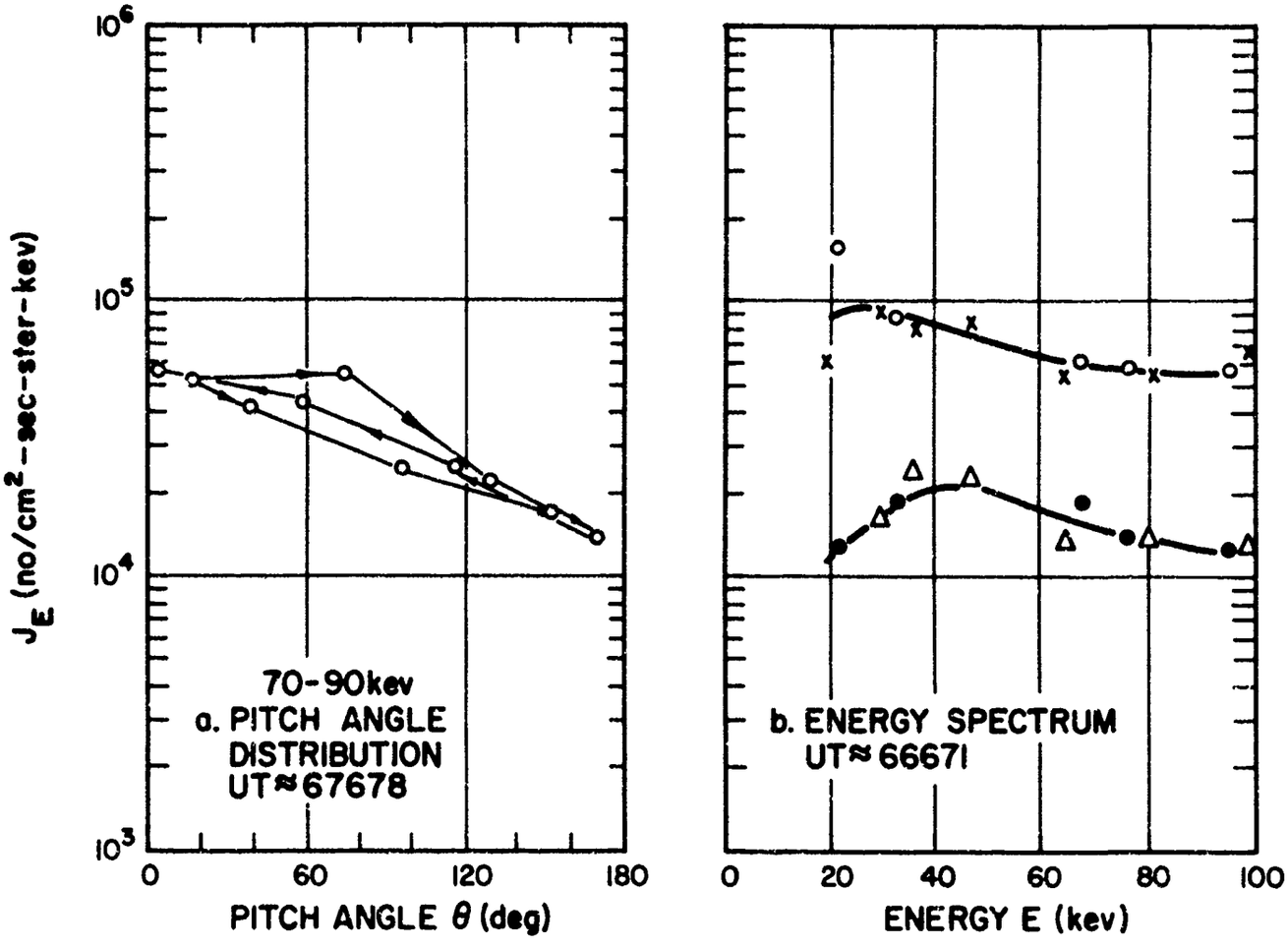

Fig. 11 Low Energy Electrons, ϕ 25

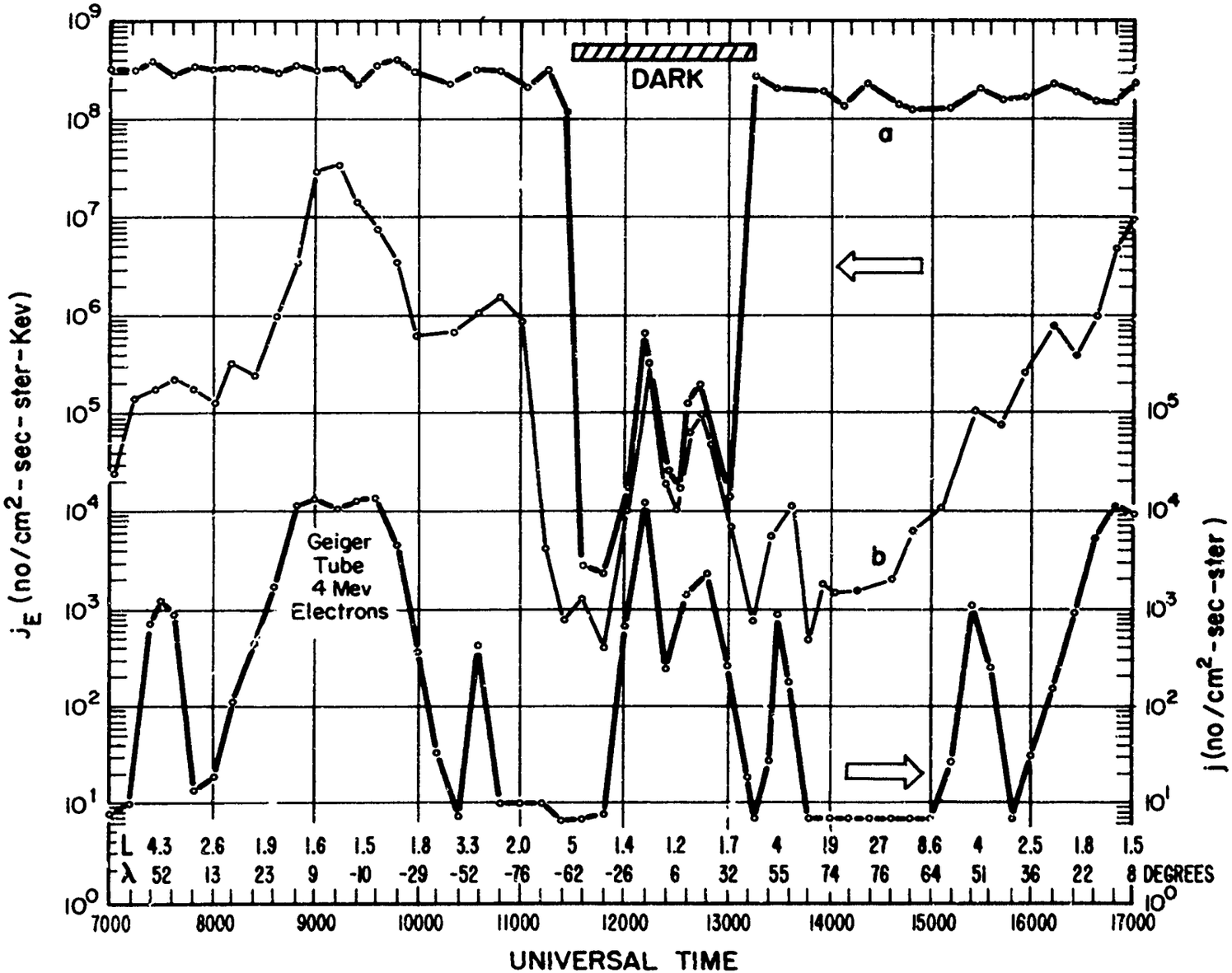

Fig. 12 40 kev Protons, ϕ 431

through the heart of the inner belt (around UT 9000 sec and 17000 sec). This peak can be attributed to energy deposited in the scintillator by high energy particles which penetrate the shielding around the instrument. Similar peaks were recorded by the electron ESA with intensities lower by factors of 50 to 100. A difference in response is to be expected due to the different scintillators used in the two instruments. Correlated variations in proton ESA and Geiger tube counting rates, indicating shielding penetration, are observed at the perigee pass through the inner belt (UT ~ 12000 to 13000 sec). Some penetration, but much less pronounced, is occasionally seen also during outer belt passes (e.g., UT ~ 13500 in Figure 12).

During the rest of the sunlit part of the orbit the minimum intensity presents fluctuations which can be understood in terms of the orientation of the detector with respect to the Sun or to Sunlight reflected off the surface of the Earth.

In the dark part of the orbit the maximum intensity is very low and about equal to the minimum intensity. Occasionally higher maximum intensities are observed (i.e. spikes) in the direction of the Moon.

As noted before, the energy spectra are always close to the form $1/E^2$ expected for a constant rate of energy input. Figure 13 gives two such pairs of maximum and minimum spectral curves in the light (13a) and in the dark (13b). The $1/E^2$ curve is given also for comparison.

A typical pitch angle distribution in the Sun is given in Figure 14a. The peak corresponds approximately to the direction of the Sun. The observed asymmetry around the peak can be understood by the different exposure of the scintillator to sunlight through satellite geometry and reflection through the analyzer plates. Occasionally a second peak due to the reflection of the sunlight off in the ocean can also be seen. During the

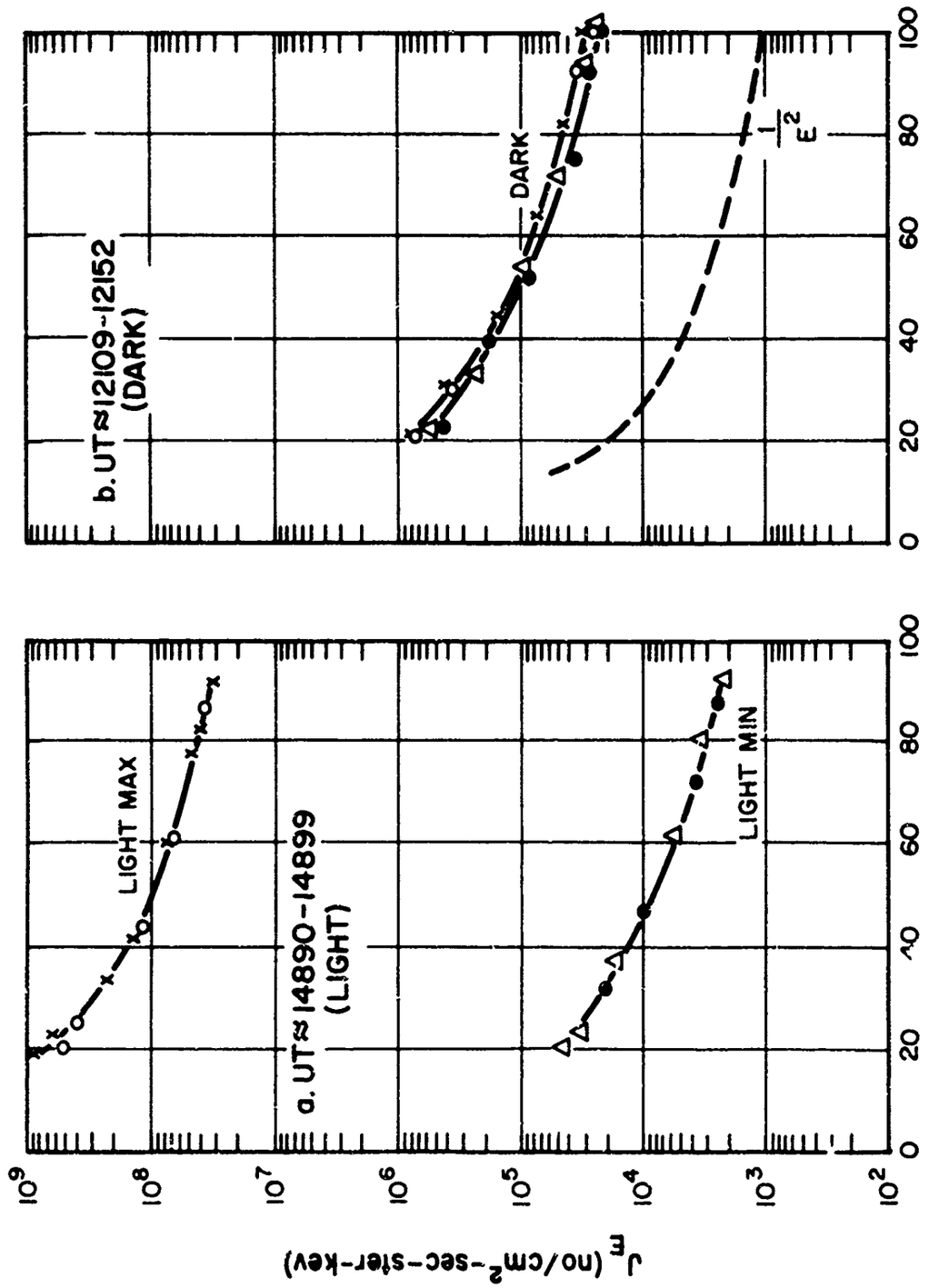

Fig. 13 Low Energy Proton Spectra, ϕ 431

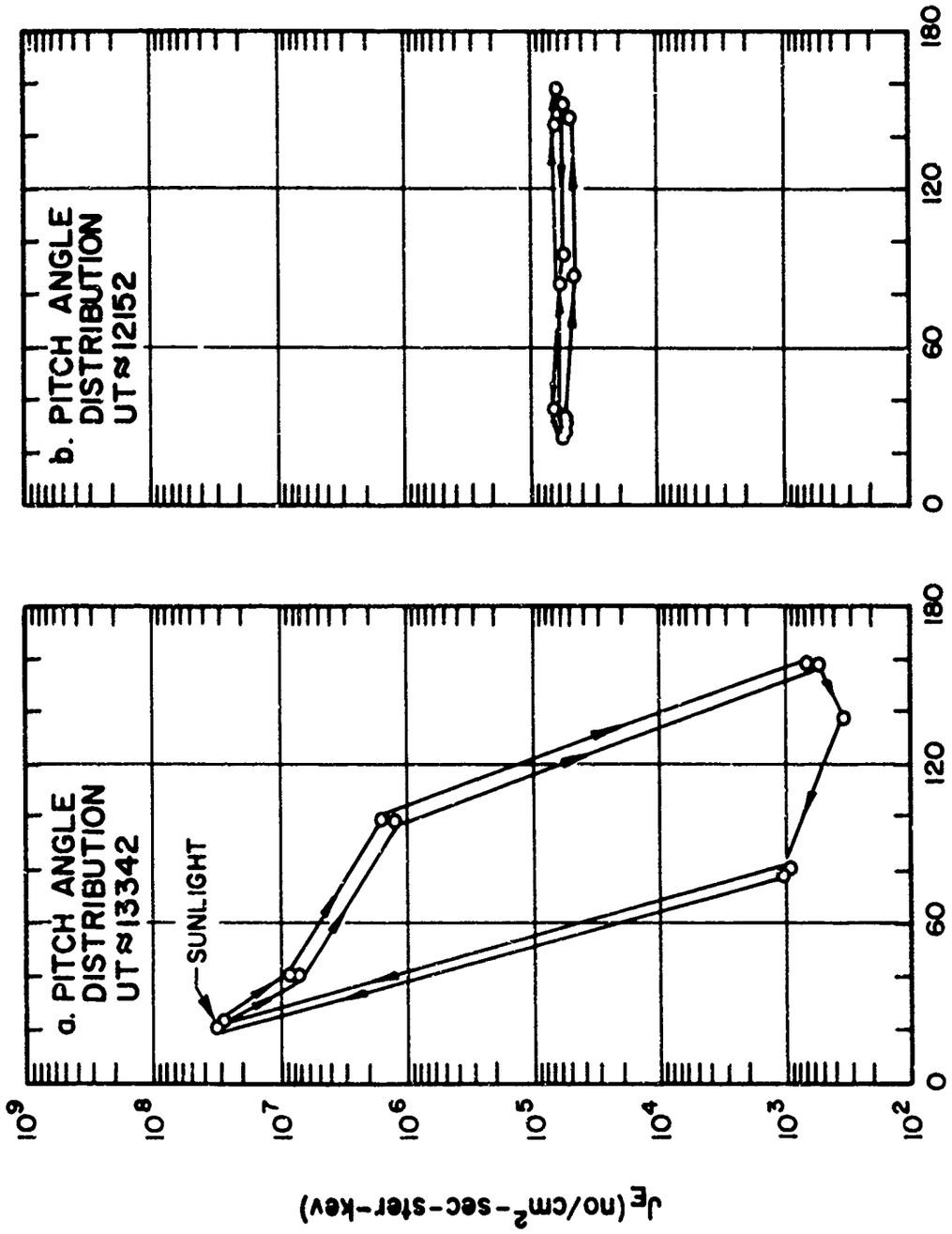

Fig. 14 70 - 90 kev Protons, ϕ 431

dark portion of the orbit, angular modulation is usually low (Figure 14b); in some instances, spikes corresponding to the direction of the Moon are recorded.

2.3 Electron Scintillation Spectrometer

Results from the electron scintillation spectrometer are presented in Appendices A, C, and D; A being the most comprehensive. In Appendix A, data from the rate of energy deposition channel of the instrument have been used in regions where the count rate channel approached saturation.

2.4 Proton Scintillation Spectrometer - Low Energy Channel

Data obtained from this instrument are presented as graphs of unidirectional intensity, energy spectra, and pitch angle distributions, in Appendix B. The intensity levels obtained in certain regions were substantially higher than results obtained from Relay I (Fillius and McIlwain 1964) and Injun IV (Krimigis and Van Allen 1965). We will, therefore, consider the possible contamination of the proton spectrometer data by electrons entering through the main aperture. Note that the sharp angular dependence observed excludes significant contamination from omnidirectional sources.

In order for a particle to be counted in the low energy channel of the proton spectrometer it would have to deposit all its energy in the plastic scintillator, since the anticoincidence circuit eliminates from analysis all events giving simultaneous pulses in both the plastic and CsI scintillators. (The pulse height would also have to be larger than the instantaneous value of the sweep voltage used for pulse height analysis). Figure 15 gives, on the basis of data from Selinger (1955), the percentage of electrons of various energies that are stopped in 40 mg/cm^2 of Al (similar enough to plastic for the purposes of the present discussion). Included in the figure, along the electron energy scale, are the proton energies for which

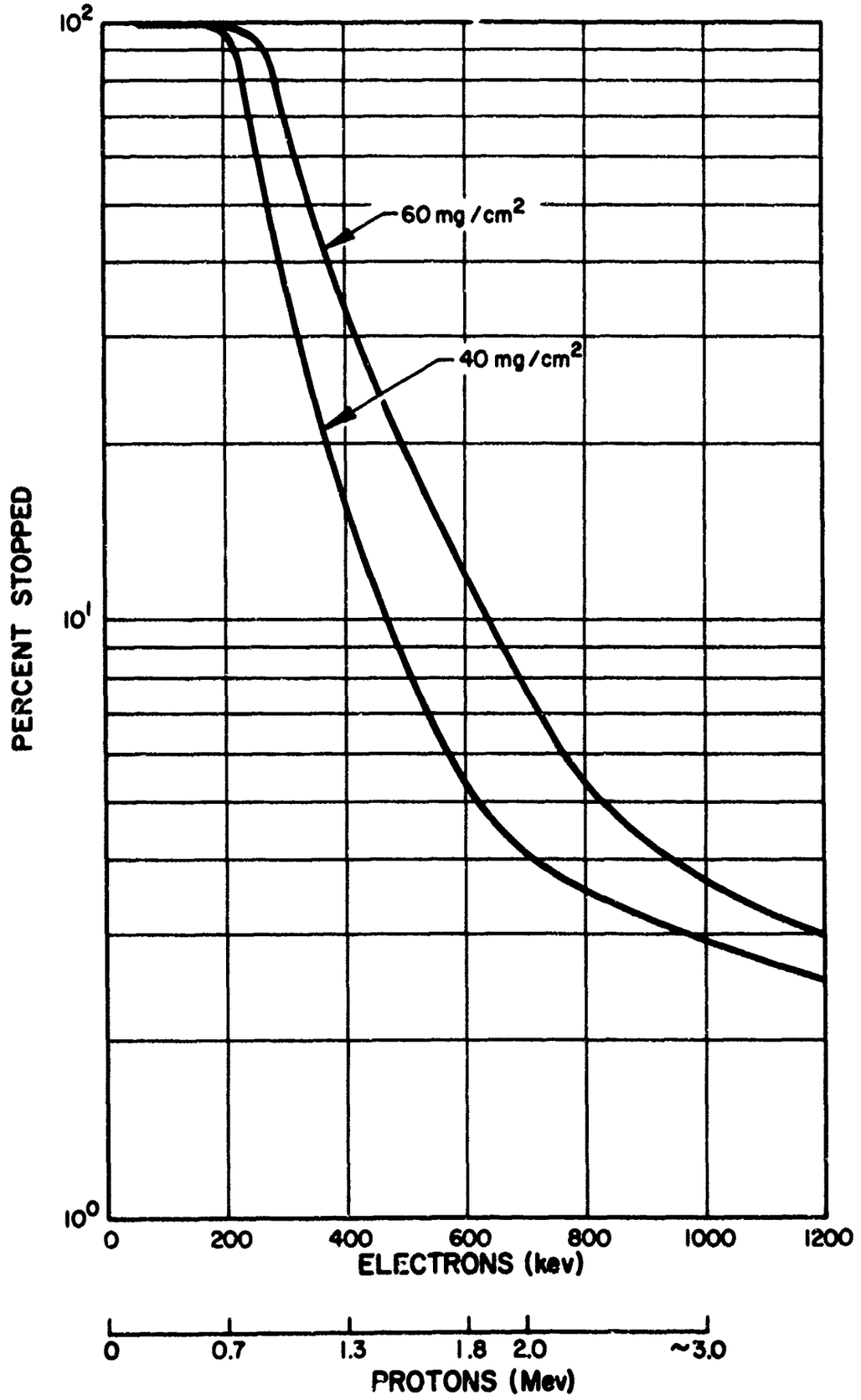

Fig. 15 Electrons Stopped in Aluminum

equivalent pulses are produced in the plastic scintillator on the basis of the electron-proton energy equivalence illustrated in the curve of Figure 16. Figure 15 indicates that for sweep voltages corresponding to proton energies above 1.5 Mev, which was the lower limit of the range of operation of the proton spectrometer, no more than 10% of the present electrons should be counted if the anticoincidence circuits were functioning.

Figure 17a contains schematic curves of proton spectrometer unidirectional intensities above 2 Mev in the inner belt. Figure 17b gives intensities of electrons above 1 Mev for the same region (reproduced from Appendix A) for comparison. Since energy spectra in the inner belt are rather flat (e-folding in about 1 Mev), the electron intensities of Figure 17b are close to those of electrons above 0.7 Mev which are approximately equivalent to protons above 2 Mev (Figure 16). Comparing Figures 17a and 17b we see that if less than 10% of the electrons are counted we have no significant electron contamination of the proton results. However, if the anticoincidence circuit failed and substantially more electrons are counted, significant contribution of electrons to the proton spectrometer counting rate could have resulted. If this were truly the case, however, it is hard to explain the marked difference in shape of the electron and proton intensity curves for $\lambda = 0^{o}$ and $\lambda = 10^{o}$ unless the electron energy spectrum at the low energy end is radically different in various inner belt regions.

A similar argument can be conducted regarding the outer zone. Figures 18a and 18b give intensity curves of protons over 2 Mev and electrons over 1 Mev in the outer zone. Figures 19a and 19b give proton and electron energy spectra in the outer belt. From Figures 18 and 19 we see again that if all electrons were counted in the proton spectrometer, instead of 5 to 10 percent, as expected from Figure 15, significant contamination of proton data by electrons would have resulted.

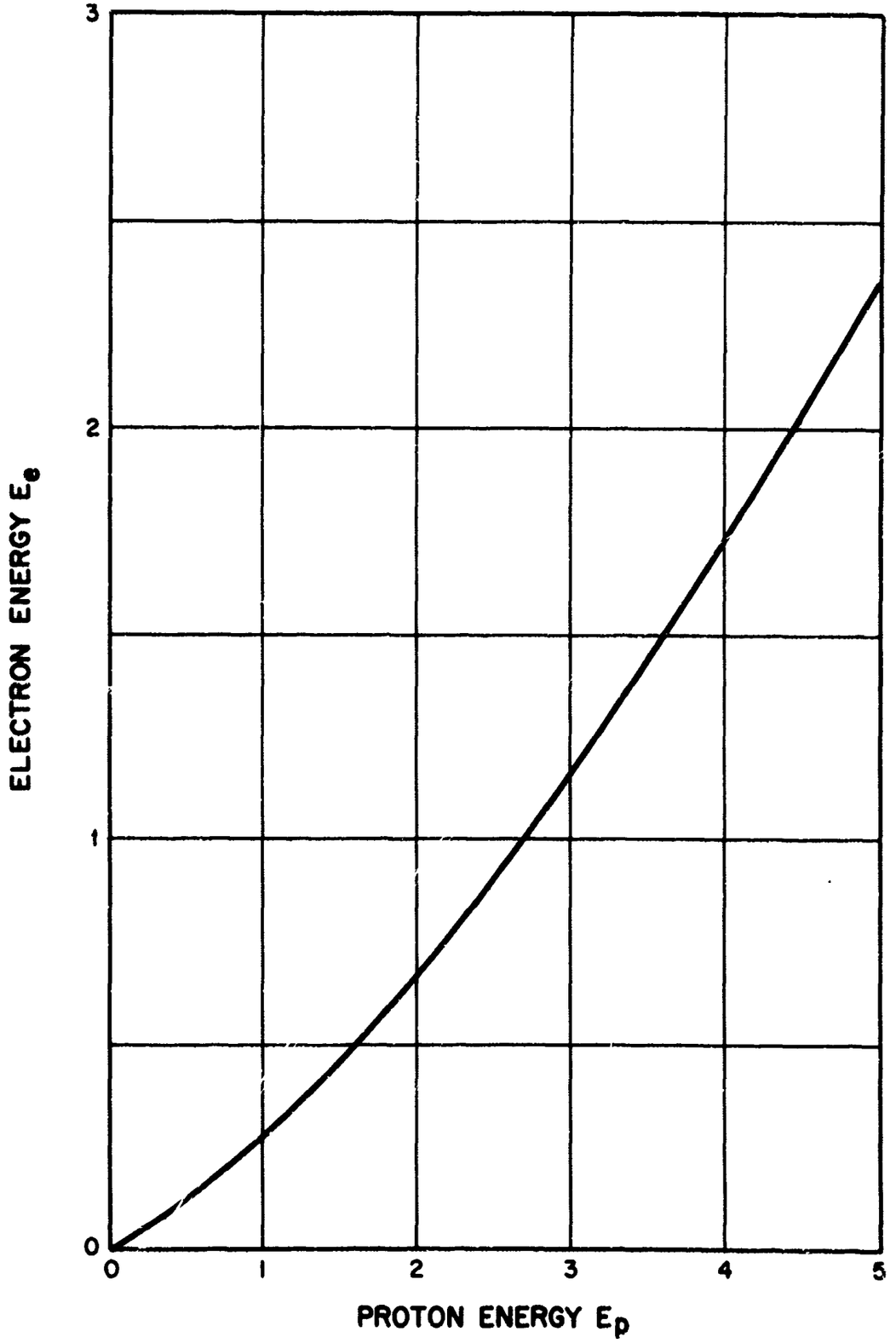

Fig. 16 Electron-Proton Scintillation Light Equivalents in Anthracene

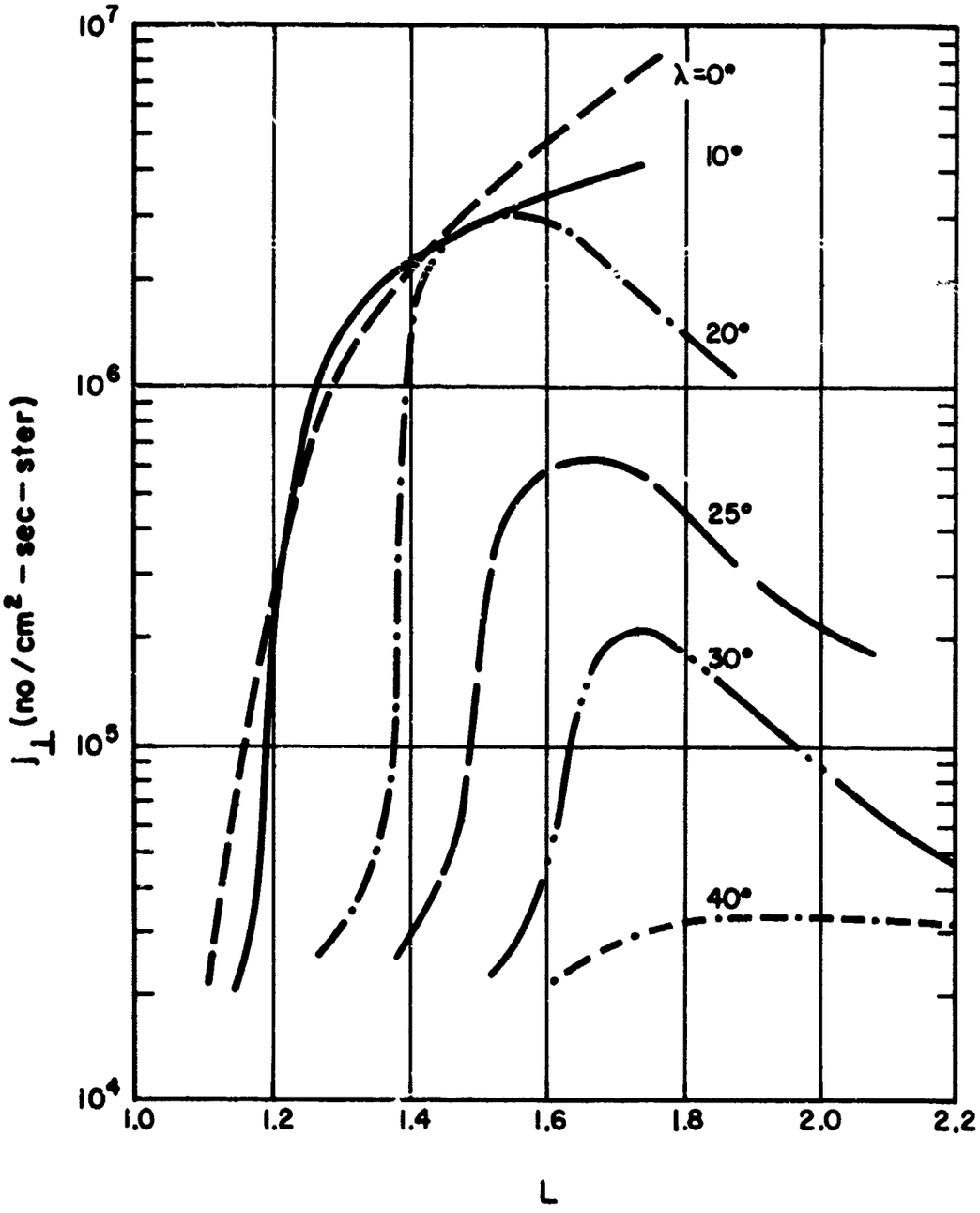

Fig. 17a Protons, >2 Mev, Inner Belt (Unidirectional Intensities at 90°)

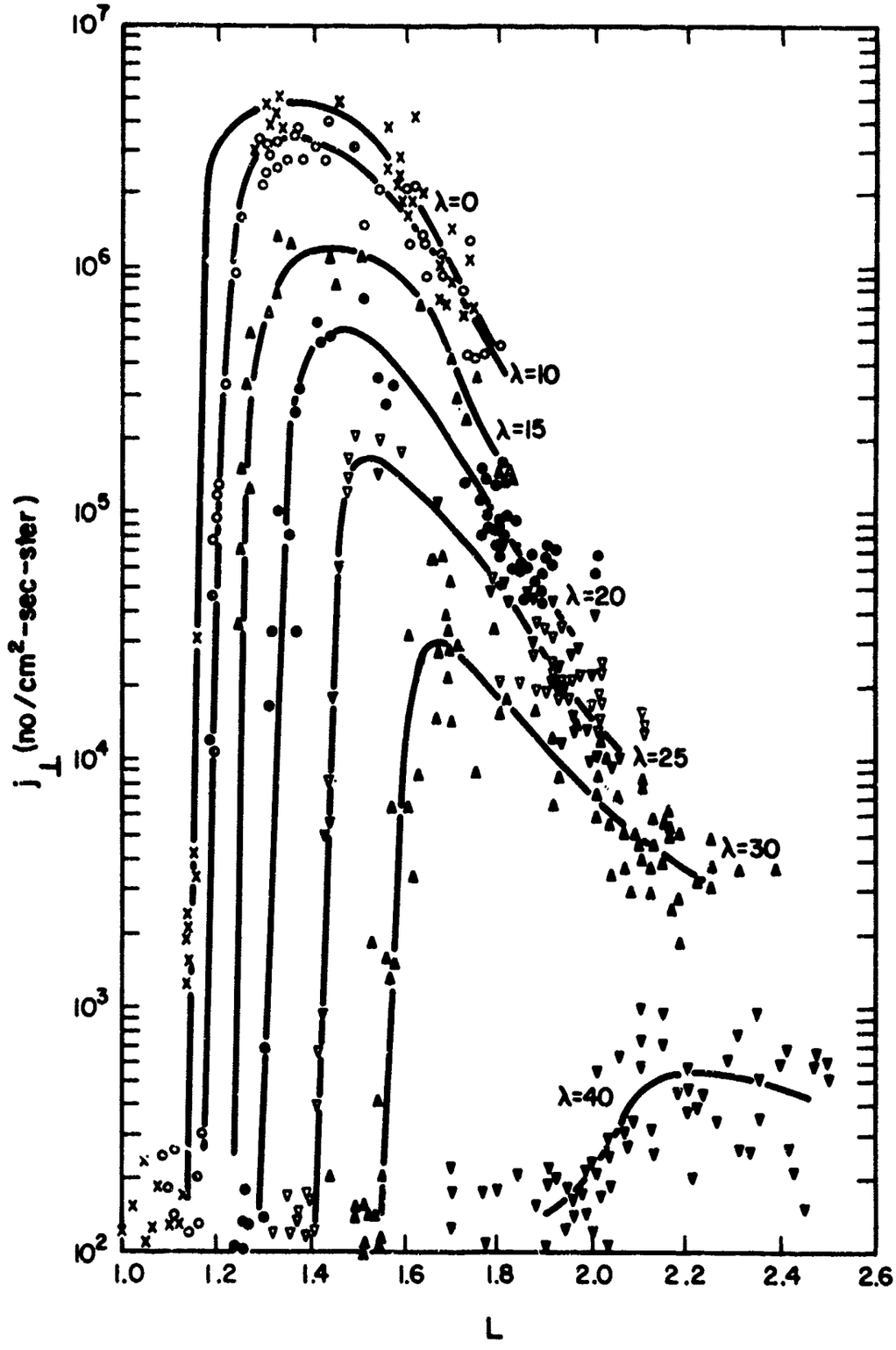

Fig. 17b Unidirectional Intensities of Electrons (> 1 Mev) at 90° for Comparison

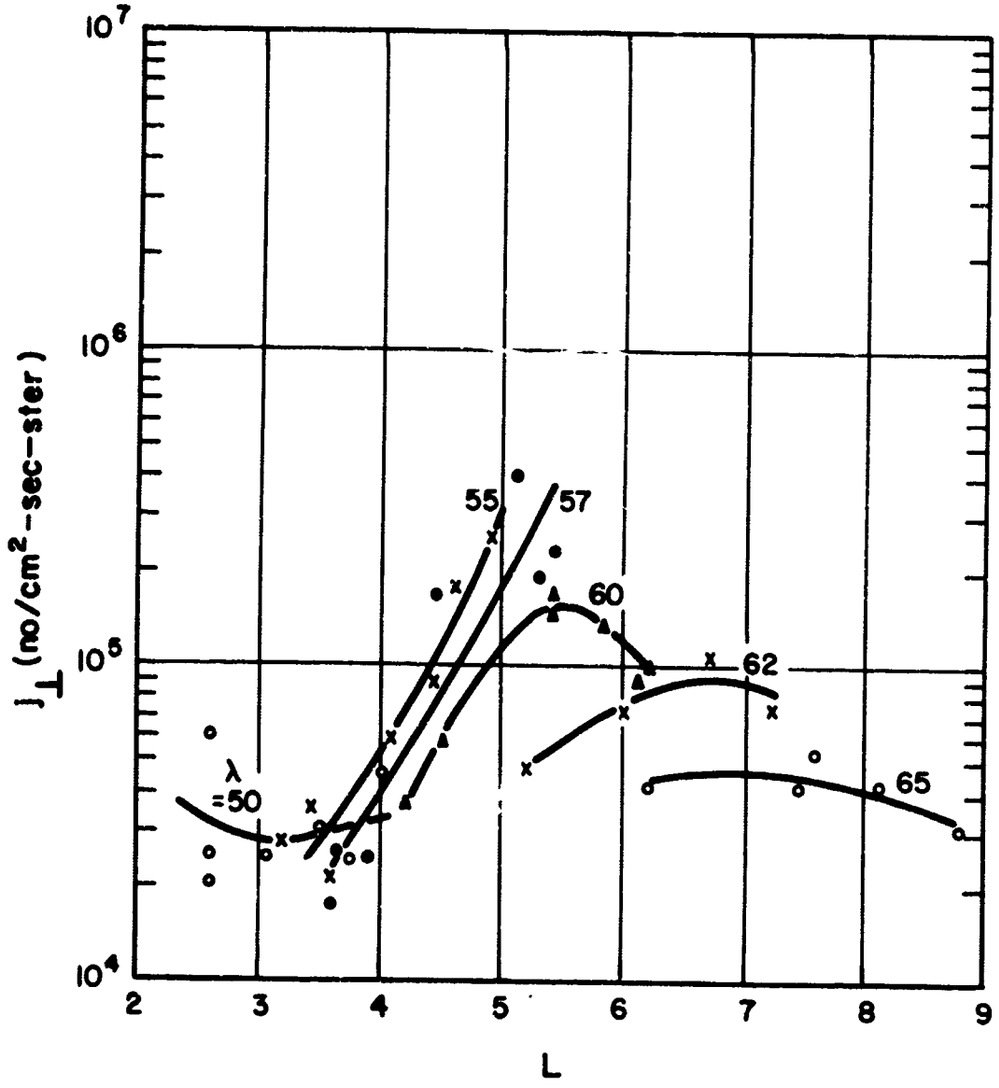

Fig. 18a Protons, >2 Mev, Outer Belt (Unidirectional Intensities at 90°)

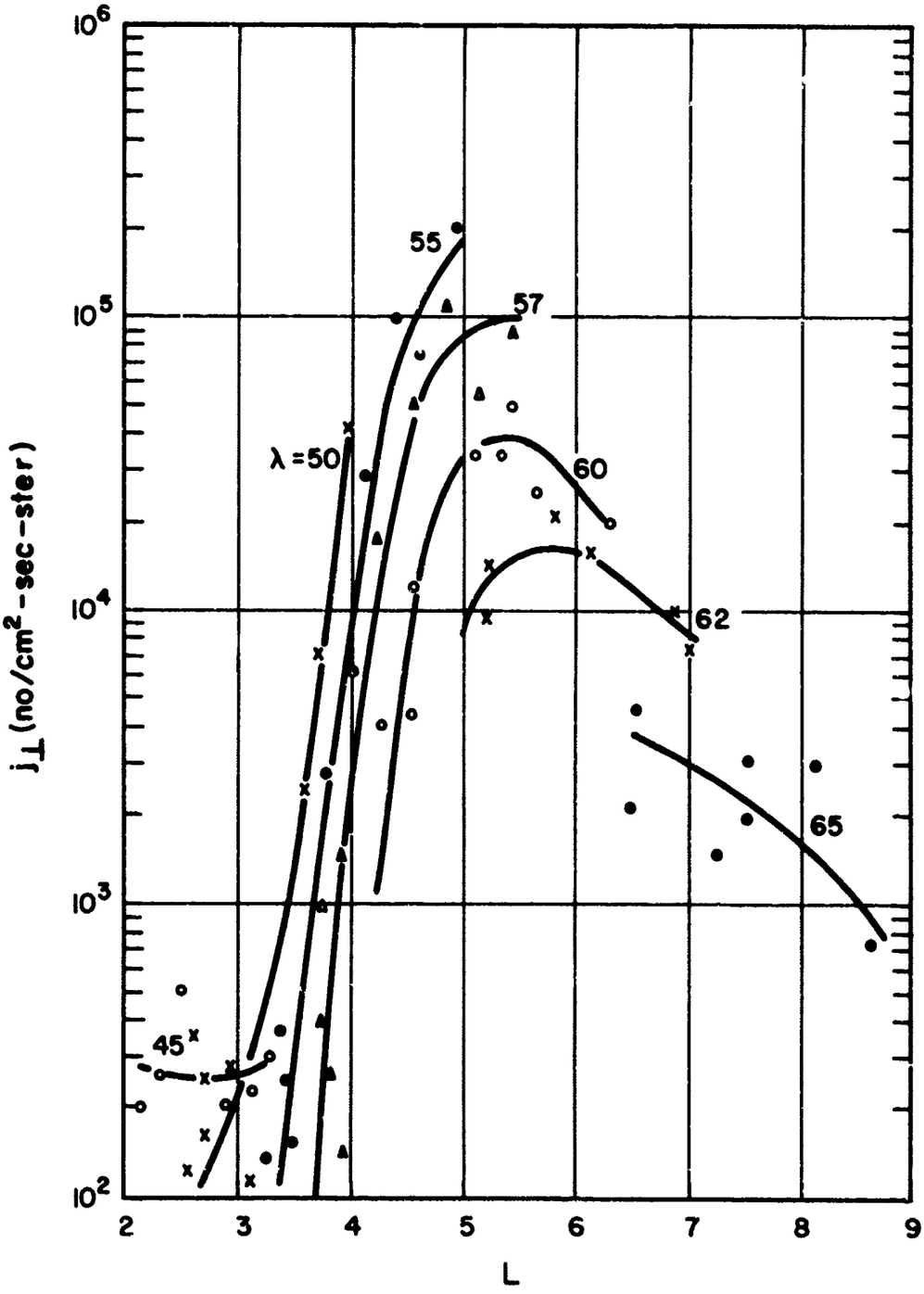

Fig. 18b Electrons > 1 Mev, Outer Belt (Unidirectional Intensities at 90°)

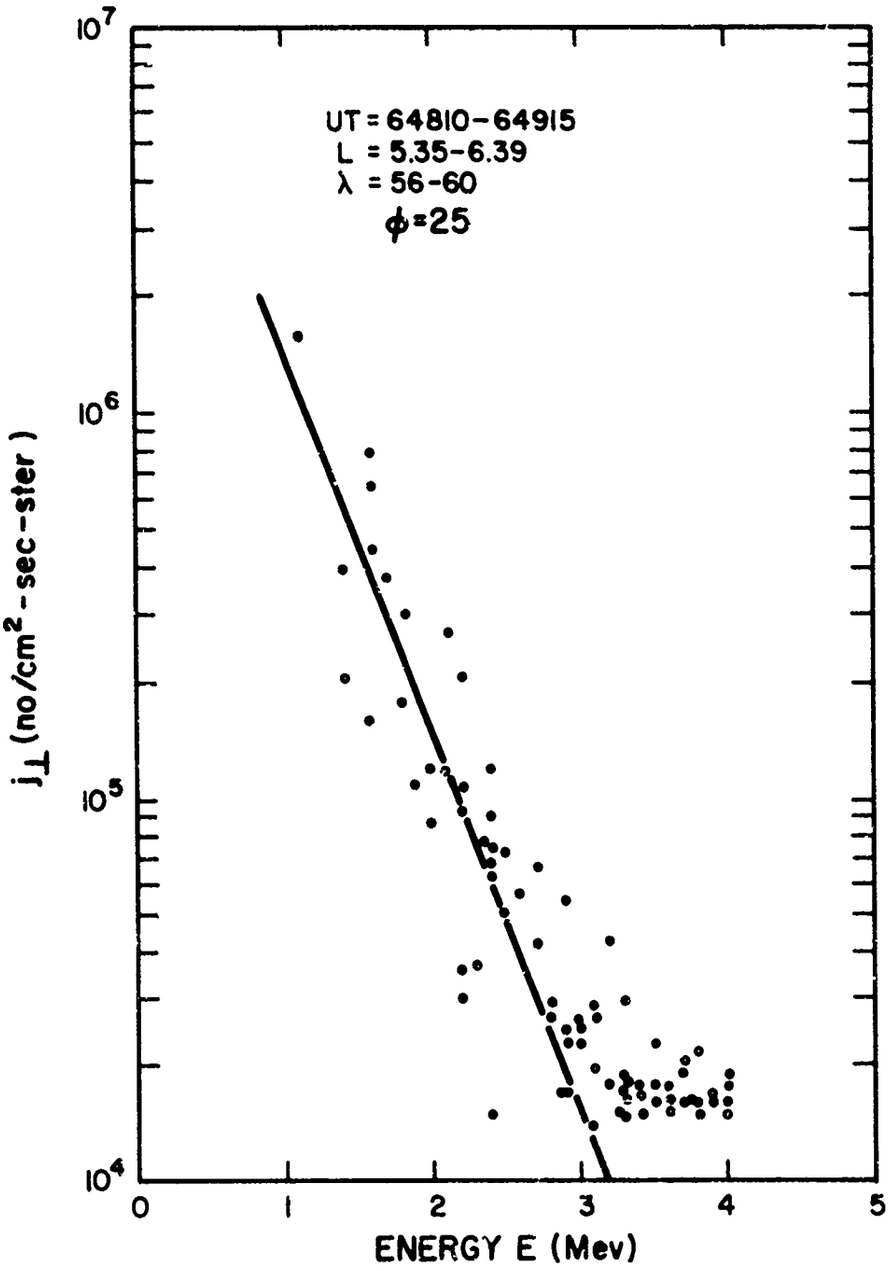

Fig. 19a Protons, 1 - 4 Mev, Outer Zone Energy Spectrum

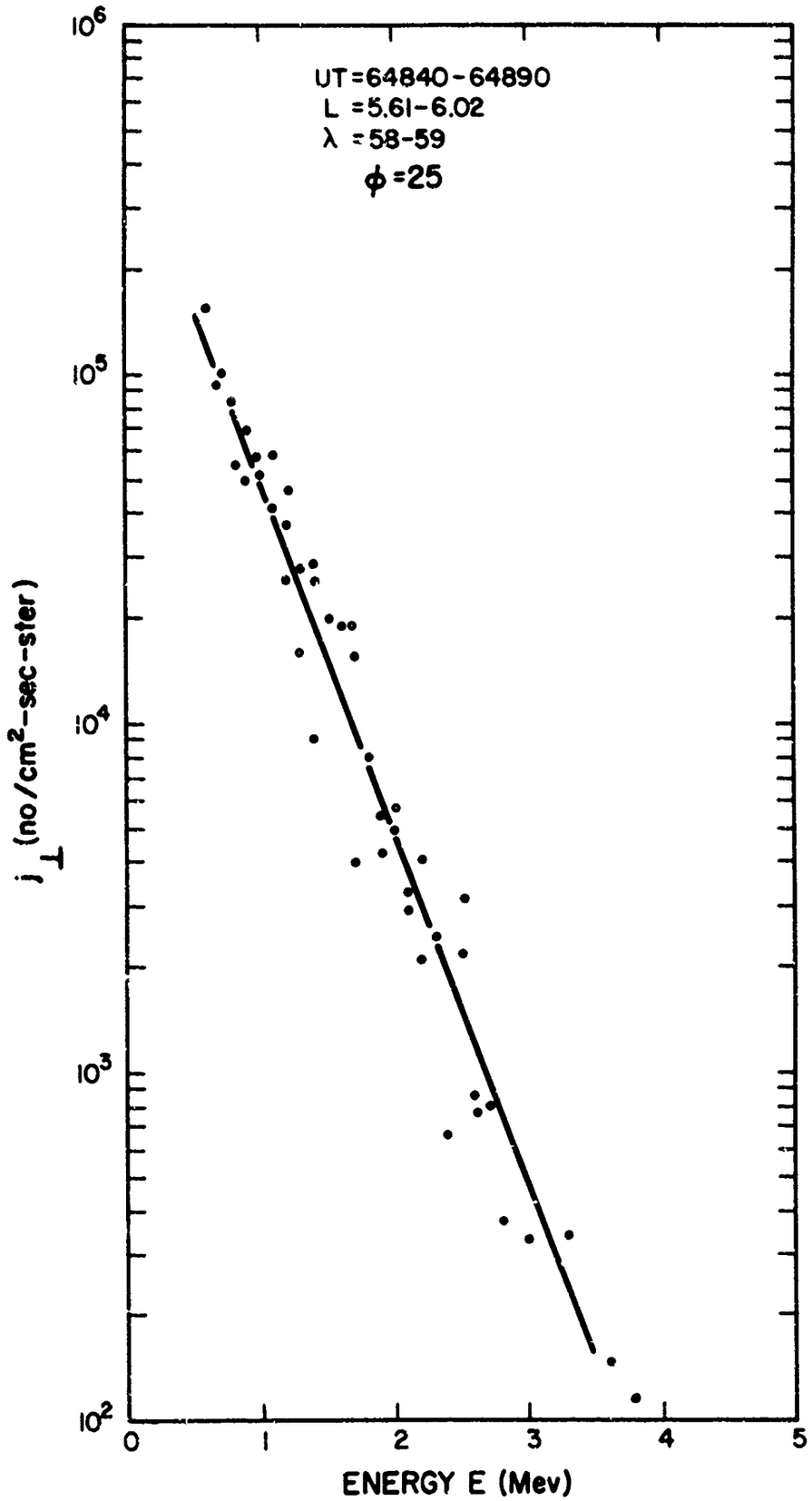

Fig. 19b Protons, 1 - 4 Mev, Outer Zone Energy Spectrum for Comparison

The anticoincidence circuit is triggered by pulses occurring in the CsI crystal. As calculated in the next section in connection with the high energy channel of the proton spectrometer, bremsstrahlung from electrons above 1 Mev hitting the shielding might have caused up to 5×10^6 pulses/sec in the CsI crystal in the heart of the inner belt. Since the anticoincidence circuit is normally effective for a period of the order of one microsecond after each pulse, and then is dead for a time of about 2 microseconds following, the bremsstrahlung pulse rate of 5×10^6/sec would result in totally suppressing the low energy channel counting for about 1/3 of the time while allowing it to be free from any anticoincidence requirement for the remaining 2/3 of the time. Thus, we conclude that the anticoincidence circuit was essentially incapacitated in the high intensity portion of the inner belt, merely introducing a factor of approximately 2/3 on the pulse rate counted in the plastic scintillator.

Another way in which electrons that penetrate the plastic scintillator may fail to trigger the anticoincidence circuit is by being backscattered out of the CsI crystal before they deposit in it a large enough amount of energy. From Brinkhoff (pp. 131 - 132) it can be estimated that for CsI ($z \approx 54$) about 60% of the impinging electrons around 700 kev are backscattered, and more than half of them have deposited less than 20% of their energy in the crystal. It is conceivable therefore that a substantial part of the electrons that penetrate the plastic scintillator may be backscattered by the high Z CsI crystal before depositing enough energy to trigger the anticoincidence circuit.

From the above discussion we conclude that in regions of high electron intensities in the inner and outer belt significant numbers of electrons may not have been rejected by the anticoincidence circuitry and may therefore have substantially contributed to the low energy proton spectrometer counting rates.

2.5 Proton Scintillation Spectrometer: High Energy Channel

The output intensities obtained from the high-energy channel throughout the observation period varied widely and continuously over its output range, signifying that the scaler (scale of 32) in this circuit recycled an indeterminant number of times. The observed exceptionally high counting rates could have been accidental coincidences between pulses in the CsI crystal and in the plastic scintillator. The geometrical factor ($A\Omega$) for particles which penetrate the shielding is about 50 cm^2 ster versus ($A\Omega$) $\approx 10^{-3} cm^2$ ster for particles which enter through the instrument aperture. The inch thick stainless steel shielding can be penetrated by protons above approximately 100 Mev (Evans p. 652). In the inner belt high energy proton intensities up to $10^2 - 10^3$ protons/cm^2 sec ster have been observed so that about 5×10^3 to 5×10^4 events/sec could have occurred within the CsI crystal from this source.

Bremsstrahlung from electrons stopped in the shielding could also lead to high accidental coincidence rates. All γ-rays of energy greater than about 1 Mev appreciably penetrate the shielding (~ 20 g/cm^2 of Fe) and are then (with a high probability) counted in the massive CsI crystal. (Evans pp. 713 - 717).

Due to the relatively steep electron spectra, most of the bremsstrahlung production will come from electrons whose energy is around 1 Mev. Since 1 Mev electrons in Fe convert about 3% of their energy in bremsstrahlung (Evans p. 610) and an appreciable part of the generated photons have energies close to the 1 Mev limit (Evans pp. 605 - 606) it is reasonable to estimate that about 10^{-2} of the intensity of 1 Mev electrons will cause events in the CsI crystal through bremsstrahlung. Since electron intensities in this energy range are about 10^3 to 10^7/cm^2sec ster, about 5×10^2 to 5×10^6 pulses/sec can be expected in the CsI crystal from bremsstrahlung.

However, since most of the bremstrahlung events will not deposit enough energy to be recorded by the 7.5 to 120 Mev pulse height analyzer circuits, the main contribution in the high energy channel will be the 5×10^3 to 5×10^4 pulses/sec generated in the CsI crystal at the heart of the inner belt by high energy penetrating protons. With a coincidence time resolution of the order of a few microseconds the CsI would be generating pulses about 20% of the time in the heart of the inner belt. The pulse rate in the plastic scintillator can be estimated from the readings of the low energy proton channel. Observed fluxes reach up to $10^8/cm^2$sec ster in the inner belt, with corresponding pulse rates of 10^5/sec in the plastic scintillator. We can expect, therefore, accidental coincidence rates up to about 2×10^4/sec, equivalent to high energy channel intensities of about $2 \times 10^7/cm^2$ sec ster. Clearly, therefore, in the high intensity inner belt regions accidental coincidences alone exceed the counting capacity of the instrument (0 to $4 \times 10^5/cm^2$sec ster). However in the low intensity portions of the orbits counting rates should be well within the scaler limits and scaler recycling should not occur. Since no such cases were observed it is possible that some additional factor, such as a malfunction in the counting circuit, may be responsible for the observed counting rate behaviors.

2.6 Geiger Counter

The Geiger counter output was extremely helpful in obtaining a concise picture of the satellite passes through the radiation belts, and as a guide for the analysis of the data from the other instruments. The counting rates obtained showed the same gross pattern and temporal variations as the 1 - 4 Mev electron data obtained from the scintillation spectrometer. For Geiger tube shielding generation by 4 Mev electrons and a geometrical factor $A\Omega \approx 1$ cm^{2}ster, quantitative agreement with inner belt electron

spectrometer data is fairly good. Geiger tube counting rates in the outer belt however appear higher (by factors of 2 to 10) than those expected from the scintillation spectrometer data. Inner belt high energy protons (McIlwain 1964) can account for less than one-tenth of the observed inner zone Geiger counting rates, which therefore appear to be due predominantly to penetrating electrons.

During the latter half of the 50-day observation period a gradual increase in Geiger tube counting rates by factors of 2 to 5 was observed without any simultaneous marked change in electron spectrometer intensity levels or energy spectra. A possible cause of this gradual increase might be deterioration of the quenching mechanism in the Geiger tube.

BLANK PAGE

3.0 SUMMARY OF DATA

Hitch-hiker I data on trapped particles in the radiation belts provide information on perpendicular intensities, pitch angle distributions, and energy spectra.

Perpendicular intensity contour maps can yield complete information on pitch angle distributions and omnidirectional intensities. Thus, on the basis of Liouville's theorem the unidirectional intensity $j(\theta, B, L)$ at a pitch angle θ at a position (B, L) is equal to the perpendicular intensity at the point on the magnetic shell L where the electrons with pitch angle θ mirror, i.e.,

$$j(\theta, B, L) = j(90^{\circ}, \frac{B}{\sin^2\theta}, L) \equiv j_{\perp}(\frac{B}{\sin^2\theta}, L) \qquad (1)$$

Furthermore the omnidirectional intensity $J(B, L)$ at any point can be calculated by integrating the unidirectional intensity j over all pitch angles:

$$J(B, L) = 2\pi \int_0^{\pi} j(\theta, B, L) \sin\theta \, d\theta \qquad (2)$$

Maps of the perpendicular intensities of electrons above 1 Mev in the inner belt as measured throughout the observation period are given in Figures 1 and 3 of Appendix A. These data are plotted also on a (B, L) iso-intensity contour map in Figure 20a for convenience in applying Equation (1). A similar (B, L) iso-intensity contour is given in Figure 20b for the outer belt as seen on 3 July 1963, a day when outer belt intensities were highest.

Figure 21a and 21b give inner and outer belt (B, L) iso-intensity contour maps of the proton spectrometer perpendicular intensities above 2 Mev. replotted from the data of Figures 17a and 18a.

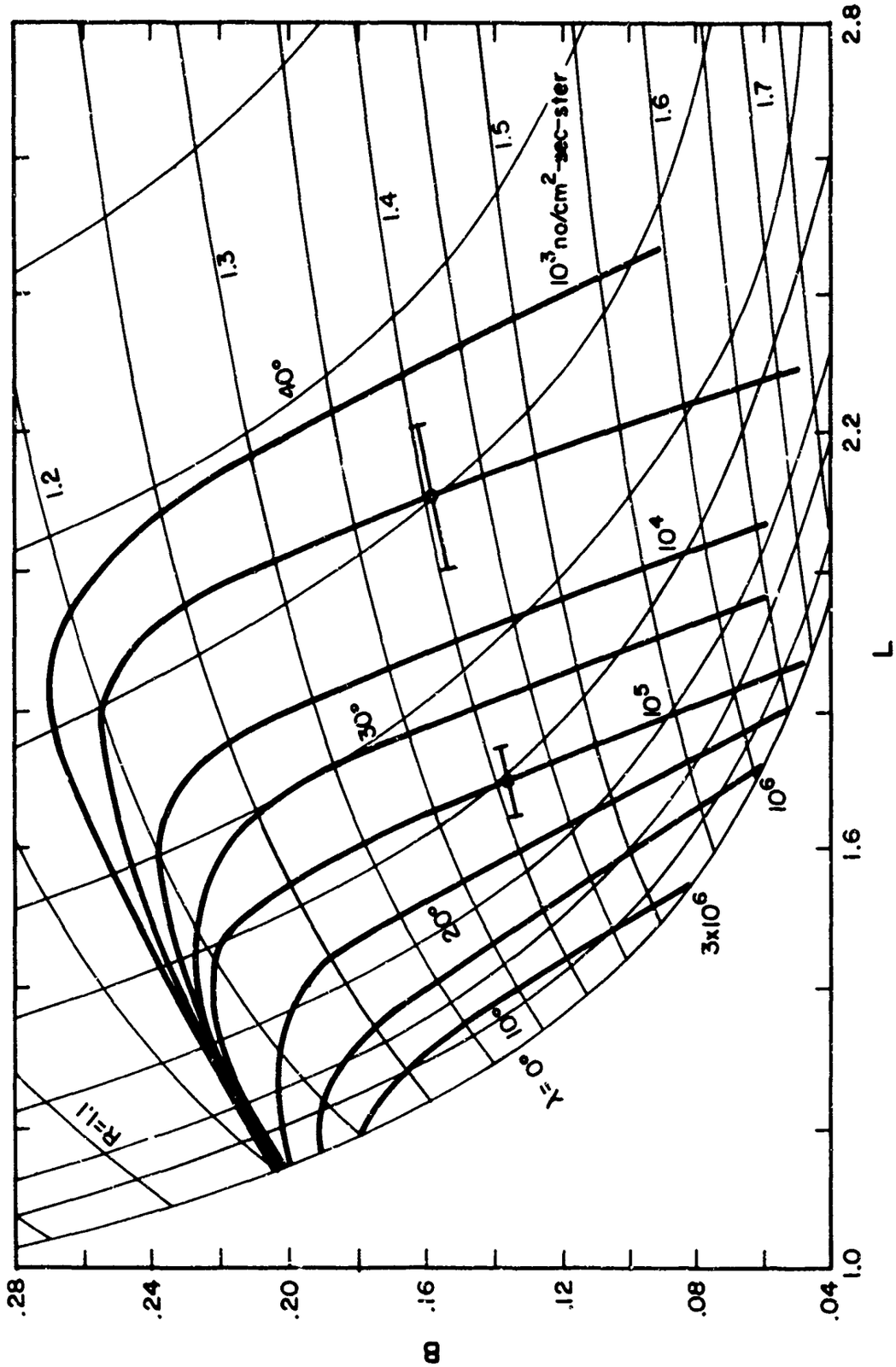

Fig. 20a Iso-Intensity (j_1) Contours of Electrons > 1 Mev (Typical)

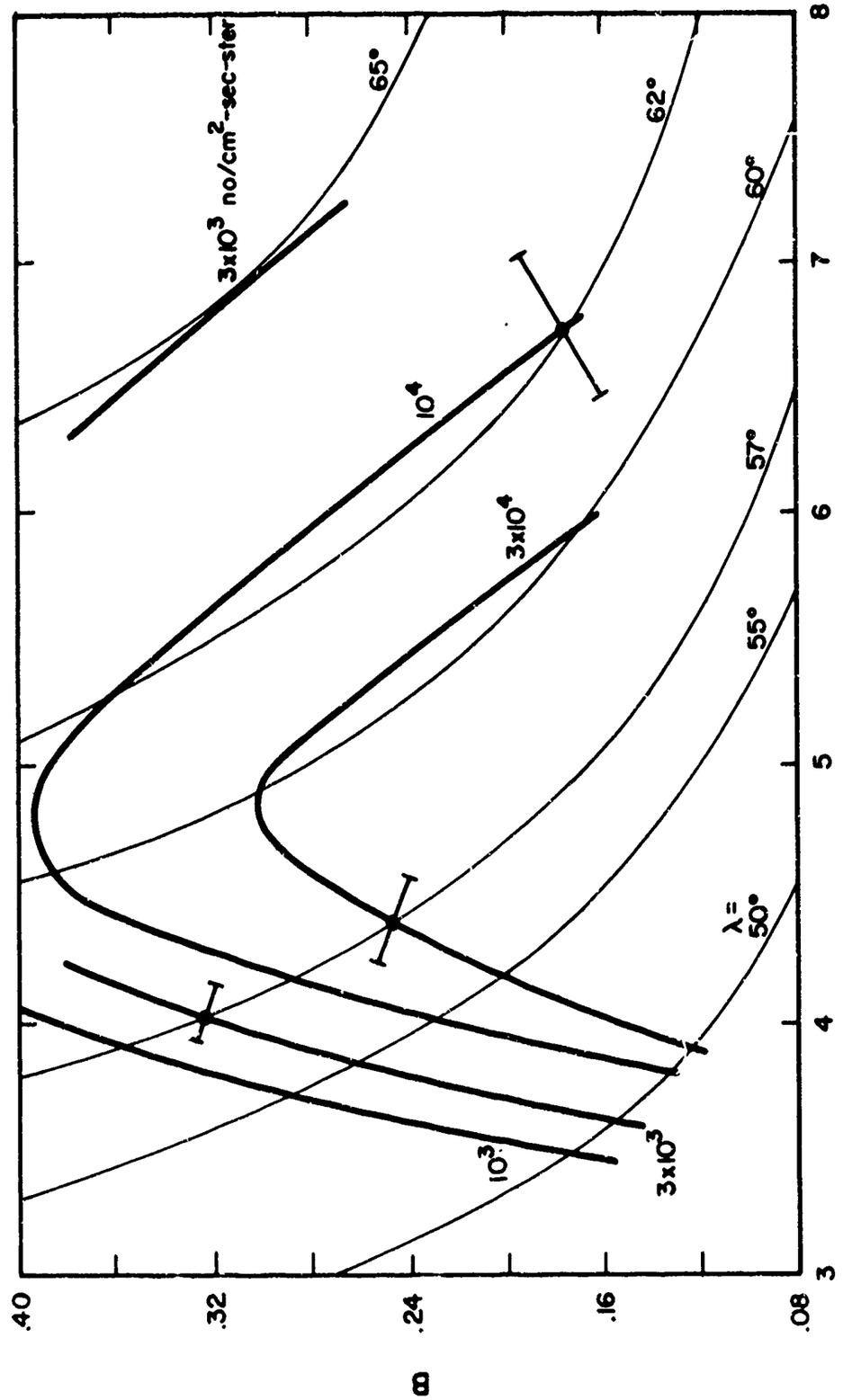

Fig. 20b Iso-Intensity (j_1) Contours of Electrons > 1 Mev Maximum, ϕ 25

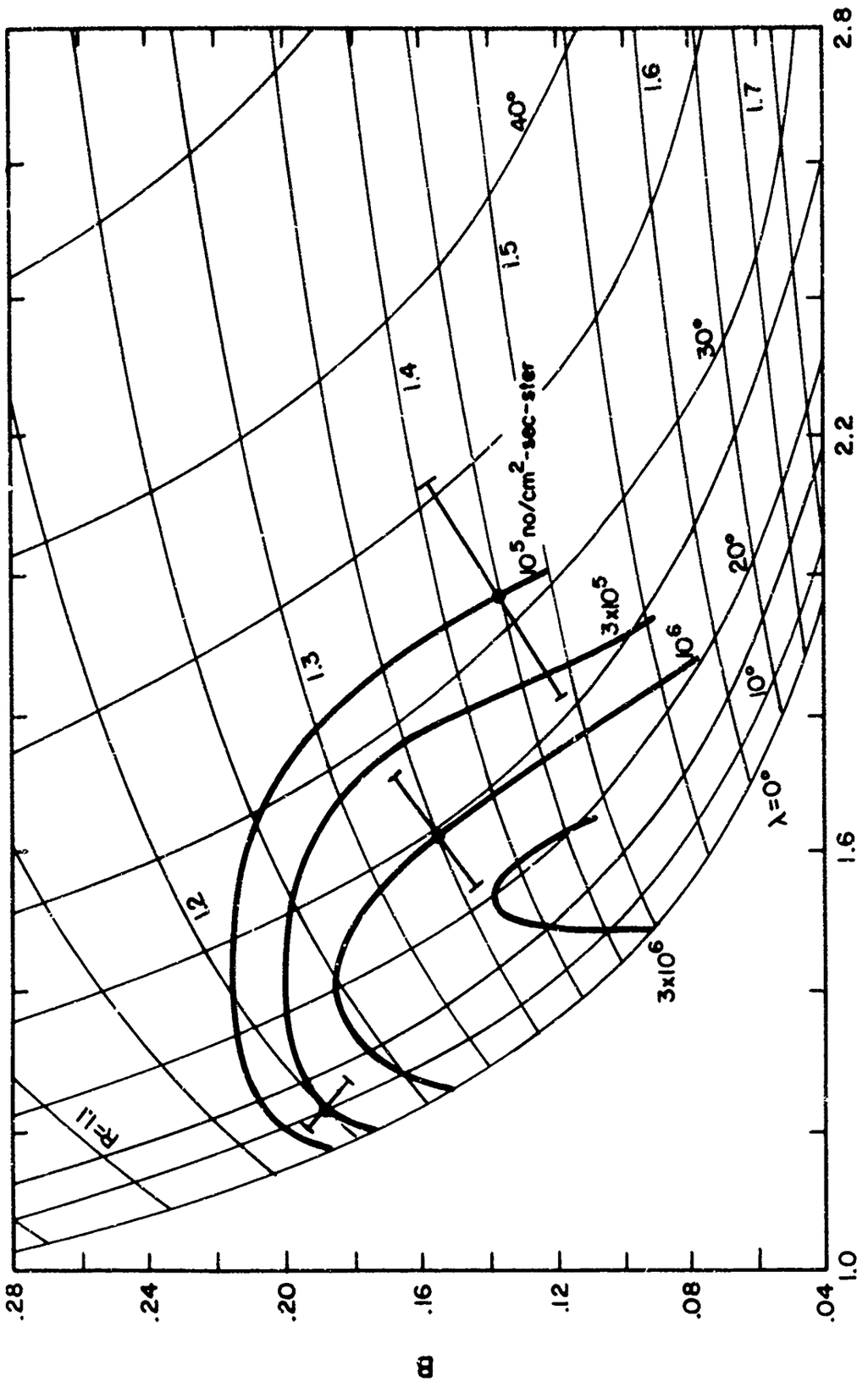

Fig. 21a Iso-Intensity ($J_\perp$) Contours of protons >2 Mev Typical

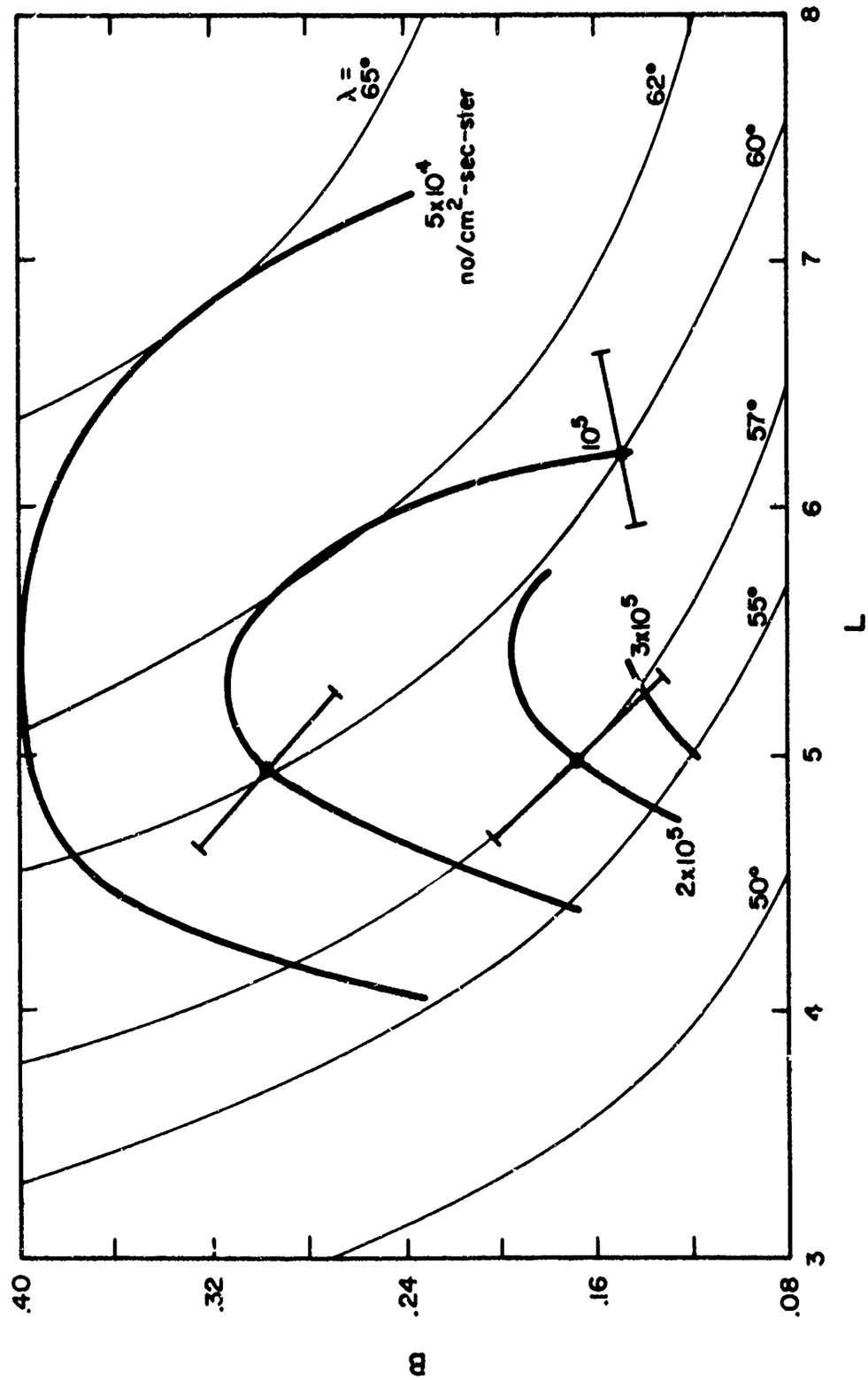

Fig. 21b Iso-Intensity ($J_\perp$) Contours of Protons > 2 Mev Maximum, ϕ 25

Measured pitch angle distributions given in Appendices A, B, C, and D are consistent within the accuracy of measurement with those derived from the intensity contours using Equation (1). (See these appendices for examples.)

Spectra obtained from the scintillation spectrometers could always be fitted (within statistical limitations) by an exponential energy dependence $\exp(-E/E_o)$. Tables I and II summarize the ranges of spectral slopes E_o obtained from the spectrometers in the inner and outer belts. The data of these tables, together with the data of Figures 20 and 21, thus allow determination of energy-angle distributions for any region of the magnetosphere covered by the satellite.

Measured electron spectra between 0.7 Mev and 4 Mev in the inner belt had slopes E_o close to about 1 Mev (Table I) not much different from the fissionlike spectra observed after the Starfish explosion. In inner belt regions where energy spectra could not be obtained from the count rate channel of the electron spectrometer, the output of the rate of energy deposition channel of the instrument and that of the Geiger counter were consistent with exponential spectral slopes E_o around 1 Mev. Electron spectra obtained in the outer belt were considerably steeper, with exponential slopes E_o around 0.4 Mev (Table I). In the slot region ($L \approx 2$ to 3) the electron spectrometer yielded extremely flat spectra between 0.7 and 4 Mev but this was probably due to a significant contribution from protons above 5 Mev which penetrated the front shield through the aperture proper of the instrument.

Spectra obtained from the proton spectrometer (Table II) have exponential slopes E_o in the vicinity of 0.4 Mev.

TABLE I: ELECTRON ENERGY SPECTRA (0.7 to 4 Mev)

	L	λ	E_o (Mev)
INNER	1.2 - 1.3	10 - 16°	0.8 - 1.0
BELT	1.3 - 1.5	20 - 27°	~0.9
	1.5 - 1.6	27 - 30°	0.7 - 0.9
OUTER	3.5 - 4.0	47 - 56°	0.3 - 0.6
BELT	4.0 - 5.0	50 - 62°	0.3 - 0.5
	5.0 - 6.5	57 - 65°	0.3 - 0.5

TABLE II: PROTON ENERGY SPECTRA (1.5 to 4 Mev)

	L	λ	E_o
INNER BELT	1.2 - 1.7	5 - 25°	0.30 - 0.45
OUTER BELT	4.5 - 5.3	55 - 59°	0.4 - 0.5

4. REFERENCES

Fillius, R. W.; C. E. McIlwain, Phys. Rev. Letters 12, 609 (1964).

Krimigis, S. M.; J. A. Van Allen, Transactions AGU 46, 140 (1965).

Selinger, H. H., Phys. Rev. 100, 1029 (1955).

Brukhoff, R. D., in "Encyclopedia of Physics, Corpuscules and Radiation in Matter II", Vol. 34, p. 131-132 (1958).

Evans, R. D., "The Atomic Nucleus" McGraw-Hill Publishing Co., Inc., (1965).

McIlwain, C. E.; R. W. Fillius; J. Valerio; A. Dave; NASA TND-2516 (1964).

This is a preprint of a paper to be presented to the Advanced Study Institute at the Christian Michelson Institute in Bergen, Norway, on 16 August - 3 September 1965.

ASE-992

Appendix A

A STUDY OF ENERGETIC ELECTRONS IN THE RADIATION BELTS WITH THE HITCH-HIKER I*

G. C. Theodoridis and F. R. Paolini

American Science and Engineering, Inc.
Cambridge, Massachusetts

and

L. Katz and D. Smart

Air Force Cambridge Research Laboratories
Bedford, Massachusetts

*Research funded wholly by the Air Force In-house Laboratory Independent Research Fund.

A STUDY OF ENERGETIC ELECTRONS IN THE RADIATION BELTS WITH HITCH-HIKER I*

G. C. Theodoridis and F. R. Paolini

American Science and Engineering, Inc.
Cambridge, Massachusetts

and

L. Katz and D. Smart

Air Force Cambridge Research Laboratories
Bedford, Massachusetts

ABSTRACT

A survey of relativistic electrons in the Van Allen radiation zones was performed in July and August 1963 with instruments on board the polar orbiting Air Force subsatellite Hitch-hiker I. Unidirectional intensity maps, energy spectra and pitch angle distributions are presented for electrons between 0.7 and 4 Mev. Peak inner belt intensities for electrons above 1 Mev were about 5×10^6 electrons/cm^2 sec ster and the energy dependence was exponential with slope $0.7 \leq E_o \leq 1.2$ Mev. Outer belt intensities fluctuated substantially with severe depletions at times of magnetic and solar activity, and subsequent recoveries in periods of a few to several days. Maximum observed intensities of electrons above 1 Mev at the horns of the outer belt were about 10^5 electrons/cm^2 sec ster. Loss of outer belt electrons through dumping at high latitudes in the Anomaly was detected at rates up to 2×10^{11} ergs/sec. Outer belt spectra between 0.7 and 4 Mev were approximately exponential with slope $E_o = 0.4 \pm 0.1$ Mev. No drastic spectral changes were seen during the observed time variations. Directly measured pitch angle distributions throughout the radiation belts were consistent with the perpendicular intensity profiles. Shifts in mirror point distribution during time variations in the outer belt did not change appreciably the measured pitch angle distributions.

---

*Research funded wholly by the Air Force In-house Laboratory Independent Research Fund.

INTRODUCTION

The Air Force Sub-satellite Hitch-hiker I (1963-25B) was launched on 1 July 1963 into a polar orbit of 82.14° inclination with perigee at 326 km and apogee at 4150 km. The angle between the ascending node of the orbit and the Earth-Sun line was initially about 63°, and regressed at a rate of approximately -1 1/2°/day. The orbital period was 133 minutes. The sub-satellite was spin stabilized at 68 rpm with its axis of rotation at an angle of about 25° to the axis of the Earth. Data presented in this paper were derived from orbits covering a period of about 50 days.

INSTRUMENTATION

Electrons in the Mev energy range were measured by a scintillation spectrometer. An Anton 302 Geiger counter was also included in the instrument package and provided additional reference information on high energy electrons and protons.

The sensor of the scintillation spectrometer was a 2.5 g/cm^2 Pilot "B" plastic scintillator, equivalent to the range of a 5.0 Mev electron or a 55 Mev proton. The plastic scintillator was shielded on the sides and back with stainless steel against electrons of energy less than about 10 Mev and protons of energy less than about 65 Mev. The entrance aperture was shielded with 50 mg/cm^2 of Aluminum, corresponding to the range of a 200 kev electron or a 5 Mev proton. The amount of contamination of the measured electron intensities by protons over 5 Mev is well within the statistical uncertainty of the data. The entrance aperture was calculated to be a cone of about 25° FWHM and the total geometrical factor was $A\Omega \approx 0.12$ cm^2 ster.

This instrument had a "count rate channel" and a "rate of energy deposition channel". The count rate channel yielded integral spectral information for electrons between 0.7 Mev and 4 Mev and had an absolute dynamic range of 8 x 10^1 to 10^6 particles/cm^2 sec ster. The rate of energy

deposition channel measured the power deposited in the scintillator by electrons of energy greater than about 0.2 Mev. It could accommodate much higher intensities than the count rate channel, having a dynamic range of 8×10^2 to 8×10^8 Mev/cm^2 sec ster.

Spectral information was derived by pulse height analysis. The scintillation pulses were fed to one input of a comparator, the other input of which was fed by a linear sweep of about 16 sec period. The comparator output signal repetition rate thus corresponded to intensities of electrons of energy greater than some threshold energy E linearly proportional to the sweep voltage. The energy resolution of this instrument varied from $\pm$ 15% at 0.7 Mev to about $\pm$ 6% at 3 Mev. A Van de Graaff accelerator was used in calibration.

The spectrometer output was sampled 6 times/sec for the count rate channel and 2 times/sec for the rate of energy deposition channel, while the satellite spin frequency was about 1.1 rotation/sec. Thus pitch angle distributions with fair angular resolution could also be obtained. Two sets of 3 axis flux gate magnetometers of different sensitivities were used for aspect determination.

The rate of energy deposition channel was used to derive electron intensity levels and pitch angle distributions near the heart of the inner belt where the count rate channel saturated. For an exponential integral spectrum $j(E) = j(0) \exp(-E/E_o)$ the ratio of the rate of energy deposition $I_E \left(\frac{\text{Mev}}{\text{cm}^2\text{sec ster}} \right)$ to the intensity $j(1\ \text{Mev})$ is given in Table 1 for various values of E_o. For $E_o \geq 0.5$ Mev the rate of energy deposition is roughly proportional to the flux of electrons above 1 Mev and we have approximately:

$$\frac{I_E \left(\frac{\text{Mev}}{\text{cm}^2\text{sec ster}} \right)}{j(1\ \text{Mev}) \left(\frac{\text{electrons}}{\text{cm}^2\text{sec ster}} \right)} \approx 3 \frac{\text{Mev}}{\text{electron}} \qquad (1)$$

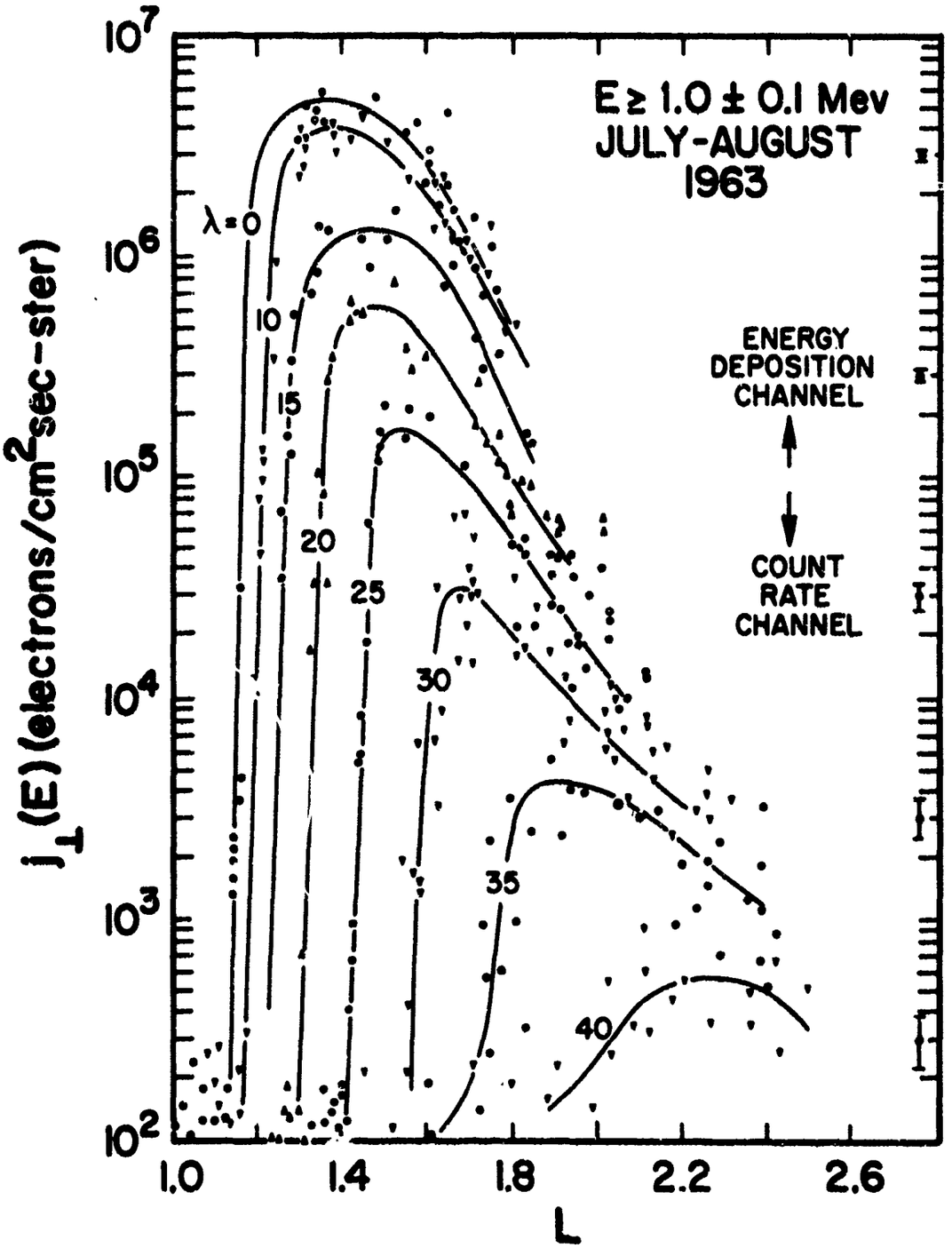

Fig. A1. Electron Intensities in the Inner Belt at Various λ.

TABLE 1

FACTORS FOR CONVERTING RATE OF ENERGY DEPOSITION INTO INTENSITY

E_o (Mev)	$\frac{L_E \left(\frac{\text{Mev}}{\text{cm}^2 \text{ sec ster}}\right)}{j(1 \text{ Mev}) (\text{el/cm}^2 \text{sec ster})}$
0.2	23
0.3	7.2
0.4	4.3
0.5	3.4
0.7	2.9
1.0	2.7
1.5	2.3
2.0	3.1
3.0	3.4
5.0	3.9
10.0	4.4
20.0	4.6

RESULTS

Unidirectional Intensities

Figure 1 presents unidirectional intensities of electrons with energy $E \geq 1.0 \pm 0.1$ Mev and pitch angles $90^{\circ} \pm 10^{\circ}$ in the inner belt. Data obtained during the whole observation period are presented in curves of intensity vs. L at a constant $\frac{B}{B_o}$ or, equivalently, at a constant magnetic latitude λ, defined by

$$\frac{B}{B_o} = \frac{(1 + 3 \sin^2\lambda)^{1/2}}{\cos^6\lambda}$$

Above 10^5 el/cm^2 sec ster the count rate channel approaches saturation and the intensities given in Figure 1 have been derived from the energy deposition channel on the basis of Equation 1. This relation holds provided the spectrum is not too steep ($E_o \geq 0.5$ Mev for an exp $(-E/E_o)$ spectrum) which is the case in the inner belt. (See Figure 8 for example). In regions with intensities within the range of both spectrometer channels, agreement between the electron intensities measured by the count rate channel and those derived from the rate of energy deposition is well within the statistical scatter of the data.

In the outer belt, time variations of one to two orders of magnitude occurred during the observation period. Figure 2a presents unidirectional intensities of electrons with energy $E \geq 1.0 \pm 0.1$ Mev and pitch angles $90^{\circ} \pm 20^{\circ}$ as mapped during three orbits on 3 July 1963, a day when intensities were high, and Figure 2b is a similar plot from 2 orbits on 5 and 6 July 1963, while intensities were low as a result of a solar flare on 4 July 1963. The effects of this flare are further discussed later on.

On the basis of the intensity curves of Figures 1 and 2a, the iso-intensity contours of Figure 3 have been constructed in the polar geomagnetic coordinates λ and $R = L\cos^2\lambda$. (Figure 3a), and in the coordinates B and L (Figure 3b). The dotted line included in Figure 3a is the

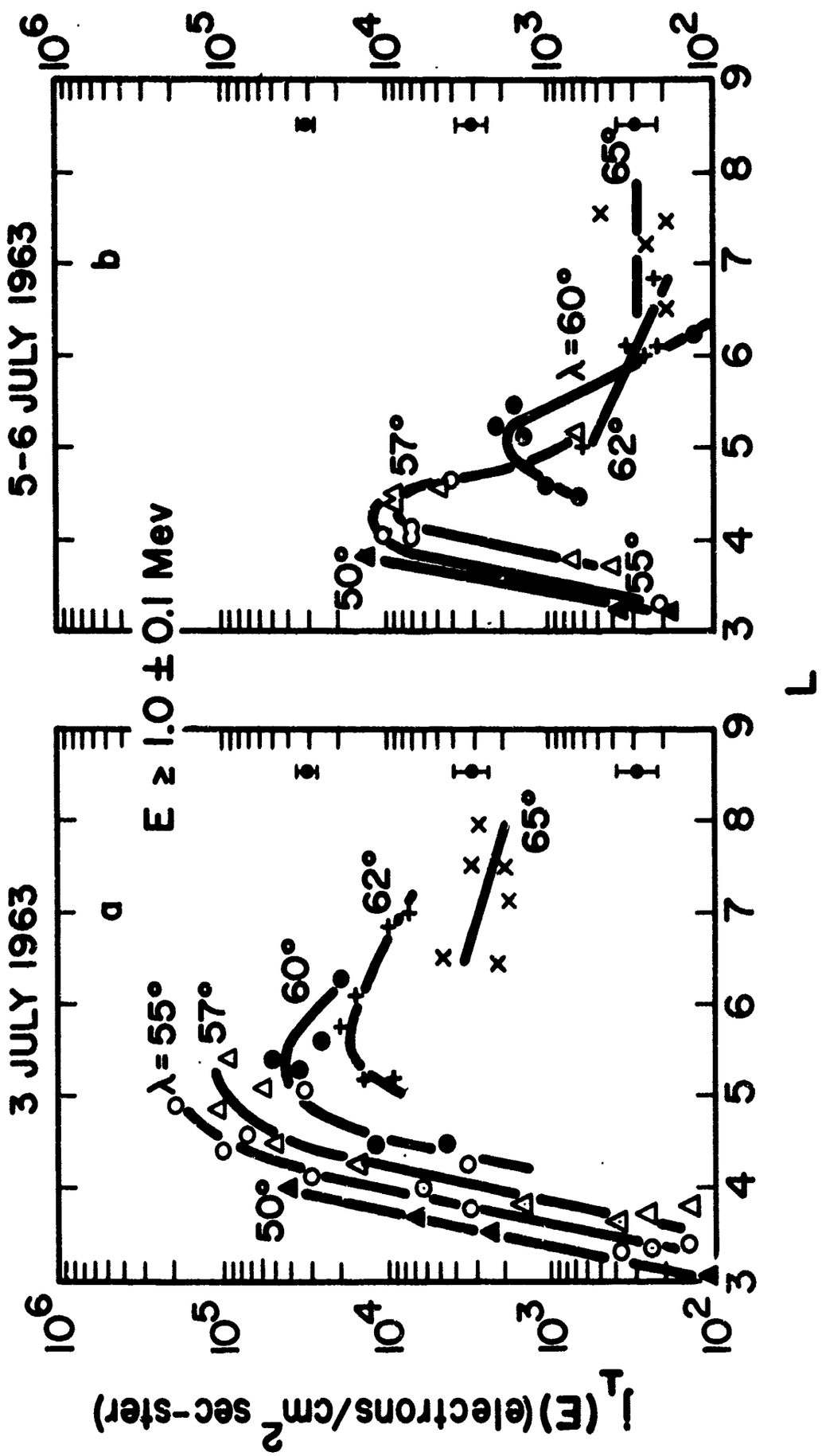

Fig. A2 Electron Intensities in the Outer Belt at Various λ.

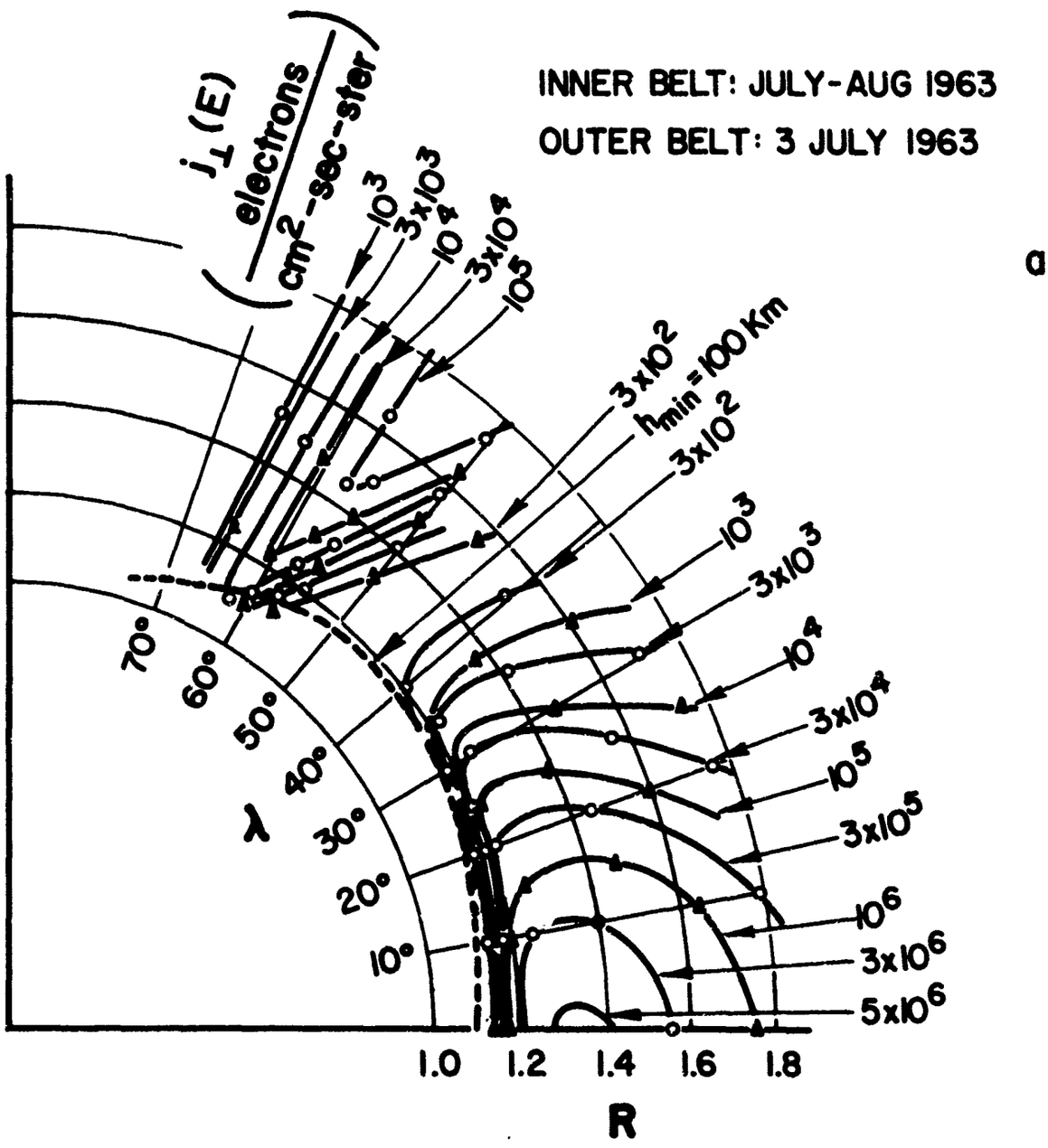

Fig. A3 Electron Iso-Intensity Contours ($E \geq 1.0 \pm 0.1$ Mev).

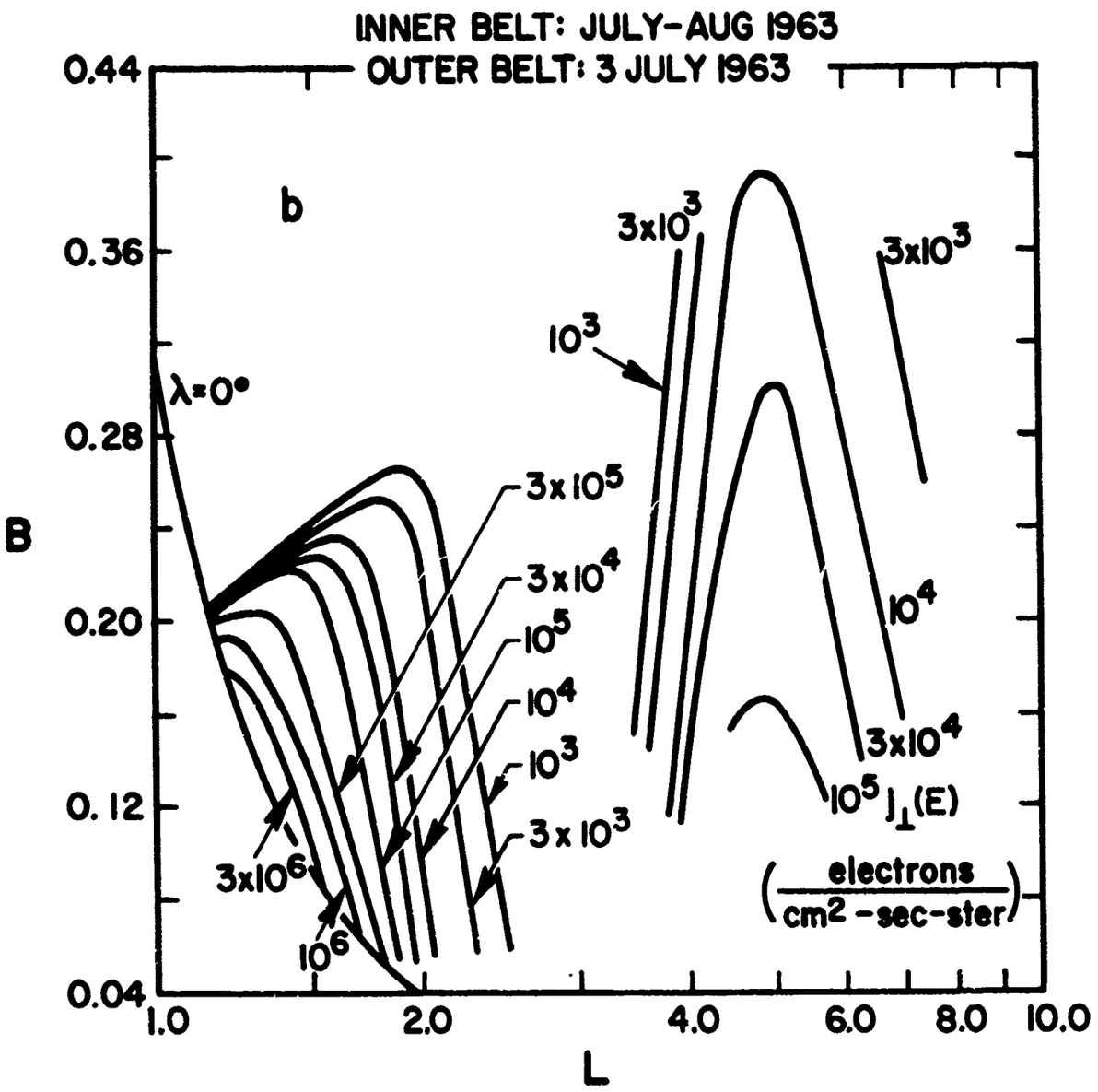

Fig. A3 Electron Iso-Intensity Contours ($E \geq 1.0 \pm 0.1$ Mev).

trace of the (R, λ) surface which has a minimum altitude of 100 km. This line has been constructed as the locus of the maximum R's corresponding to given λ's and 100 km altitude. Magnetic field calculations throughout this paper used the Jensen and Cain 48-term expansion coefficients.

For $\lambda \approx 20^{\circ} - 40^{\circ}$ ($L \approx 1.3 - 2.0$) the isointensity contour of Figure 3a near the lowest limit of sensitivity of our instrument closely approaches the 100 km minimum altitude surface while for lower magnetic latitudes the intensity cutoff corresponds to higher altitudes. In the outer belt region for $\lambda \approx 55^{\circ}$ to 62° significant electron fluxes reach beyond the 100 km minimum altitude surface being therefore scattered in the atmosphere. This point will be discussed in some detail later on.

Pitch Angle Distributions

Figure 4 shows pitch angle distributions obtained at various points throughout the inner belt. Curves 4a, b, c and d give fluxes of electrons above 1.0 ± 0.1 Mev from the count rate channel while curves 4e, f, g and h give rate of energy deposition. For the latter curves the equivalent intensity of electrons above 1 Mev is given also, computed on the basis of Equation 1. The accuracy of the aspect determination ranges from a few degrees around 90° pitch angle to about ten degrees at 0° and 180°, thus adding little to the pitch angle uncertainty due to the 25° field of view of the instrument. The dotted curves presented with the measured pitch angle distributions in Figure 4 indicate the distributions expected on the basis of the 90° intensities of Figures 1 and 3. Besides some apparent broadening of the measured distributions to be expected because of the wide aperture of the instrument, a considerable background intensity within the loss cone is evident in each case and most clearly in Figures 4a and 4e. This background is very likely due to electrons of energy above 10 Mev and/or protons above 65 Mev which penetrate the shielding around the scintillator. Since the geometrical factor for such penetration is approximately $4.5\ cm^2 \times 2\pi$ ster $\approx 28\ cm^2$ ster versus $A\Omega \approx 0.12\ cm^2$ ster for the entrance aperture of the

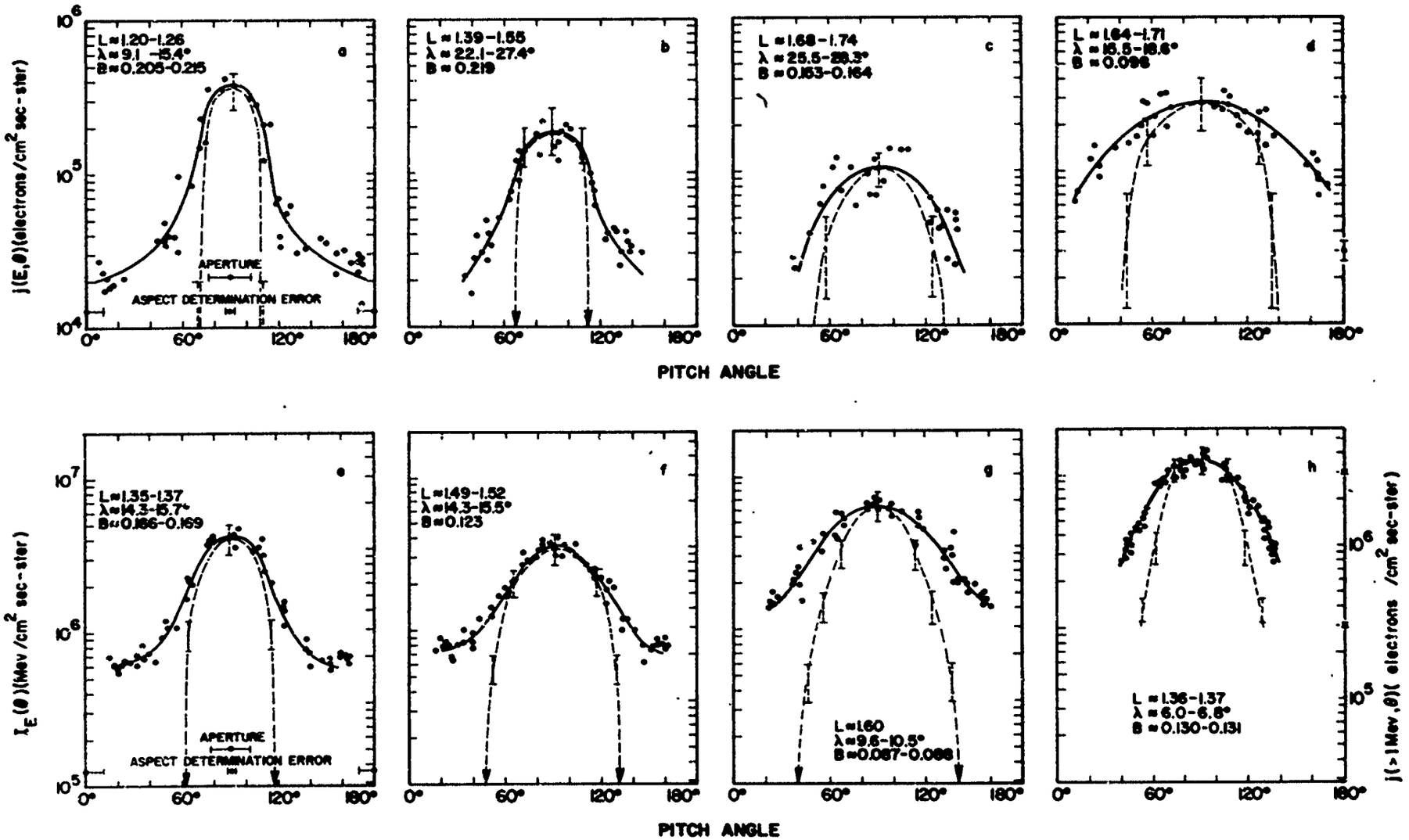

Fig. A4 Electron Pitch Angle Distributions in the Inner Belt ($E \geq 1.0 \pm 0.1$ Mev).

instrument, the background can be the result of a 250 times lower average intensity of penetrating particles. Observed backgrounds range from 10^4 to 3 x $10^5/cm^2$ sec ster so that penetrating particles must have intensities of about 50 to $1000/cm^2$ sec ster. High energy protons are present in the inner belt in comparable intensities (e.g., McIlwain 1963). Furthermore, extrapolation of observed electron spectra suggests presence of electrons above 10 Mev in comparable intensities as well.

Figure 5 gives pitch angle distributions for various levels of the threshold energy at the same point in space. The shape of the distribution is similar for all energy levels while the background within the loss cone shows little energy dependence, as expected if it is indeed due to high energy penetrating particles.

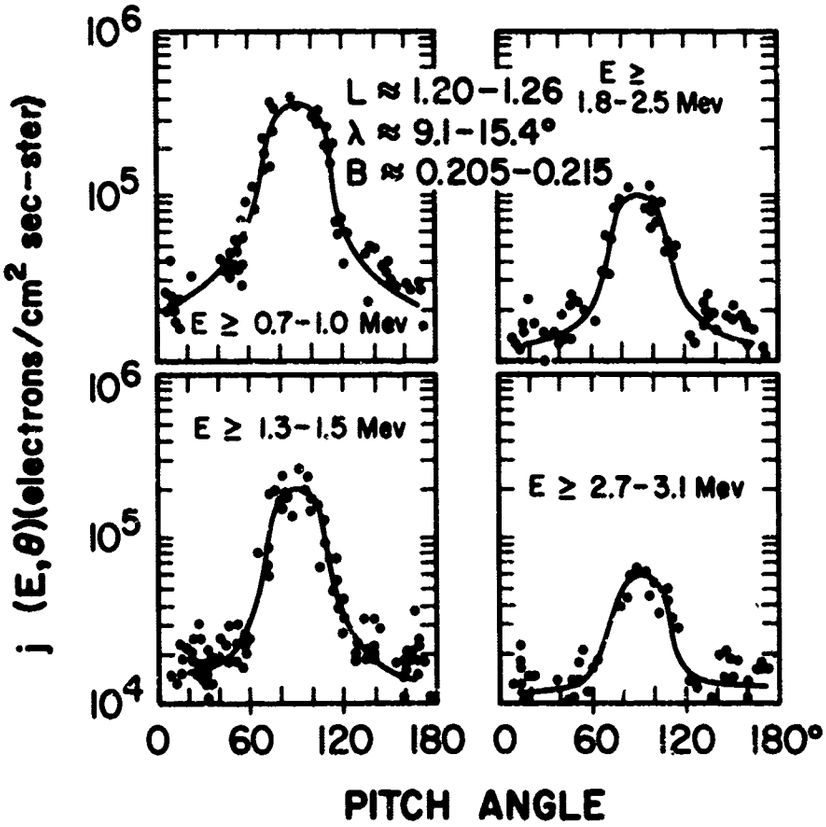

Fig. A5 Electron Pitch Angle Distributions at Various Threshold Energies.

Some equatorial pitch angle distributions derived from the 90° intensity contours of Figures 1 and 3 are given in Figure 6. Directly measured pitch angle distributions near the magnetic equator covered only a narrow range of pitch angle since the orientation of the spin axis of the satellite was almost parallel to B in these regions.

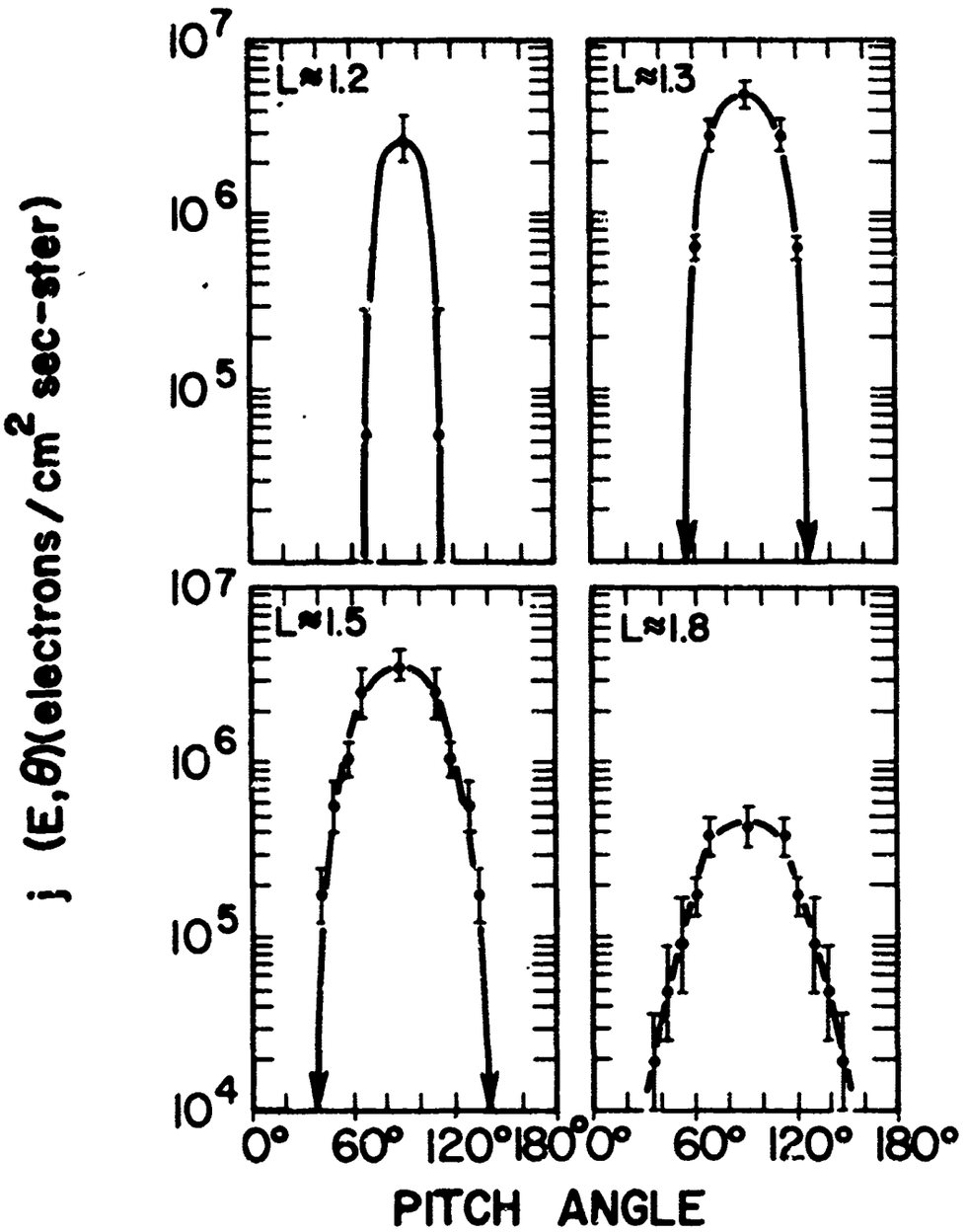

Fig. A6 Equatorial Pitch Angle Distributions Derived from Electron Intensity Contours at Various L ($E \geq 1.0 \pm 0.1$ Mev)

Figure 7 shows typical pitch angle distributions obtained in the horns of the outer belt. Some distributions appear broader than expected on the basis of the perpendicular intensities along the magnetic shell (dotted lines). The apparent broadening is consistent with the 25° FWHM field of view of the instrument and the uncertainty in aspect determination.

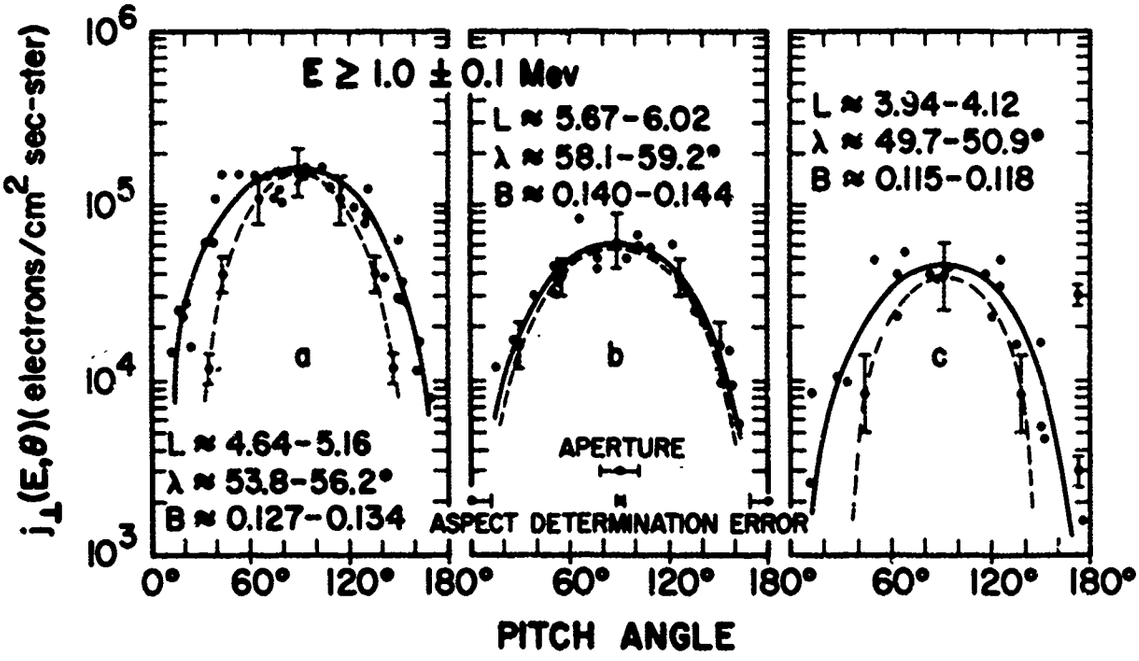

Fig. A7 Electron Pitch Angle Distributions in the Outer Belt.

Energy Spectra

In the inner belt, the shape of the measured spectra was usually distorted due to the contamination by energetic particles which penetrated the shielding around the scintillator. In regions where the loss cone was large, as for example in the case shown in Figure 5, it is possible to identify the portion of the counts that comes through the instrument aperture, by the fact that it displays sharp angular dependence. In order to correct for the omnidirectional background due to the penetrating particles, the unidirectional intensity within the loss cone (j_o (E)) was subtracted from the unidirectional intensity at 90° ($j_\perp$ (E)). Since a large loss cone is necessary to apply this correction accurately best spectra were derived

in low altitude regions of the inner belt. Some corrected spectra are given in Figure 8. The measured inner belt spectra have approximately an exponential energy dependence exp $(-E/E_o)$ with E_o between 0.7 and 1.2 Mev.

At higher altitudes in the inner belt some spectral information can also be obtained by comparing the intensities of electrons above 1 Mev derived from the electron spectrometer, with the intensities of electrons above approximately 4 Mev, derived from the Geiger counter. Assuming an exponential spectrum, values of E_o obtained in this manner are found to be in the same range with those measured with the electron spectrometer at lower altitudes in the inner belt.

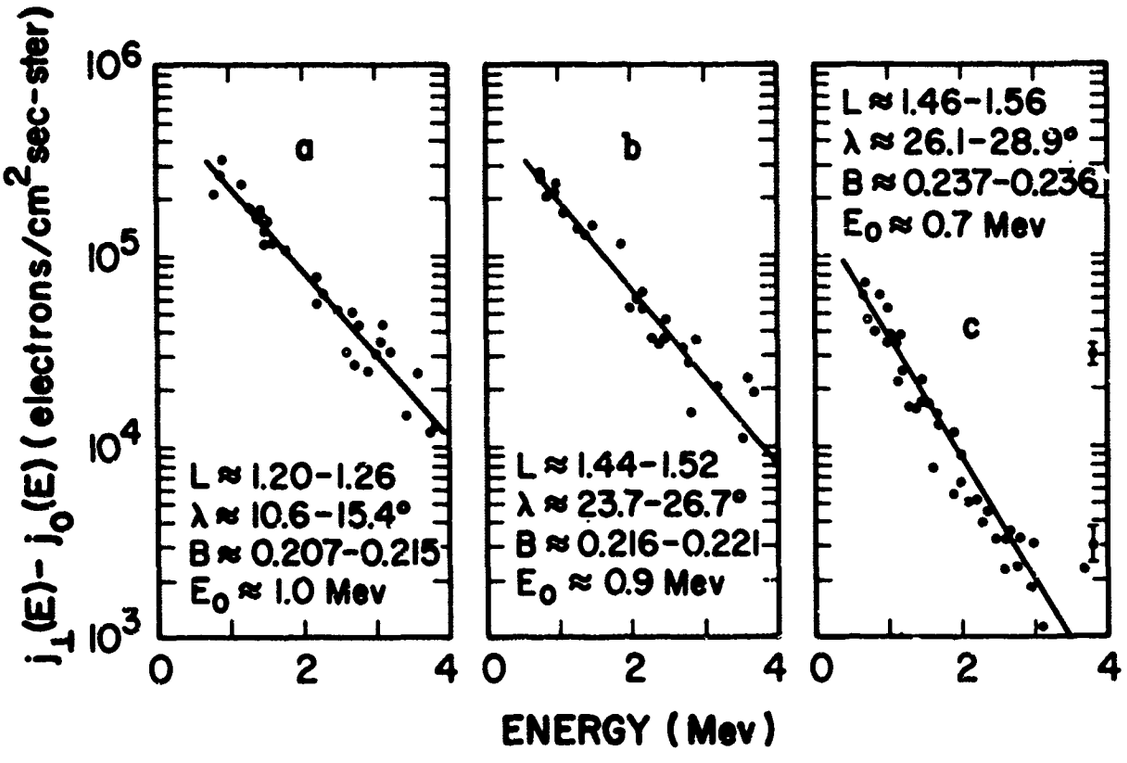

Fig. A8 Electron Integral Energy Spectra in the Inner Belt.

Figure 9 shows a typical outer belt electron integral energy spectrum between 0.7 and 4 Mev derived from the scintillation spectrometer. The spectrum has approximately an exponential dependence exp $(-\frac{E}{E_o})$ with $E_o \approx 0.4$ Mev. Throughout the observation period and in outer belt regions with high enough intensities for an adequate spectrum determination, all spectra obtained could be fitted with $E_o \approx 0.4 \pm 0.1$ Mev.

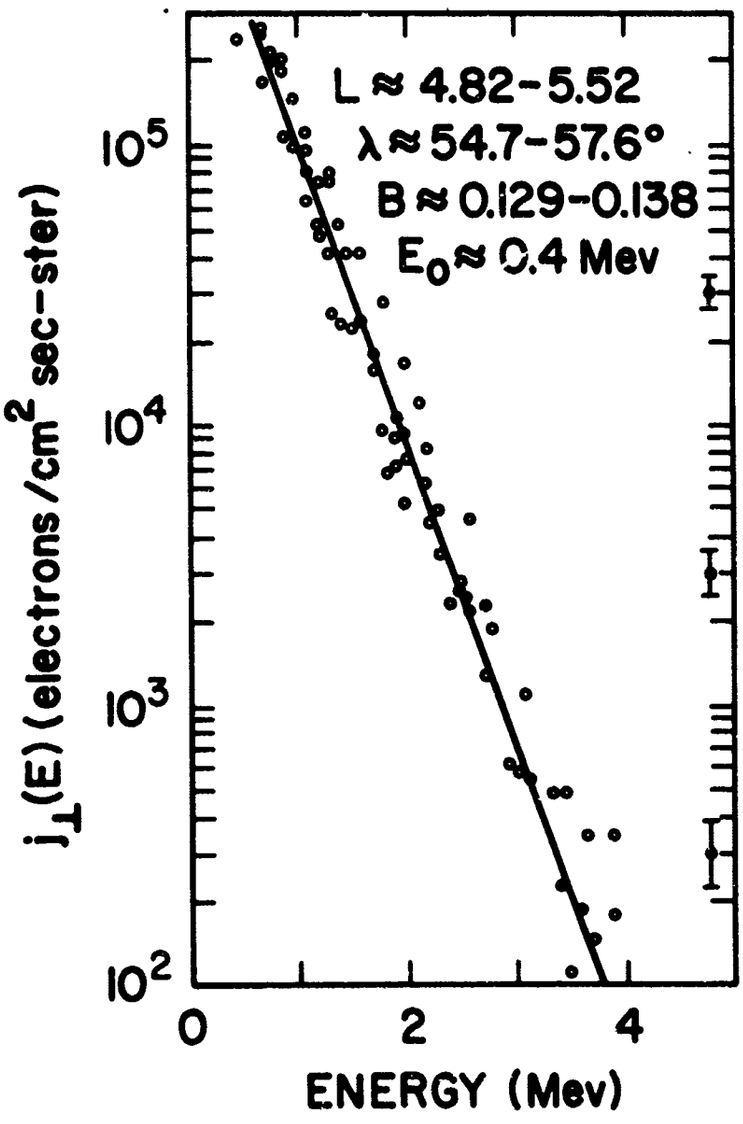

Fig. A9 Electron Integral Energy Spectrum in the Outer Belt.

Dumping of Electrons in the Anomaly

As was already pointed out in connection with the isointensity contours of Figure 3, the contour close to the lowest limit of sensitivity of our instrument closely approached the 100 km minimum altitude surface for $\lambda \sim 20^{\circ} - 40^{\circ}$ ($L \approx 1.3 - 2.0$). Around this region of the inner belt, Paulikas and Freden (1964), using an instrument with a lower limit of sensitivity, have observed electrons in regions with minimum altitudes such that precipitation into the atmosphere occurs in the Anomaly.

A similar situation exists at times in regions of the outer belt. In Figure 3 for $\lambda \approx 55^{\circ}$ to 62° significant electron intensities are measured in regions with a minimum altitude below 100 km. Such electrons scatter into the atmosphere when they reach the Anomaly. Additional information about electron intensities at altitudes below the levels reached by the satellite is provided by pitch angle distributions obtained during the low satellite passes. Two such pitch angle distributions are shown in Figure 10. For each pitch angle the R and λ coordinates of the corresponding mirror point are given. Also the approximate minimum altitude h_{min} that the electrons at this pitch angle will reach is indicated in the figure. For the largest part of the shown pitch angle distributions, h_{min} is negative showing clearly that precipitation into the atmosphere will occur. The dumping of electrons between $\lambda \sim 55^{\circ}$ and 62° was observed also on days of low intensity levels in the outer belt. In the case of Figure 10b for instance, the electron intensities in all shells with $L > \sim 5$ were one to two orders of magnitude below the highest intensity levels recorded during the observation period (Figure 2a).

On the basis of the information on intensity levels and pitch angle distributions derived from Figures 3 and 10a, the loss rate from dumping in the Anomaly of electrons above 1 Mev was computed to be approximately 2×10^{17} electrons/sec or about 2×10^{11} ergs/sec.

Outer Belt Time Variations

During the present observation period large time variations which correlated with solar and geomagnetic activity were observed in the outer belt. A summary plot of intensity levels at $L \approx 5$, $\lambda \approx 60^{\circ}$ is given in Figure 11. The occurrence of solar flares and daily values of the magnetic variation A_p (Lincoln, 1963a and b) are displayed in the same figure.

In the cases of the intensity decreases around 4 July, 17 July, 30 July and 19 August 1963, sudden increases in A_p had occurred at about

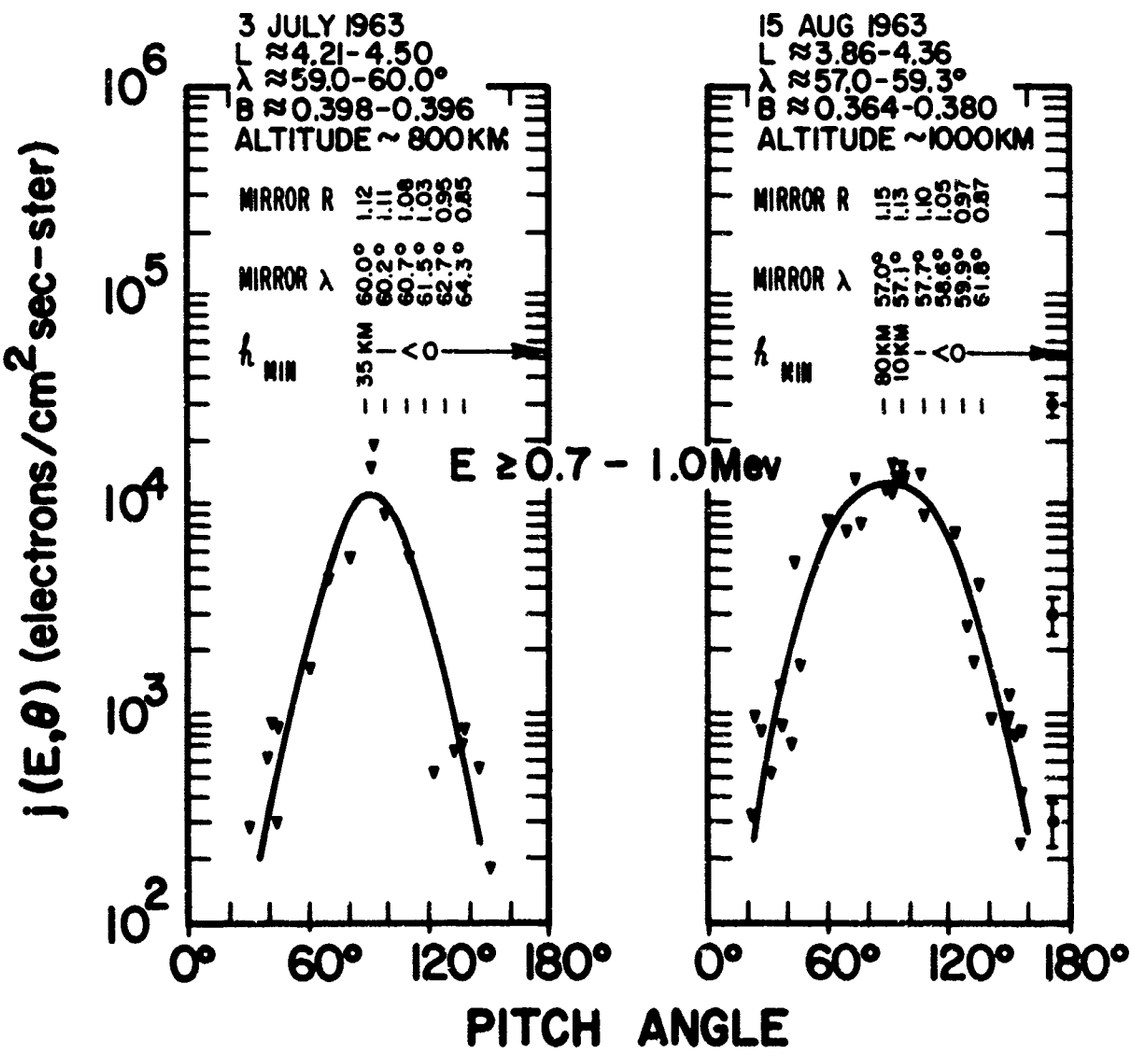

Fig. A10 Electron Pitch Angle Distributions At Low Altitudes in the Outer Belt.

the time of the fall in intensity. Solar flares had been observed in three of these four instances. The intensity decrease during the magnetically quiet period between 10 August and 17 August occurred gradually with a simultaneous shift of the intensity peak toward lower L values. Following the depletions of 4 July, 17 July and 30 July the outer belt recovered to pre-storm intensity levels with recovery times which varied from a few to about 10 days.

For $L < \sim 4$ no significant time variations were observed during the observation period. The steep inner edge of the outer belt (Figures 2 and 3) remained relatively unchanged with time while the outer part of the belt underwent considerable variation. Due to the relative invariance of intensity levels at the low L edge of the outer belt, whenever the rest of the belt was depleted the intensity peak shifted toward lower L shells.

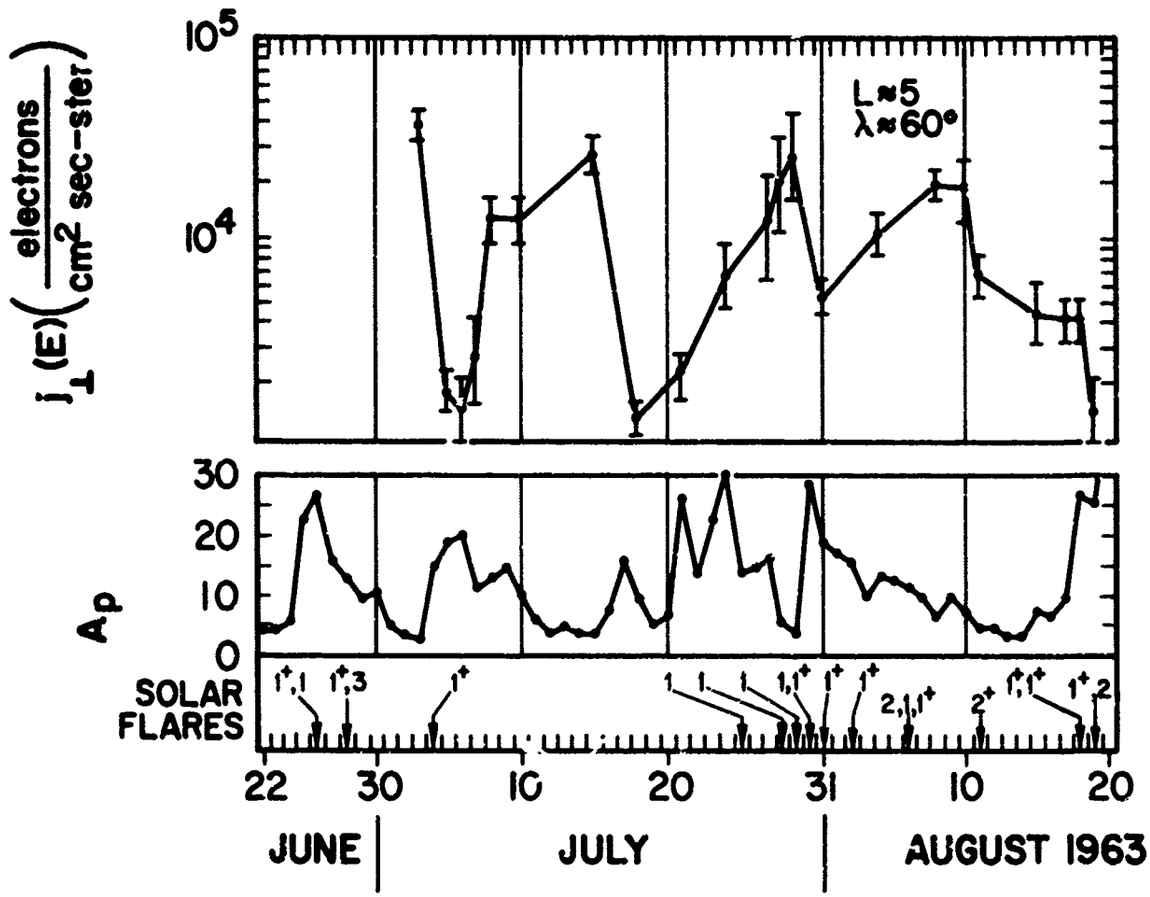

Fig. A11 Electron Intensity Fluctuations in the Outer Belt ($E \geq 1.0 \pm 0.1$ Mev).

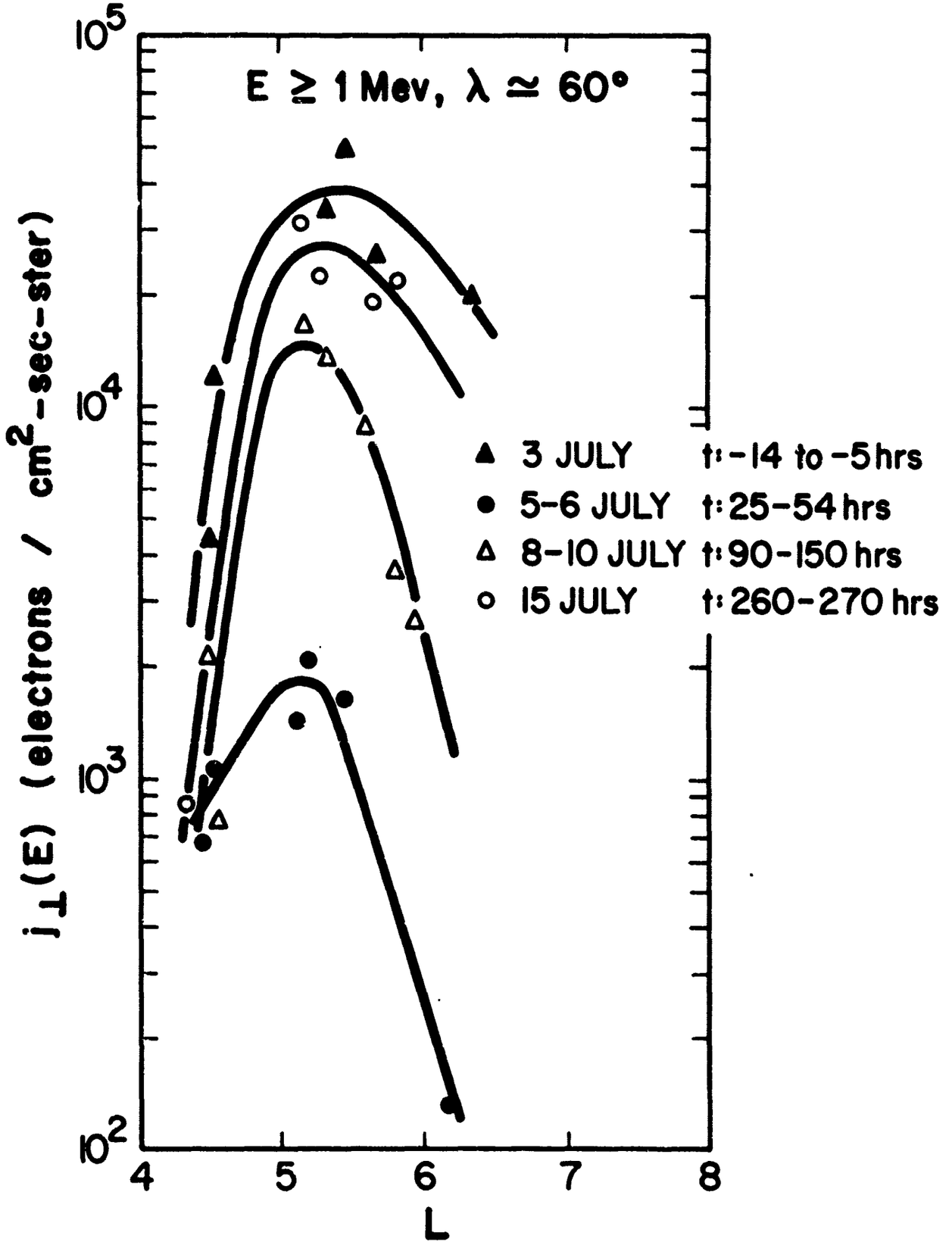

Fig. A12 Electron Intensities in the Outer Belt at Various Times Around the Solar Flare of 4 July 1963.

The depletion and recovery cycle that occurred from 3 July to 15 July 1963 will now be examined in more detail. A class 1^+ solar flare occurred at 0734 UT, 4 July 1963 (4th quadrant, 8° latitude, 79° to meridian). Prior solar activity consisted of two flares on 28 June (class 1^+ in quadrant 4, class 3 in quadrant 1) and subsequent activity consisted of a flare on 25 July (class 1, quadrant 4). The magnetic variation A_p was 3 on 2 and 3 July, went up to 14 on 4 July and stayed at 10 - 20 until 10 July; there was also Thule Riometer activity on 5 July. The occurrence of the flare will be taken as a time reference point in the subsequent discussion.

The change that occurred in the intensity profiles of the outer belt can be seen by comparing Figure 2a (data obtained 1 hr to 5 hrs before the flare) with Figure 2b (25 to 54 hrs after the flare). Electrons above 1 Mev are depleted by 1 order of magnitude at $L \approx 4.5$ to about two orders of magnitude for $L > 5.5$.

After the depletion, the electron intensity started to build up again until it essentially returned to the pre-storm level. The recovery process is illustrated in Figure 12 where the curve for $\lambda \approx 60^\circ$ is followed from about 15 hrs before the flare until 270 hrs later. Provided that the whole outer belt is depleted in the same way as the observed region and with the assumption of a constant logarithmic loss mechanism, it is found that a source of electrons of the order of $10^{13} - 5 \times 10^{13}$ ergs/sec must be present in order to account for the observed recovery time.

During the observed time variations the relative position of various constant λ profiles changed considerably, particularly at higher L's, as can be seen, for instance, by comparing Figures 2a and 2b. This indicates that changes in mirror point distributions on certain magnetic shells occurred as well as variations in intensity alone. Such changes should also be evident from the pitch angle distributions on those magnetic shells. Unfortunately, for the regions where the intensity levels remained high enough to permit

an adequate direct measurement of pitch angle distributions (i.e., around L ~ 4.5) no significant changes were expected from the intensity profiles. Two such distributions obtained in about the same region 13 hrs before and 45 hrs after the flare are given in Figure 13 together with the expected distributions on the basis of the intensity contours. Although the intensities are considerably different, the shape of the distribution remains essentially unchanged.

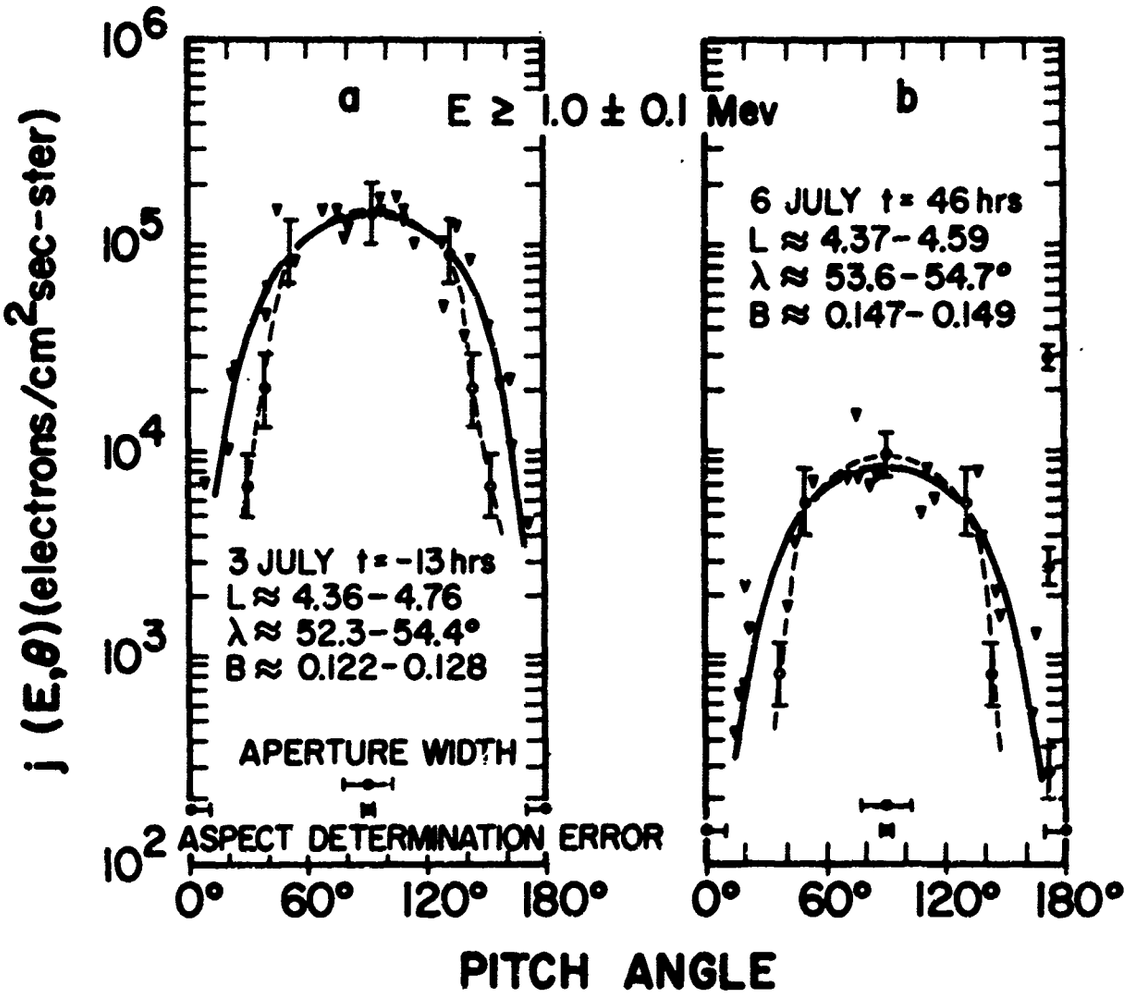

Fig. A13 Electron Pitch Angle Distributions in the Outer Belt Before and After the Solar Flare of 4 July 1963.

Figure 14 shows electron integral energy spectra between 0.7 Mev and 4 Mev in a given region before and after the flare and during the recovery period. The parameter E_o of an exp $(-E/E_o)$ spectral shape, changes from about 0.4 Mev to about 0.3 Mev after the flare returning later to 0.4 Mev. Since the very low intensity after the flare reduces the accuracy with which E_o can be determined, the observed steepening may not be significant.

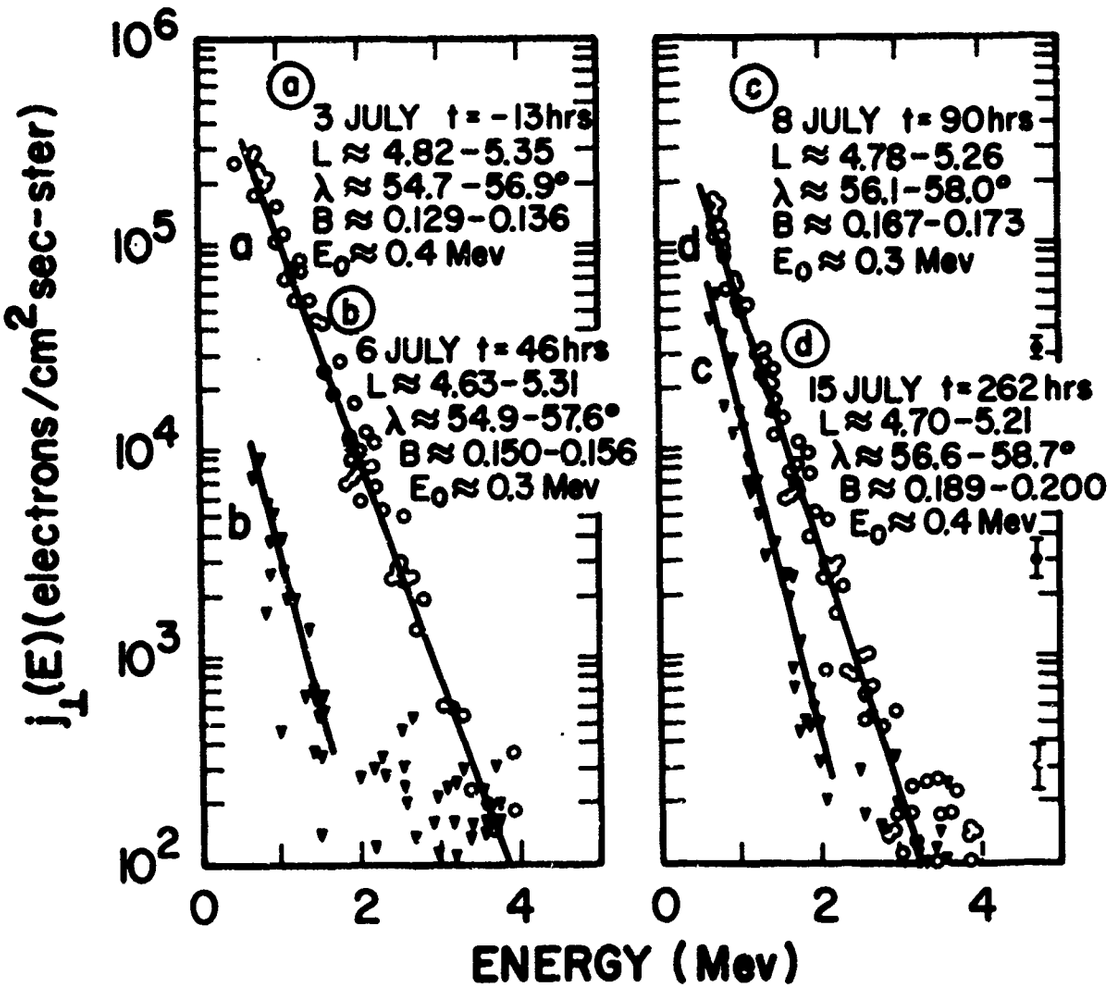

Fig. A14 Electron Integral Energy Spectra in the Outer Belt at Various Times Around the Solar Flare of 4 July 1963.

DISCUSSION

Electron intensities detected by Hitch-hiker I in the inner belt during July - August 1963 were at about the level reported by Van Allen (1964) from Injun III data for June 1963. They are about one order of magnitude lower than electron fluxes measured by Explorer XV around January 1963 (McIlwain 1963) and Relay I for May through September 1963 (McIlwain et al., 1964). Electron data from a low altitude polar satellite reported by Bostrom and Williams (1965) for October 1963 refer mainly to regions near the steep edge of the inner belt where comparison is rather difficult, although their intensity levels seem to be comparable to the ones reported here.

Measured inner belt spectra with exponential slope 0.7 Mev $\leq E_o \leq$ 1.2 Mev are not much different from the fission like spectra observed after the Starfish explosion (Mozer et al., 1963, Brown and Gabbe, 1963).

The range of observed intensities for electrons above 1 Mev at the horns of the outer belt was roughly 10^3 - 10^5 electrons/cm^2 sec ster. Intensities measured with polar satellites near the horns of the outer belt by Williams and Smith (1965) and Paulikas and Freden (1964) vary roughly around the same levels, while considerably lower hard electron intensities are reported by Armstrong (1965). Similar intensities for energetic electrons are reported in outer belt regions closer to the magnetic equator by Frank (1965), Frank, et al., (1964), Frank et al., (1963), and Hoffman et al., (1962).

The observed location of the intensity peak at the horns of the outer belt was between $L \approx 4.5$ and 6 with a very sharp and rather stable cutoff at $L \approx 4$. During Explorer 7 measurements (Forbush et al., 1962) the peak of the outer zone at the horns was considerably lower, at $L \approx 3$ to 5.

Spectral data for the outer belt electrons in the literature refer mostly to the energy range from about 40 kev to 1.6 Mev. The steep spectra observed (Williams and Smith, 1965, Frank et al., 1964, Paulikas and Freden, 1964, Mozer et al., 1963 and Rosser et al., 1962) are not inconsistent with the 0.7 Mev to 4 Mev spectra reported in this paper.

The directly measured pitch angle distributions in the inner and outer belt are seen to be consistent with the distribution derived from j_1 within uncertainties due to the angular resolution of the instrument and the accuracy of the aspect determination and the limitations imposed by the existent omnidirectional background. Some directly measured pitch angle distributions near the horns of the outer belt are given by Cladis et al., 1961. Their measurements were taken at a lower altitude and consequently the distributions are considerably narrower than those presented here.

The observed presence of energetic electrons in high latitude portions of outer belt magnetic shells that plunge into the atmosphere at the Anomaly is consistent with observations by Forbush et al., 1962 and Paulikas and Freden 1964. Based on the data of this paper, the estimated loss rate of energetic outer belt electrons due to such dumping (about 2×10^{11} ergs/sec) is about two orders of magnitude smaller than the electron source that is estimated from the recovery time constants after outer belt depletions (about 10^{13} to 5×10^{13} ergs/sec). Therefore loss of hard outer belt electrons through this mechanism must be of minor importance in the electron balance of the outer belt compared to other loss mechanisms such as scattering into the loss cone and immediate dumping into the atmosphere or escaping from the trapping region through broken magnetic lines (Dessler and Karplus, 1961).

The pattern of time variations observed in the outer belt is consistent with previous observations performed at high magnetic latitudes as well as close to the equator. Observations near the equator seem to agree on a pattern of a decrease in the intensity of energetic electrons around the time of magnetic disturbances by factors ranging from less than 10 (Frank et al 1964, Hoffman et al., 1962, Arnoldy et al., 1960) up to 1000 (Rosser, 1963). Subsequently the intensities recover over a period of a few to several days, often going up to several times the pre-storm levels (Freeman, 1964, Frank et al., 1964, Hoffman et al., 1962). In the region of the horns of the belt Forbush et al., 1962 have observed about a 10-fold

intensity decrease for $L > 3.5$ at the time of magnetic storms with a simultaneous increase at lower L's. Williams and Smith, 1965, observe a rise of hard electron intensities a few days after magnetic disturbances.

Although no major magnetic storm occurred during the present observation period a number of substantial depletions and subsequent recoveries of the hard electron outer belt component were observed, associated with solar and magnetic activity. Considering the general pattern indicated by the quoted references the observed intensity decreases in the horns seem to be part of a general depletion of the energetic electrons in the belt rather than mere redistributions of magnetic shells in space.

The recovery times observed after outer belt depletions are similar to times mentioned in the quoted papers. The estimated electron source required ($\sim 10^{13}$ to 5×10^{13} ergs/sec) would have to arise from the solar wind ($\sim 10^{20}$ ergs/sec) with an acceleration mechanism.

The integral electron spectra measured between 0.7 Mev and 4 Mev are relatively constant in shape during the observed time variations, with possibly a slight steepening at the time of the intensity drop. This is to be contrasted with the considerable spectral steepening that occurs at lower energies where the soft electron intensities actually increase at the time of the hard electron depletion (e.g., Frank et al., 1964).

SUMMARY

Unidirectional electron intensities, integral energy spectra, and pitch angle distributions were obtained in the radiation belts during July and August 1963. Peak inner belt intensities for electrons above 1 Mev were about 5×10^6 electrons/cm^2-sec-ster at $L \sim 1.3 - 1.4$ at the magnetic equator. Inner belt spectra could be fitted with the shape $\exp(-E/E_o)$, with $0.7 \leq E_o \leq 1.2$ Mev.

Outer belt peak intensities fluctuated widely with maximum observed values around 10^5 electrons/cm^2sec ster. Outer belt spectra between 0.7 Mev and 4 Mev had exponential shapes, with $E_o \approx 0.4 \pm 0.1$ Mev. Pitch angle distributions obtained throughout the radiation belts were consistent with the observed perpendicular intensity profiles.

Dumping of energetic electrons in the S. Atlantic Anomaly was observed at high latitudes in the outer belt. Loss of electrons above 1 Mev through such dumping was of the order of 2×10^{11} ergs/sec.

Severe depletions of the hard outer belt electrons occurred at times of magnetic and solar activity. Subsequent recoveries had time constants ranging from a few to about ten days. No drastic spectral changes between 0.7 Mev and 4 Mev were recorded during such time variations. Although some changes in mirror point distributions along magnetic shells did occur, they were not radical enough to substantially alter the pitch angle distributions in the high intensity region of the horns of the outer belt.

REFERENCES

Armstrong, T., J. Geophys. Res. 70, 2077-2110 (1965).

Arnoldy, R. L., R. A. Hoffman and J. R. Winckler, J. Geophys. Res. 65, 1361-1376 (1960).

Bostrom, C. O., and D. J. Williams, J. Geophys. Res. 70, 240-242 (1965).

Brown, W. L., and J. D. Gabbe, J. Geophys. Res. 68, 607-618 (1963).

Cladis, J. V., L. F. Chase, W. L. Imhof and D. J. Knecht, J. Geophys. Res. 66, 2297-2312 (1961).

Dessler, A. J. and R. Karplus, J. Geophys. Res. 66, 2289-2295 (1961).

Forbush, S. E., G. Pizzella and D. Venkatesan, J. Geophys. Res. 67, 3651-3668 (1962).

Frank, L. A., J. Geophys. Res 70, 1593-1626 (1965).

Frank, L. A., J. A. Van Allen and H. K. Hills, J. Geophys. Res 69, 2171-2191 (1964).

Frank, L. A., J. A. Van Allen, W. A. Whelpley and J. D. Craven, J. Geophys. Res. 68, 1573-1579 (1963).

Freeman, J. W., J. Geophys. Res. 69, 1691-1723 (1964).

Hoffman, R. A., R. L. Arnoldy and J. R. Winckler, J. Geophys. Res. 67, 4543-4575 (1962).

Lincoln, J. V., J. Geophys. Res 68, 6199-6200 (1963a).

Lincoln, J. V., J. Geophys. Res. 68, 6537 (1963b).

McIlwain, C. E., Science 142, 355-361 (1963).

McIlwain, C. E., R. W. Fillius, J. Valerio and A. Dave, NASA TND-2516 (1964).

Mozer, F. S., D. D. Elliot, J. D. Mihalov, G. A. Paulikas, A. L. Vampola and S. C. Freden, J. Geophys. Res. 68, 641-649 (1963).

Paulikas, G. A. and S. C. Freden, J. Geophys. Res. 69, 1239-1249 (1964).

Rosser, W. G. V., J. Geophys. Res. 68, 3131-3148 (1963).

Rosser, W. G. V., B. J. O'Brien, J. A. Van Allen, L. A. Frank and C. D. Laughlin, J. Geophys. Res., 67, 4533-4542 (1962).

Van Allen, J. A., Nature 203, 1006-1007 (1964).

Williams D. J. and A. M. Smith, J. Geophys. Res. 70, 541-556 (1965).

This is a preprint of a paper to be presented at the Forty-sixth Annual Meeting of the American Geophysical Union at Washington, D. C. on 19 - 22 April 1965.

ASE-914

Appendix B

MEASUREMENTS ON 1.5 TO 4 MEV PROTONS IN THE RADIATION BELTS*

G. C. Theodoridis and F. R. Paolini

American Science and Engineering, Inc.
Cambridge, Massachusetts

*Work supported by the Air Force Cambridge Research Laboratories

MEASUREMENTS ON 1.5 TO 4 MEV PROTONS IN THE RADIATION BELTS*

G. C. Theodoridis and F. R. Paolini

American Science and Engineering, Inc.
Cambridge, Massachusetts

ABSTRACT

Integral energy spectra from 1.5 to 4 Mev and pitch angle distributions of protons in the radiation belts were measured using a scintillation spectrometer flown on Hitch-hiker I. The protons defined two belts, with hearts at $L \sim 1.6$ and $L \sim 4.5$, and a slot at $L \sim 3.0$. The integral spectra observed were all similar in shape, with approximately an exponential energy dependence. The spectra tended to be much steeper than electron spectra in the same energy range in the inner belt. Typical omnidirectional intensities for energy $E > 2$ Mev were $10^8/cm^2$ sec at $(L, \lambda) \sim (1.6, 8^\circ)$ and $2 \times 10^6/cm^2$ sec at $(L, \lambda) \sim (4.5, 55^\circ)$. Pitch angle distributions observed were peaked at 90° and had cutoffs consistent with theory.

---

*Work supported by the Air Force Cambridge Research Laboratories

BLANK PAGE

INTRODUCTION

The proton scintillation spectrometer flown on the Air Force sub-satellite Hitch-hiker I (1963-25B) used a "phoswich" of 40 mg/cm^2 of Pilot "B" plastic scintillator (corresponding to the range of a 5.3 Mev proton or a 0.20 Mev electron) on 22.5 g/cm^2 of CsI (Tℓ) scintillator (corresponding to the range of a 130 Mev proton or a 50 Mev electron). The scintillators were shielded on the sides to prevent penetration by electrons of energies less than 50 Mev and protons of energies less than about 150 Mev. The scintillator light shield was 5000 A aluminum, corresponding to a proton range of about 150 kev. The pulses arising from energy deposited in each of the scintillators could be separated by pulse-shape discriminating logic. Pulses of sufficient amplitude from the plastic alone, in anticoincidence with pulses from the CsI(Tℓ), were predominantly due to protons of energies 1 to 5.3 Mev with some contamination at lower energies due to straggling electrons. Because of the thinness of the plastic scintillator, electrons which stop in it produce significant contamination only at pulse heights corresponding to protons of 0.7 Mev or less, which is below the energy range investigated. Spectral information was derived by pulse height analysis using a comparator with a linear sweep of 16 sec. period. The comparator output corresponded to fluxes of protons with energy above the variable energy threshold defined by the sweep and below 5.3 Mev, thus measuring integral proton spectra between approximately 1.5 and 4 Mev. The energy resolution varied from about $\pm$20% at 1.5 Mev to about $\pm$4% at 4 Mev. A Van de Graaff accelerator was used in calibration.

The entrance aperture was calculated to be a cone of vertex angle 8° and the total geometrical factor was $A\Omega = 8.4 \times 10^{-4}$ cm^2 ster. The output stage was a logarithmic count rate meter and the absolute dynamic range was 1.4×10^4 to 2×10^8 particles/cm^2 sec ster. The spectrometer output was sampled 6 times/sec while the satellite spin frequency was about 1.1

rotation/sec; thus pitch angle distributions with good resolution were also obtained.

RESULTS

Unidirectional Intensities

Figure 1 presents unidirectional intensities of protons with energy between 2.0 ± 0.1 Mev and 5.3 Mev and pitch angle $90^{\circ} \pm 10^{\circ}$ for various points in the radiation belts. The data are presented in curves of perpendicular intensity vs. L at a constant magnetic latitude λ.

During the period of observation the inner belt intensity levels displayed no systematic variations outside statistical fluctuations. The outer belt intensities exhibited variations by factors of 2 - 5 during the same period, following roughly the same pattern as the variations of 1 - 4 Mev electrons although less drastic. These effects are discussed in a subsequent paper.

Data from several orbits between 1 July and 20 August 1963 have been included in the inner belt data of Figure 1. The data for the outer belt are taken from orbits 25 and 26 of 3 July 1963 when intensity levels were rather high.

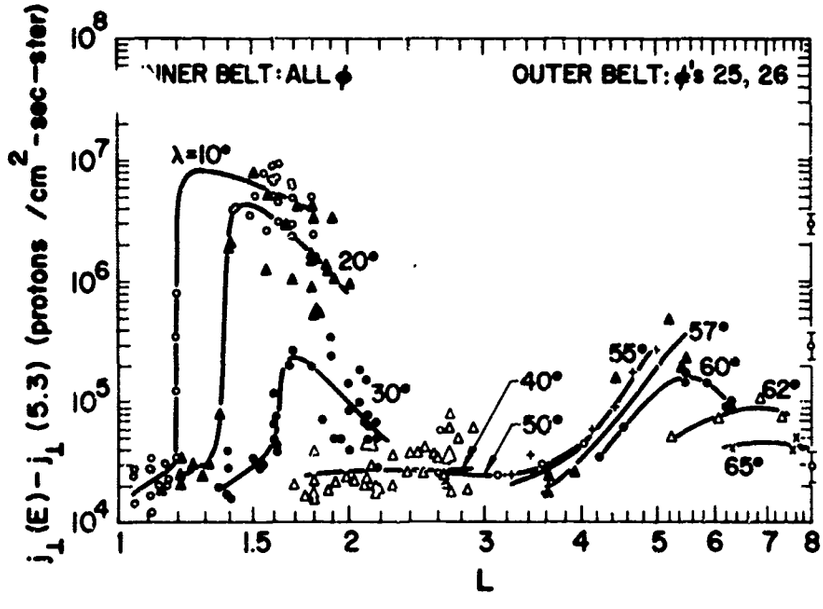

Fig. B1 Proton Fluxes at Various λ ($E \geq 2$ Mev).

Pitch Angle Distributions

Some proton pitch angle distributions obtained in the inner and outer belt are given in Figure 2. The values of the loss cone angle are computed on the basis of a cutoff at $R \sim 1.14$ as expected from atmospheric scattering. Uncertainties in aspect determination range from a few degrees around 90° pitch angle to about ten degrees at 0° or 180°, being therefore of the same order of magnitude as the uncertainty due to the 8° field of view of the instrument.

It appears that the inner belt distributions are somewhat narrower than expected. For example, in Curve B the cutoff pitch angle is about 70° compared to a computed cutoff of $53 - 60^{\circ}$. This would roughly correspond to an edge of the inner belt as defined by the proton component at $R \approx 1.17 - 1.19$, that is about 200 - 300 km above the limiting surface expected from atmospheric scattering. The intensity curves of Figure 1 seem to indicate a similar trend but the data points in the region of the edge are rather scarce so that no definite conclusion can be drawn.

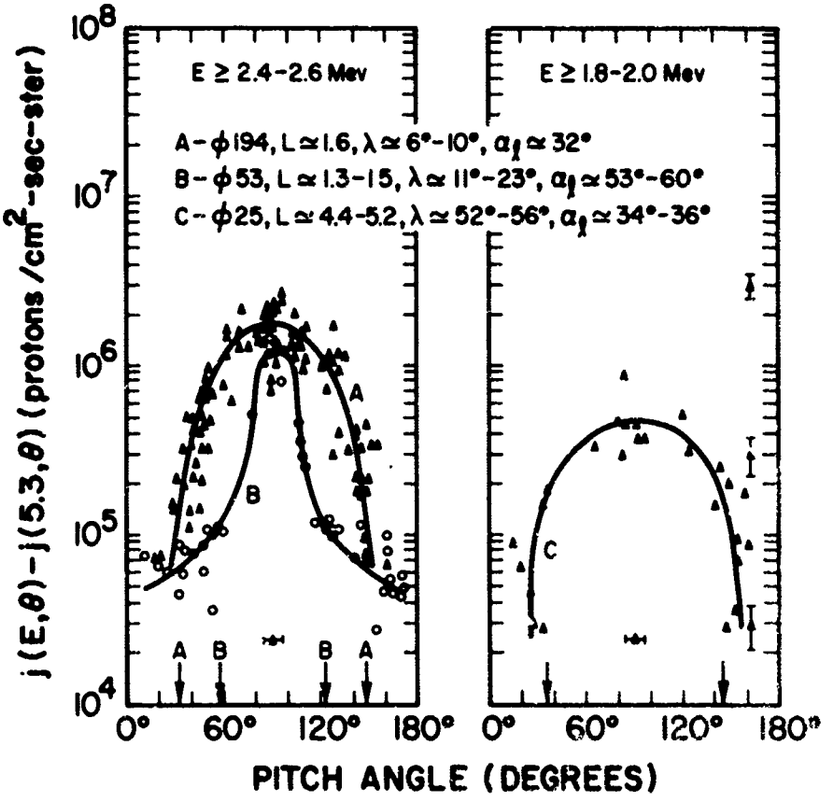

Fig. B2 Proton Pitch Angle Distribution.

Each pitch angle curve in Figure 2 includes data points in a narrow range of threshold energies but similar curves are obtained for any threshold energy between 1.5 and 4 Mev. Due to the steepness of the proton energy spectra, even a range of 0.2 Mev in threshold energy contributes appreciably to the scatter of the data points.

Energy Spectra

The measured proton integral spectra have approximately an exponential energy dependence exp $(-E/E_o)$ with E_o ranging between 0.3 Mev and 0.4 Mev. Some typical spectra are shown in Figure 3 for points in the inner and the outer belt. Unidirectional intensities at pitch angle $90^o \pm 10^o$ are included in these graphs. The spectra give the intensities of protons between a threshold energy and 5.3 Mev vs. the threshold energy.

The slopes of the spectra are essentially the same. It should be noted, though, that the regions in which a complete 1.5 - 4 Mev spectrum can be obtained are rather limited since, due to the steep slope, a large part of the spectrum is below the instrument sensitivity for all but the most intense radiation regions.

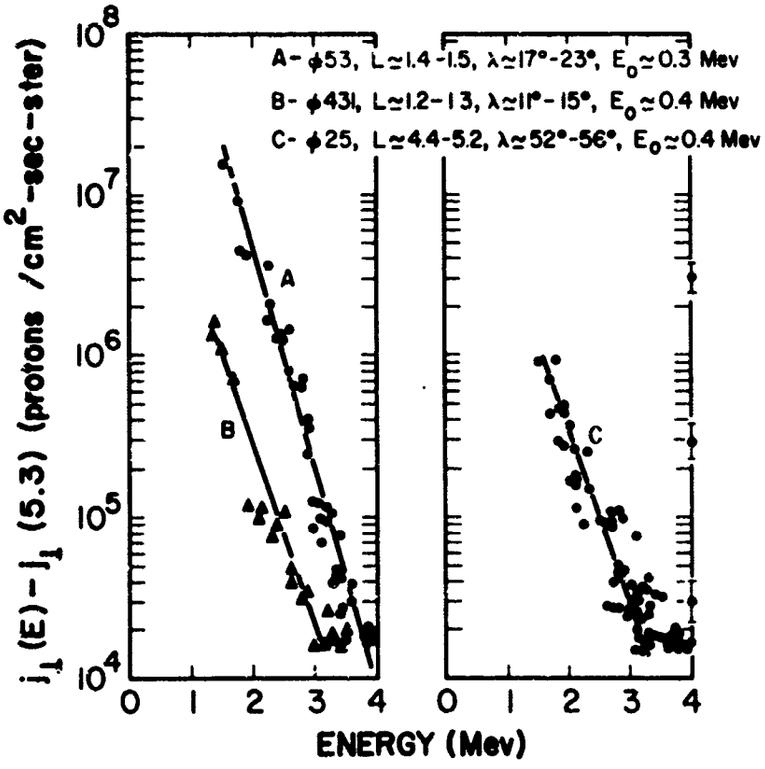

Fig. B3 Proton Integral Energy Spectra.

Comparison of Protons and Electrons

Figures 4 and 5 display proton and electron pitch angle distributions and energy spectra obtained simultaneously in several regions of space. The proton pitch angle distributions in the inner belt appear to be narrower than the corresponding electron pitch angle distributions (Figure 4, Curves A and B) indicating that the proton intensity falls off at the edge of the inner belt at a somewhat higher altitude than the electron intensity. This conclusion should be accepted with some reservation since the larger field of view of the electron spectrometer (25^{o}) would tend to widen the apparent electron distribution. An additional distortion is brought about by the presence of a considerable background due to energetic particles penetrating the electron scintillator shielding.

Comparing the electron and proton integral spectra (Figure 5) we see that the slopes are about equal in the outer belt while the proton spectra are considerably steeper in the inner belt. The intensity of protons above ~ 2 Mev is higher than the intensity of electrons above the same energy by factors ranging from about 3 to 30 in the various regions of space.

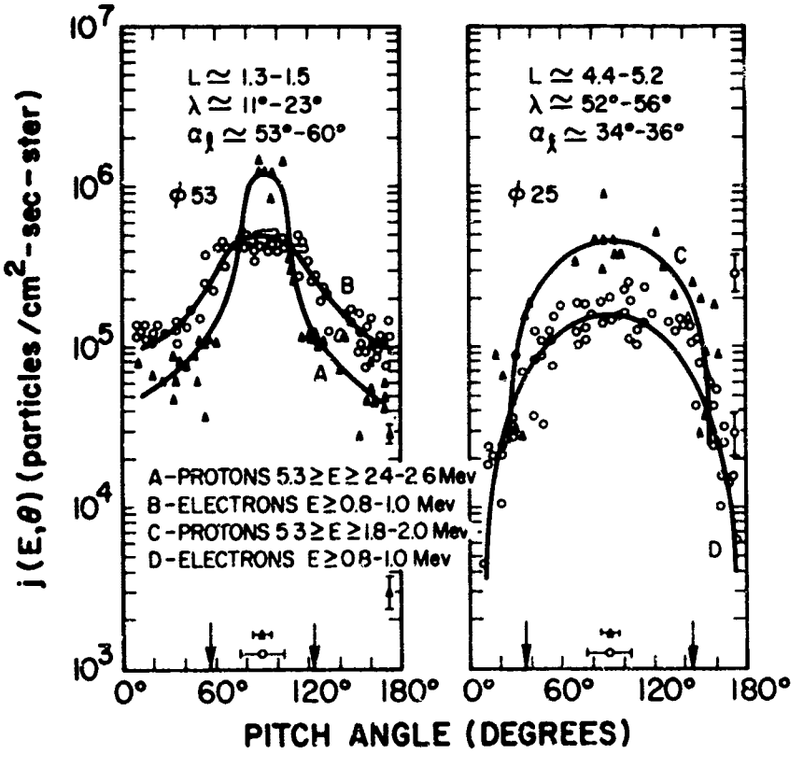

Fig. B4 Electron and Proton Pitch Angle Distributions.

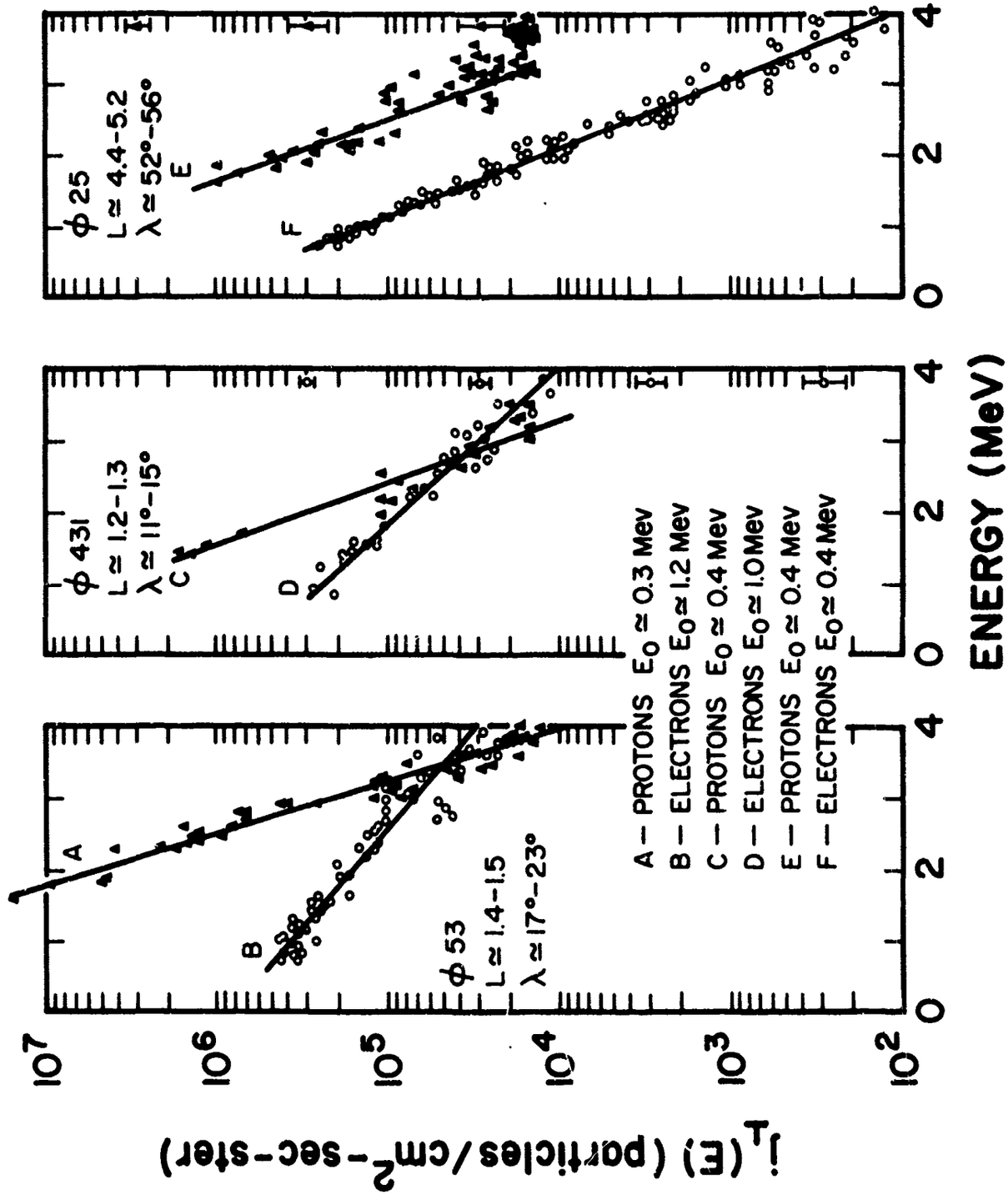

Fig. B5 Electron and Proton Integral Energy Spectra.

Discussion

Some data on protons in the energy range examined in this paper have been given by Davis and Williamson (1963), Bame et al., (1963) and Pieper et al., (1962). These experimenters mention intensities of $10^4 - 10^5/cm^2$sec ster in the outer belt for protons above 1 Mev. These levels seem to be lower by about a factor of ten than the present data, although the different locations of the measurements as well as variations in the outer zone may account for the difference. Bame et al., (1963) give an intensity of ~ $5 \times 10^5/cm^2$sec ster for protons above ~ 1 Mev at $L \approx 2.5$ and $\lambda \approx 30^o$, which fits well with our data. Unfortunately they give no data for those regions where we observed the highest intensities.

The integral spectra given by Bame et al., (1963) and Davis and Williamson (1963) are very steep and agree relatively well with the spectra derived in this work, allowing for the different locations and the accuracy of the measurements.

Proton data are much more abundant in the literature for energies above 30 to 100 Mev, where inner belt intensities are known to be of the order of 10^2 to $10^3/cm^2$ sec ster with very flat spectra (e.g., see Imhof and Smith 1964, Freden and Paulikas 1964, Valerio 1964, Naugle and Kniffen 1963, etc.).

Summarizing our results, we observe that 1.5 - 5 Mev protons are present with maximum intensities of the order of $10^7/cm^2$sec ster in about the same region as the energetic electrons in the inner belt, and with relatively lower intensities, up to about $5 \times 10^5/cm^2$ sec ster, in the investigated portion of the outer belt. Outer belt variations seem to follow a similar pattern with the variations of energetic electrons but are much less drastic.

Proton spectra are as steep as electron spectra in the outer belt but much steeper than the electron spectra in the inner belt. They fit an exponential form $\exp(-E/E_o)$ with $E_o \approx 0.4$ Mev. Proton pitch angle distributions are about 10^o narrower than expected from atmospheric scattering alone in the inner belt, and are consistent with the computed loss cones in the outer belt.

REFERENCES

1. Bame, Conner, Hill and Holly, JGR 68 55 (1963).

2. Davis and Williamson, Space Research, pp 365 - 375, North Holland Publishing Co., Amsterdam (1963).

3. Freden and Paulikas, JGR 69 1259 (1964).

4. Imhof and Smith, JGR 69 91 (1964).

5. Naugle and Kniffen, JGR 68 4065 (1963).

6. Pieper, Zmuda, Bostrom and O'Brien, JGR 67 4959 (1962).

7. Valerio, JGR 69 4949 (1964).

This is a preprint of a paper to be presented at the Forty-sixth Annual Meeting of the American Geophysical Union at Washington, D. C. on 19 - 22 April 1965.

ASE-913

Appendix C

MEASUREMENTS ON 0.7 TO 4 MEV ELECTRONS IN THE RADIATION BELTS FROM HITCH-HIKER I*

G. C. Theodoridis and F. R. Paolini

American Science and Engineering, Inc.
Cambridge, Massachusetts

*Work supported by the Air Force Cambridge Research Laboratories

MEASUREMENTS ON 0.7 TO 4 MEV ELECTRONS IN THE RADIATION BELTS FROM HITCH-HIKER I*

G. C. Theodoridis and F. R. Paolini

American Science and Engineering, Inc.
Cambridge, Massachusetts

ABSTRACT

Omnidirectional intensities, pitch angle distributions, and integral spectra from energy E = 0.7 to 4 Mev were measured with a scintillation spectrometer flown on Hitch-hiker I. The electrons exhibited the usual two belt morphology, with inner belt heart at L ~ 1.6, slot at L ~ 3.0, and outer belt heart at L ~ 4.5. Typical omnidirectional intensities for E > 1.0 Mev were 4 x 10^5/cm^{2}sec at (L, λ) ~ (4.5, 55°), 10^3/cm-sec at (L, λ) ~ (3, 45°), and 3 x 10^6/cm^{2}sec at (L, λ) ~ (1.7, 15°). For E > 4 Mev the omnidirectional intensities were 10^3/cm^2-sec, 10/cm^2-sec, and 10^5/cm^2-sec respectively. The angular distributions observed all had maxima in directions perpendicular to the field lines and exhibited cutoff angles consistent with theory. Outer belt spectra, 3 < L < 7, all had the approximate shape exp (-kE) with k of the order of 2.0 Mev^{-1}. In and below the slot, spectra were also approximately exponential, but less steep, with 0.6 Mev^{-1} < k < 1.5 Mev^{-1}.

*Work supported by the Air Force Cambridge Research Laboratories

INTRODUCTION

The Air Force sub-satellite Hitch-hiker I (1963-25B) was launched on 1 July 1963 into a polar orbit of 82.14° inclination with perigee at 326 km and apogee at 4150 km. The angle between the ascending node of the orbit and the earth-sun line was initially about 63°, and regressed at a rate of approximately -1 1/2°/day. The orbital period was 133 minutes. The sub-satellite was spin-stabilized at 68 rpm with its axis of rotation at an angle of about 25° to the axis of the earth.

The data to be presented in this paper concern electrons of energy 0.7 to 4 Mev and were obtained from a scintillation spectrometer using a 2.5 gm/cm^2 Pilot "B" plastic scintillator, equivalent to the range of a 5.0 Mev electron or a 55 Mev proton. The plastic scintillator was shielded on the sides and back against electrons of energy less than about 10 Mev and protons of energy less than about 65 Mev. The entrance aperture was shielded with 50 mg/cm^2 of aluminum, corresponding to the range of a 200 kev electron or a 5 Mev proton. The amount of contamination of the measured electron fluxes by protons over 5 Mev is well within the statistical uncertainty of the data, since estimates of proton intensities at that energy from spectra obtained from a proton spectrometer indicate proton intensities one to three orders of magnitude below the measured electron intensities.

Spectral information was derived by pulse height analysis. The scintillation pulses were fed to one input of a comparator, the other input of which was fed by a linear sweep of about 16 sec period. The comparator output signal repetition rate thus corresponded to fluxes of electrons of energy greater than some threshold energy E linearly proportional to the sweep voltage. The energy resolution of this instrument varied from ±15% at 0.7 Mev to about ±6% at 3 Mev. A Van de Graaff accelerator was used in calibration.

The entrance aperture was calculated to be a cone of about 25° FWHM and the total geometrical factor was $A\Omega \approx 0.12$ cm^2 ster. The output circuit was a logarithmic count rate meter with an absolute dynamic range from 6×10^1 to 10^6 particles /cm^2-sec-ster.

The spectrometer output was sampled 6 times/sec, and the satellite spin frequency was about 1.1 rotation/sec. Thus pitch angle distributions with good angular resolution could also be obtained. Two sets of 3 axis flux gate magnetometers of different sensitivity were used for aspect determination.

RESULTS

Unidirectional Intensities

Figure 1 presents unidirectional intensities of electrons with energy $E \geq 1.0 \pm 0.1$ Mev for various regions of the radiation belts. The range of pitch angles included was $90^{\circ} \pm 10^{\circ}$ in the inner belt and $90^{\circ} \pm 20^{\circ}$ in the outer belt. The data are presented as intensity vs. L at a constant $\frac{B}{B_o}$ or, equivalently, at constant magnetic latitude λ, defined by

$$\frac{B}{B_o} = \frac{(1 + 3 \sin^2\lambda)^{1/2}}{\cos^6\lambda}$$

For in the inner belt, data from several orbits between 1 July and 20 August 1963 are shown. The variations in electron intensities for any given λ are consistent with expected statistical fluctuations.

In the outer belt, time variations of one to two orders of magnitude occurred during the observation period. The data included in Figure 1 are taken from orbits 25 and 26 of 3 July 1963 when the intensity level was high. Time variations were found to be correlated to magnetic disturbances and were more pronounced at higher L shells. These effects are discussed in a subsequent paper.

On the basis of the intensity curves of Figure 1, the isointensity contours of Figure 2 have been constructed in the polar geomagnetic coordinates λ and $R = L \cos^2 \lambda$. At the lower edge of the inner belt, the intensity is seen to fall rapidly from the upper to the lower limit of the range of the instrument between $R = 1.20$ and 1.14. Analogous isointensity contours in the outer belt reach below $R \approx 1.10$.

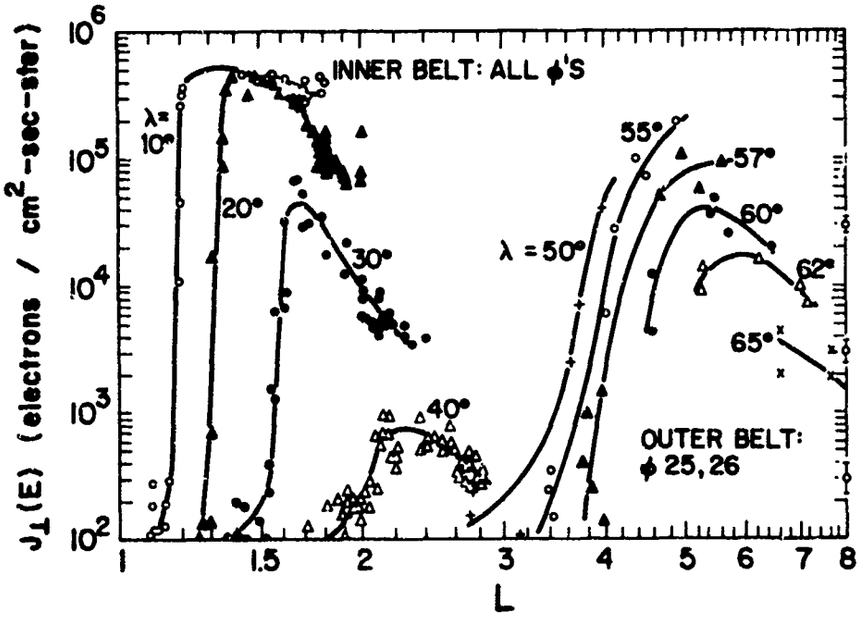

Fig. C1 Electron Fluxes at Various λ ($E \geq 1$ Mev).

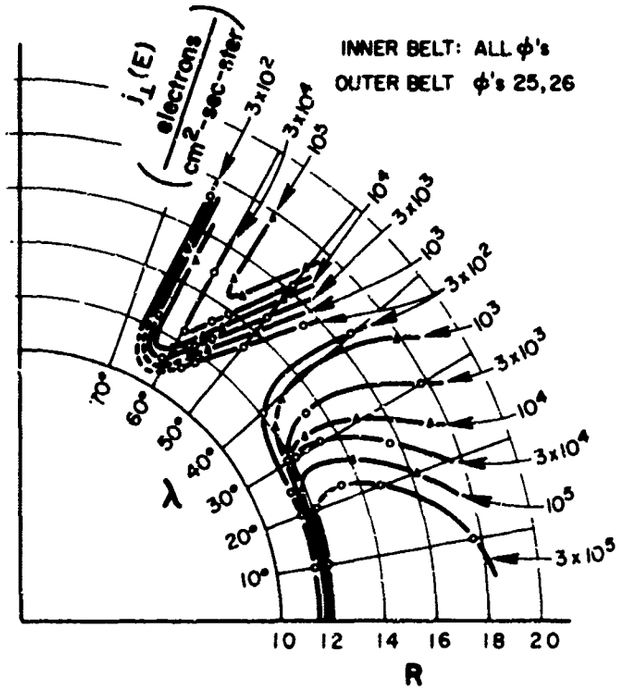

Fig. C2 Electron Iso-Intensity Contours ($E \geq 1$ Mev).

The value of R for which the minimum altitude is about 100 km varies from $R \approx 1.10$ at the magnetic equator, increasing to $R \approx 1.17$ for $\lambda \approx 30^{\circ}$ to 50°, and decreasing to $R = 1.10$ for $\lambda = 65^{\circ}$. A value of $R \approx 1.14$ is appropriate as the limit set by atmospheric scattering at the low edges of the inner and outer belt. The contours of the inner belt as shown in Figure 1 is roughly consistent with such a limit. On the other hand the outer belt is seen to penetrate into regions of (L, λ) which at some point around the earth are at altitudes where the particles must be dumped. (See also Forbush et al., 1962).

Pitch Angle Distributions

Figure 3 shows typical pitch angle distributions obtained in the inner and outer belt. The loss cone angles α given in each case are calculated on the basis of a cutoff at $R \approx 1.14$. The experimentally observed cutoff angles are in good agreement with the theoretically expected ones. The given distributions include data for electrons over the threshold range 0.7 - 1.0 Mev. Similar distributions are obtained for other threshold ranges between 0.7 and 4 Mev. The accuracy of the aspect determination ranges from a few degrees around 90° pitch angle to about ten degrees at 0° or 180°, thus adding little to the pitch angle uncertainty due to the 25° field of view of the instrument.

In the case of inner belt distributions, e.g., as in Figure 3, Curve B, there is a considerable background intensity within the loss cone. This background is very likely due to electrons of energy above ~ 10 Mev and/or protons over 65 Mev penetrating the shielding around the scintillator. Since the geometrical factor for such penetration is approximately $4.5\ cm^2 \times 2\pi$ ster $\approx 28\ cm^2$ ster against $A\Omega \sim 0.12\ cm^2$ ster of the instrument, an apparent background can be the result of a 250 times lower average intensity of penetrating particles. Observed backgrounds range from 10^4 to 10^5 / cm^2 sec ster so that penetrating particles must have intensities of about 50- 500/cm^2 sec ster. High energy protons ($E \geq 65$ Mev) are present in the

inner belt in comparable intensities (e.g., Valerio 1964 Freden and Paulikas 1964, Imhof and Smith 1964 and Freden and White 1959). Furthermore, extrapolation of observed electron spectra indicates the possible presence of electrons over ~ 10 Mev in comparable numbers as well.

In the outer belt, high energy protons are not present in substantial numbers and the electron spectra are considerably steeper so that the contribution from penetrating particles is negligible and the loss cones of the pitch angle distributions are essentially empty, as e.g., Figure 3, Curve C.

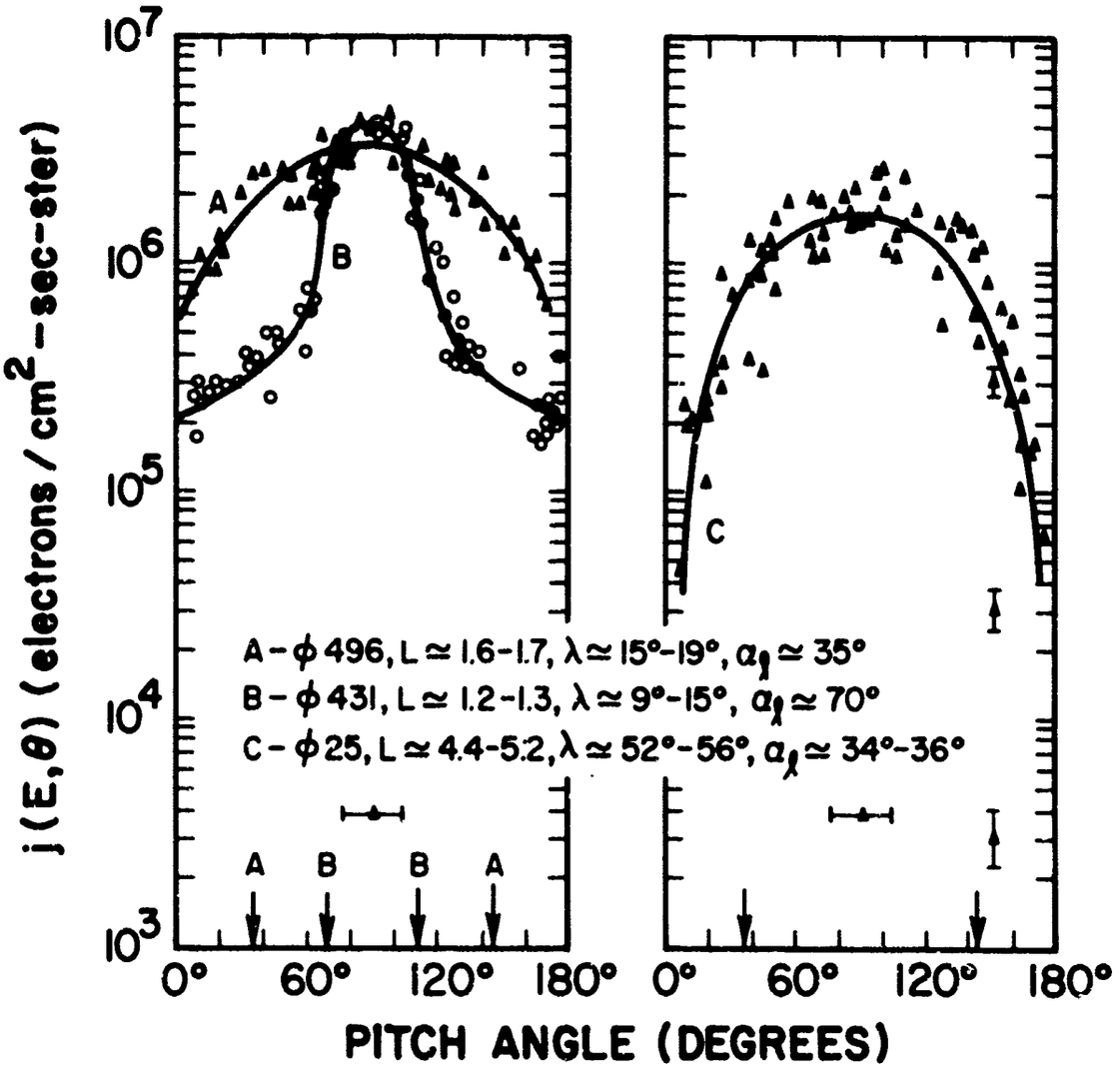

Fig. C3 Electron Pitch Angle Distribution (E ≥ 0.7 - 1.0 Mev).

Energy Spectra

Some typical integral spectra for different points in the radiation belts are displayed in Figure 4.

In the outer belt the measured spectra have approximately an exponential energy dependence $\exp(-E/E_o)$ with E_o between 0.30 Mev and 0.55 Mev at various regions and times. In the outer belt spectrum shown, Figure 4, Curve D, data points with pitch angles of $90^\circ \pm 20^\circ$ are included since the pitch angle distribution is flat in this range as Figure 3, Curve C illustrates.

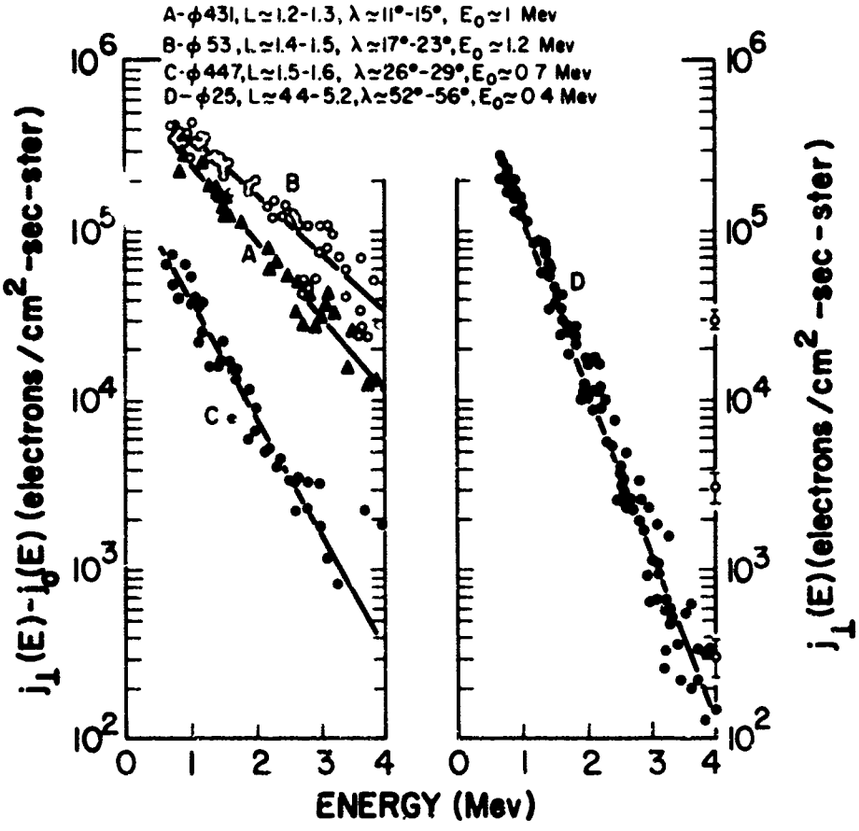

Fig. C4 Electron Integral Energy Spectra.

In the inner belt the shapes of the measured spectra are distorted because of the contamination by energetic particles penetrating the shielding around the scintillator. In order to correct for this background the unidirectional intensity within the loss cone ($j_o(E)$) was subtracted from the unidirectional intensity at 90° ($j_\perp(E)$). Thus the intensity at

pitch angles 75° - 105° was corrected by subtracting the intensity of the closest data point with pitch angle 0 - 30° or 150 - 180°. Some spectra obtained in this manner are given in Figure 4 (Curves A, B, and C). The resulting spectra are again approximately exponential with E_o between about 0.7 Mev and 1.2 Mev.

DISCUSSION

The intensity levels observed during the present experiment are in general agreement with previously available data. Maximum intensities for electrons $\geq$ 1 Mev in comparable regions of the outer belt ($\lambda \sim 50^{\circ} - 65^{\circ}$) given by Williams and Smith 1965, Paulikas and Freden 1964, and Mozer et. al. 1963 range from 10^4 to $10^5/cm^2$ sec ster, in good agreement with the present data Similar maximum intensity levels are reported in outer belt regions closer to the magnetic equator by Frank et. al. 1964, Frank et. al. 1963, Hoffman et al. 1962, and O'Brien et al. 1962.

The heart of the outer belt was located at higher magnetic shells, ($L \approx 4$ to 6), than previously observed ($L \approx 3$ to 5) e.g., by Explorer 7 in 1960 (Forbush et al, 1962).

Whenever spectral data in the outer belt are given (Williams and Smith 1965, Frank et al, 1964, Paulikas and Freden 1964, Mozer et al., 1963, Rosser et al., 1962) they roughly agree with the very steep spectra observed in this experiment, taking account of the somewhat different energy ranges and the accuracy of the data given in the mentioned references.

The inner belt intensity levels roughly agree with the available post Starfish data (Paulikas and Freden 1964, Van Allen et al., 1963, and Smith and Imhof 1963) with a peak intensity of $10^5 - 10^6/cm^2$ ster sec for electrons $\geq$ 1 Mev. The spectral slopes observed (0.7 Mev $\leq E_o \leq$ 1.2 Mev) are not much different from those of spectra observed immediately after the Starfish explosion (Hess 1963, Mozer et al., 1963, Smith and Imhof 1963, and Brown and Gabbe 1963).

Some directly measured pitch angle distributions near the horns of the outer belt are given by Cladis et al., 1961. Their measurements were taken at a lower altitude and consequently the distributions are considerably narrower than those presented here.

The general picture emerging from our present results can be summarized as follows.

Peak intensities varying with time from $10^4 - 10^5/cm^2$ sec ster for electrons above 1 Mev are found in the outer belt. Spectra are steep, with a shape $\exp(-E/E_o)$ where E_o varies from 0.3 to 0.55 Mev.

Inner belt electron intensities exceed $3 \times 10^5/cm^2$ sec ster for $E \geq 1$ Mev. Energy spectra are less steep with E_o ranging from 0.7 to 1.2 Mev.

Pitch angle distributions measured in various regions of the inner and outer belt have cutoffs consistent with the expected loss angles.

REFERENCES

1. Brown and Gabbe, JGR, 68 607 (1963).
2. Cladis, Chase, Imhof and Knecht, JGR 66 2297 (1961).
3. Frank, Van Allen, Whelpley and Craven, JGR 68 1573 (1963).
4. Frank, Van Allen and Hills, JGR 69 2171 (1964).
5. Freden and White, Phys. Rev. Let. 3 9 (1959).
6. Freden and Paulikas, JGR 69 1259 (1964).
7. Forbush, Pizzella and Venkatesan, JGR 67 3651 (1962).
8. Hess, JGR 68 667 (1963).
9. Hoffman, Arnoldy and Winckler, JGR 67 4543 (1962).
10. Imhof and Smith, JGR 69 91 (1964).
11. Mozer, Elliot, Mihalov, Paulikas, Vampola and Freden, JGR 68 641 (1963).
12. O'Brien, Laughlin, Van Allen and Frank, JGR 67 1209 (1962).
13. Paulikas and Freden, JGR 69 1239 (1964).
14. Rosser, O'Brien, Van Allen, Frank and Laughlin, JGR 67 4533 (1962).
15. Smith and Imhof, JGR 68 629 (1963).
16. Valerio, JGR 69 4949 (1964).
17. Van Allen, Frank and O'Brien, JGR 68 619 (1963).
18. Williams and Smith, JGR 70 541 (1965).

This is a preprint of a paper to be presented at the Forty-sixth Annual Meeting of the American Geophysical Union at Washington, D. C. on 19 - 22 April 1965.

ASE-915

Appendix D

EFFECT OF A SOLAR FLARE ON THE OUTER RADIATION BELT*

F. R. Paolini and G. C. Theodoridis

American Science and Engineering, Inc.
Cambridge, Massachusetts

and

Ludwig Katz

Air Force Cambridge Research Laboratories
Bedford, Massachusetts

*Work supported by the Air Force Cambridge Research Laboratories

EFFECT OF A SOLAR FLARE ON THE OUTER RADIATION BELT*

F. R. Paolini and G. C. Theodoridis

American Science and Engineering, Inc.
Cambridge, Massachusetts

and

Ludwig Katz

Air Force Cambridge Research Laboratories
Bedford, Massachusetts

ABSTRACT

The effect of the class 1^+ solar flare of 0734 UT 4 July 1963 on 0.7 to 4 Mev electrons and 1.5 to 4. Mev protons in the outer Van Allen belt was observed by the scintillation spectrometers flown on Hitch-hiker I. The outer belt was markedly depleted by this flare; at $(L, \lambda) \approx (5, 55^{\circ})$, electron intensities were reduced by more than an order of magnitude and proton intensities were reduced by about a factor of 3. Electron pitch angle distributions and electron and proton spectra observed following the flare and during the recovery period were similar in shape to those observed before. Electron intensities in this belt approached the pre-flare levels with a relaxation time of the order of 8 days. If one assumes a constant logarithmic loss mechanism and a constant source operative during the recovery period, a source strength of the order of 10^{13} erg/sec is implied for electrons of energy exceeding 1 Mev. The proton population of the outer belt recovered somewhat more slowly than the electron population. No perturbations in the inner belt, $L < 3$, were observed.

---

*Work supported by Air Force Cambridge Research Laboratories

BLANK PAGE

INTRODUCTION

The Air Force sub-satellite Hitch-hiker I was launched into a near polar orbit with perigee at 326 km and apogee at 4150 km on 1 July 1963. The orbit crossed the inner belt and the horns of the outer belt ($L \approx 3.5 - 8$, $\lambda \approx 50^{\circ} - 65^{\circ}$). The penetration into the outer belt was much deeper on the sunward side of the earth so that most of the data to be presented have been taken during local daytime.

This paper will examine time variations that occurred during the period around the class 1^{+} solar flare of 0734 U.T., 4 July 1963 (4th quadrant, 8° latitude, 79° to meridian). This flare was selected for study since it was well isolated in time. Prior activity consisted of two flares on 28 June (class 1^{+} in quadrant 4, class 3 in quadrant 1) and subsequent activity consisted of a flare on 25 July (class 1, quadrant 4). The magnetic variation A_p was 3 on 2 and 3 July, went up to 14 on 4 July and stayed at 10 - 20 until 10 July. There was auroral activity on 5 - 6 July and Thule Riometer activity on 5 July.

The data of this paper were obtained from the electron and proton scintillation spectrometers previously described. The energy range was 0.7 - 4 Mev for the electron, and 1.5 - 4 Mev for the proton, spectrometer. Integral energy spectra and pitch angle distributions were obtained from each instrument.

RESULTS

Electron Variations

The profiles of the outer belt shortly before and 25 to 54 hrs after the flare are shown in Figure 1. The unidirectional intensity of electrons above 1.0 ± 0.1 Mev at pitch angles $90^{\circ} \pm 20^{\circ}$, is plotted against L at various geomagnetic latitudes λ. The obtained curves are constant λ "cuts" through the portion of the outer belt crossed by the satellite.

The depletion of energetic electrons is apparent only for $L > 4$ and it ranges from about 1 order of magnitude at $L \approx 4.5$ to over two orders of magnitude for L greater than 5.5. In this way the peak of the belt is considerably shifted toward lower L's.

After the depletion, the electron intensity started to build up again until it essentially returned to the pre-storm level. The recovery process is illustrated in Figure 2 where the curve for $\lambda \approx 60^{\circ}$ is followed from about 10 hours before the flare until 270 hrs. later. The peak intensity is also traced through this period, and the recovery is seen to have a relaxation time of about 8 days. Provided that the whole outer belt is depleted in the same way as the observed region and with the assumption of a constant logarithmic loss mechanism, it is found that a source of electrons of the order of $10^{13} - 10^{14}$ ergs/sec must be present in order to account for the observed recovery time. Such a source could only be provided by the solar wind (energy density ~ 10^{20} ergs/sec) combined with an acceleration mechanism.

Electron pitch angle distributions observed in a given region before and after the flare, and during the recovery period, all remained constant in shape and consistent with the expected atmospheric cutoff. Figure 3 shows two such distributions taken 13 hrs. before and 60 hrs. after the flare. Although the intensities are considerably different, the shape of the distribution remains essentially unchanged.

Figure 4 shows electron integral energy spectra in given regions before and after the flare and during the recovery period. The spectral parameter E_o (for an $\exp(-E/E_o)$ energy dependence) changes from about 0.4 Mev to about 0.3 Mev after the flare returning later to 0.4 Mev. Since the very low intensity after the flare reduces the accuracy with which E_o can be determined, the observed change may not be significant.

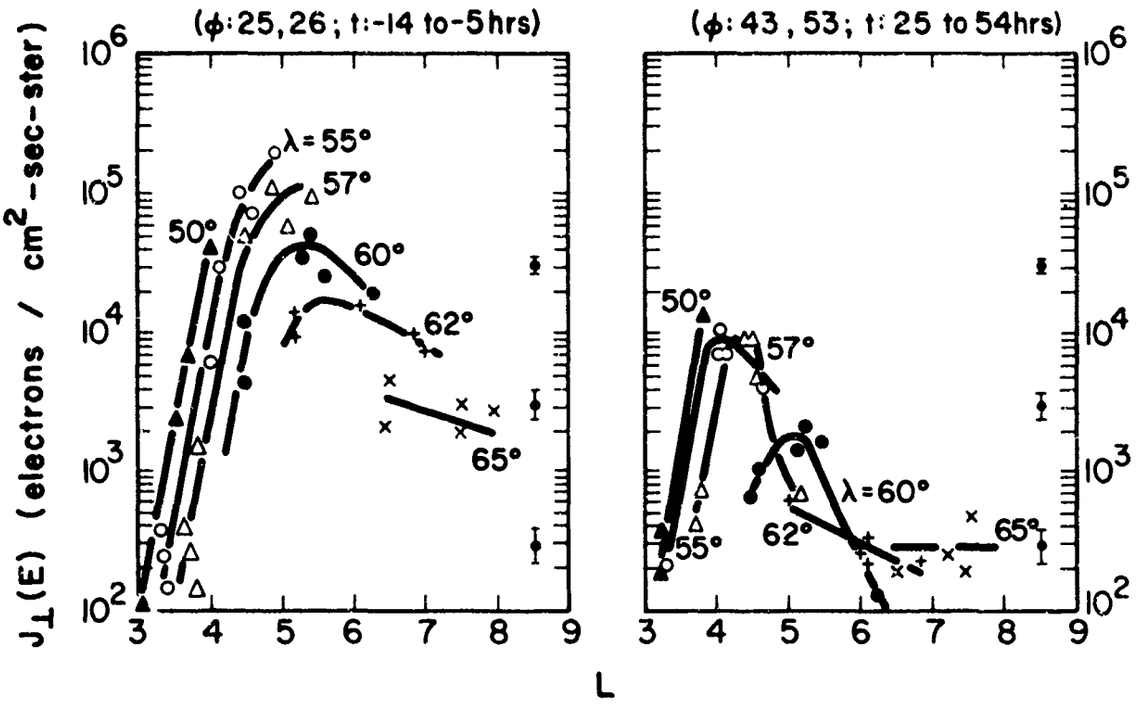

Fig. D1 Electron Fluxes in Outer Belt at Various λ (E ≥ 1 Mev).

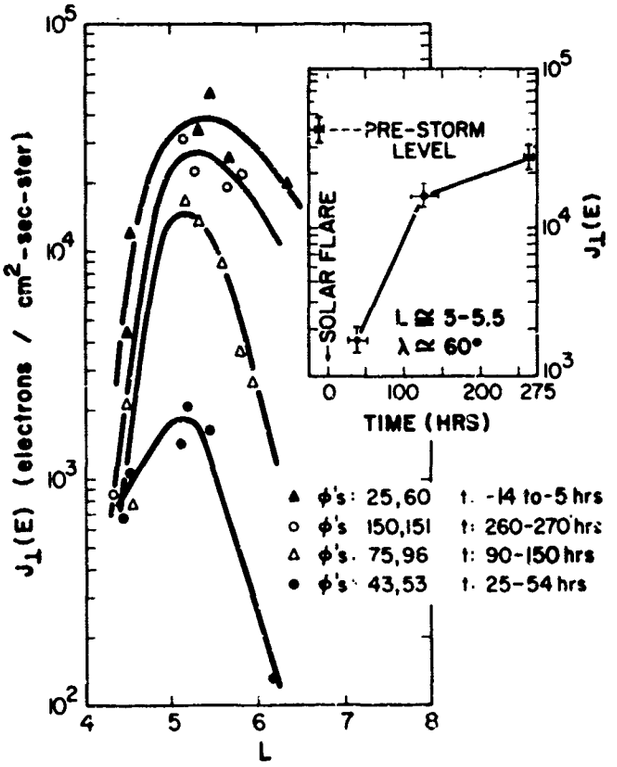

Fig. D2 Electron Fluxes in Outer Belt at Various Times (E ≥ 1 Mev, λ ≈ 60°).

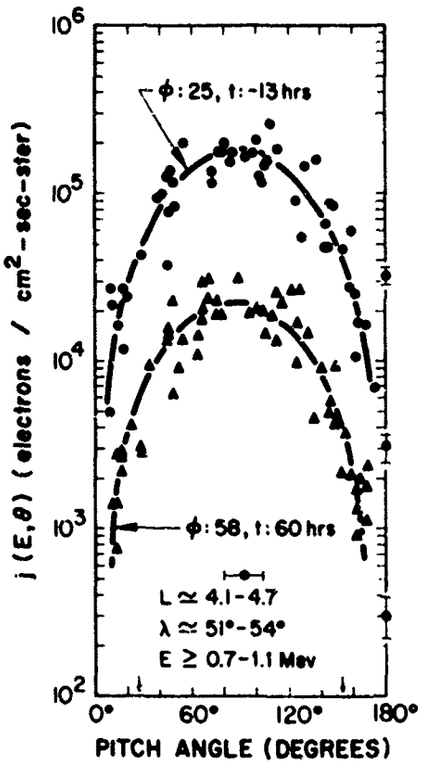

Fig. D3 Electron Pitch Angle Distributions in Outer Belt.

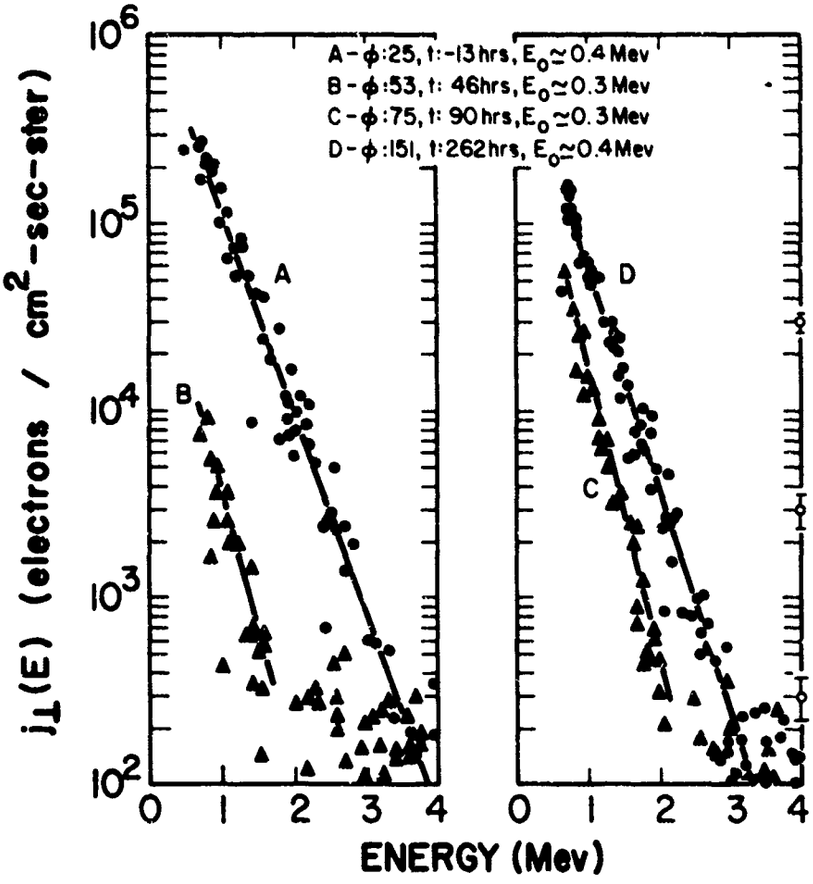

Fig. D4 Electron Integral Energy Spectra in Outer Belt at Various Times
($L \approx 4.6 - 5.3$, $\phi \approx 54^{\circ} - 59^{\circ}$)

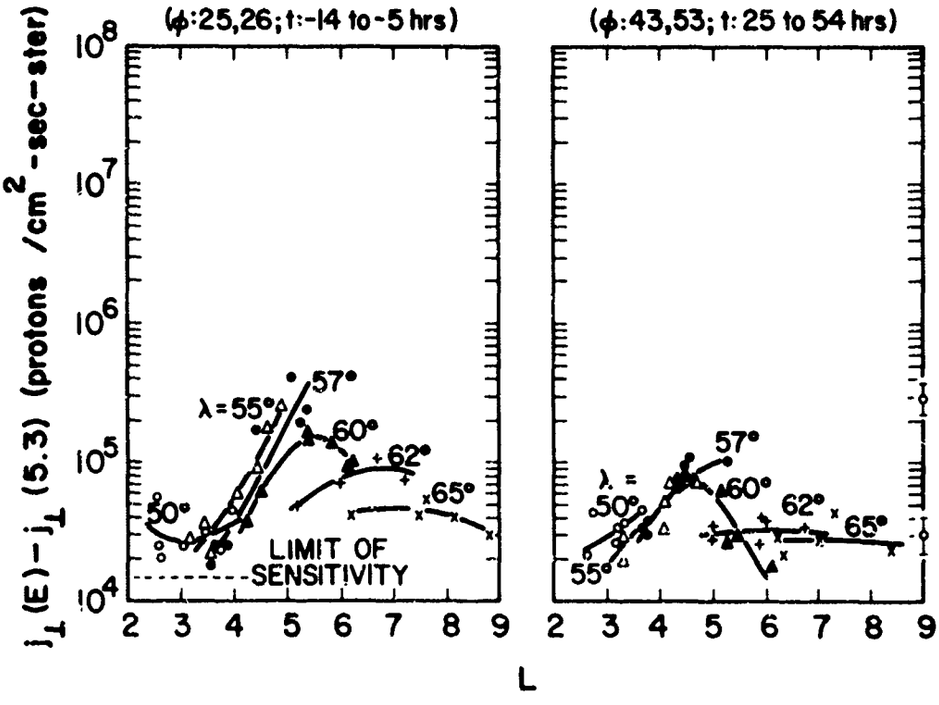

Fig. D5 Proton Fluxes in Outer Belt at Various λ ($E \geq 2$ Mev).

Proton Variation

The proton component of the outer belt appears to be affected to a considerably smaller degree than the electrons by the occurrence of the flare. The 2 - 5.3 Mev proton intensity profiles of the outer belt, as shown in Figure 5, show variations by factors of about 2 to 5 above $L \approx 4.5$. Although the measured proton intensities in the outer belt are only about an order of magnitude above the instrument limit of sensitivity, the qualitative difference of behavior from the energetic electrons is obvious.

Figure 6 displays proton spectra before and after the flare, and shows no significant change in shape.

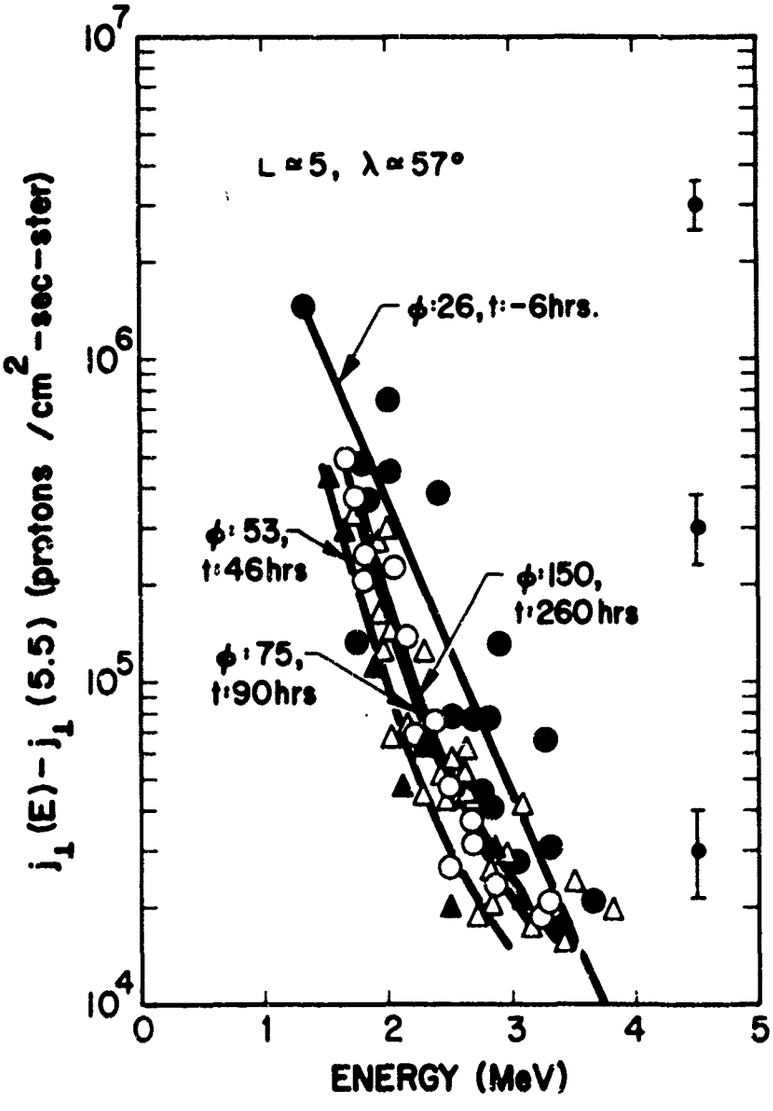

Fig. D6 Proton Integral Energy Spectra in Outer Belt at Various Times.

DISCUSSION

The marked effect of solar flares and the accompanying magnetic disturbance on the outer radiation belt have been observed on different occasions at high magnetic latitudes as well as close to the equator. Observations near the equator seem to agree on a pattern of a decrease in the intensity of energetic electrons ($E > 1$ Mev) around the time of the magnetic disturbance by factors ranging from less than 10 (Frank et al., 1964, Hoffman et al., 1962, Arnoldy et al., 1960) up to 1000 (Rosser, 1963). Subsequently, the intensities recover over a period of a few to several days, often going up to several times the pre-storm level (Freeman, 1964, Frank et al., 1964, Hoffman et al., 1962).

In the region of the horns of the outer belt, where the present observations were made, Forbush et al., 1962, have observed about a 10 fold intensity decrease for $L > 3.5$ while Williams and Smith (1965) have reported increases after magnetic disturbances, although their data seem to exhibit some decrease in the intensity of the hard electrons around the time of magnetic distrubances. Other flares and magnetic disturbances which occurred during the present observation period (1 July - 20 August 1963) were rather clustered in time so that a simple picture of each case is not apparent. A general trend, though, was that whenever an abrupt increase in magnetic disturbance occurred the energetic electron intensities in the outer belt tended to drop.

Considering the general pattern indicated by the quoted references, the presently observed severe post-flare drop in intensities at the horns of the outer belt seems to be part of a general depletion of the energetic electrons in the belt rather than a mere redistribution of magnetic shells in space.

Protons are seen to be depleted to a much smaller degree than the electrons. The relative constancy of the proton component was noticed by Frank et al. (1964) while Davis and Williamson (1963) reported some

enhancement of proton intensities in the outer belt at the time of a magnetic storm.

Different response of electrons and protons to magnetic disturbances might indeed be expected. It is quite conceivable, for instance, that electrons may be depleted preferentially over protons through scattering into the loss cone by means of hydromagnetic wave interactions. On the other hand, if particles are lost from the belt through magnetic lines broken at the periphery (Dessler and Karplus, 1961 and Anderson et al., 1965) the percentages of electrons and protons lost from a magnetic tube would be roughly inversely proportional to their respective mirroring periods ($t_e \approx 0.25 - 0.4$ sec and $t_p \approx 4 - 6$ sec) as long as the length of time for which the magnetic lines are broken is considerably smaller than the proton period t_p. Therefore, again, many more electrons than protons would escape out of the trapping region.

The 8 day recovery period observed after the flare is equal or longer than periods mentioned in the quoted papers. Therefore, the calculated loss of about $10^{13} - 10^{14}$ ergs/sec represents a minimum estimate of the required source strength. Clearly such an electron supply would have to originate in the solar wind ($\sim 10^{20}$ ergs/sec) coupled with an acceleration mechanism to account for the observed spectra.

The relatively constant shape of the measured integral spectra as well as the stability of the obtained pitch angle distributions are factors that will have to be taken into account in any explanation of the dynamics of the outer belt response to solar and magnetic activity.

REFERENCES

1. Anderson, Harris and Pauli, JGR 70 1039 (1965).

2. Arnoldy, Hoffman and Winckler, JGR 65 1361 (1960).

3. Davis and Williamson, Space Research, pp. 365-375, North Holland Publ. Co., Amsterdam (1963).

4. Dessler and Karplus, JGR 66 2289 (1961).

5. Frank, Van Allen and Hills, JGR 69 2171 (1964).

6. Forbush, Pizzella and Venkatesan, JGR 67 3651 (1962).

7. Freeman, JGR 69 1691 (1964).

8. Hoffman, Arnoldy and Winckler, JGR 67 4543 (1962).

9. Rosser, JGR 68 3131 (1963).

10. Williams and Smith, JGR 70 541 (1965).

Preprint of a manuscript submitted for publication in the Journal of Geophysical Research October, 1964.

ASE-646

Appendix E

MEASUREMENTS ON DIFFERENTIAL ENERGY SPECTRA OF ELECTRONS (15 TO 100 KEV) IN THE MAGNETOSPHERE

F. R. Paolini, R. Giacconi and J. R. Waters

American Science and Engineering, Inc.
Cambridge, Massachusetts*

and

L. Katz and D. Smart

Air Force Cambridge Research Laboratories
Bedford, Massachusetts

*Research sponsored by the Air Force Cambridge Research Laboratories, under contracts AF 19 (628) - 2392 and AF 19 (628) - 4207.

MEASUREMENTS ON DIFFERENTIAL ENERGY SPECTRA OF ELECTRONS (15 TO 100 KEV) IN THE MAGNETOSPHERE

F. R. Paolini, R. Giacconi and J. R. Waters

American Science and Engineering, Inc.
Cambridge, Massachusetts*

and

L. Katz and D. Smart

Air Force Cambridge Research Laboratories
Bedford, Massachusetts

ABSTRACT

Differential energy spectra of 15 to 100 kev electrons in the Earth's magnetosphere were obtained using an electrostatic analyzer (15% energy resolution) on board the Air Force Satellite Hitch-hiker I (1963-25B). Preliminary analysis of the data shows that electrons of these energies define a single belt extending from L less than 1.1 to beyond 7, with maximum intensities at L approximately 1.6. Differential spectra (acquired over a portion of the trajectory for which the magnetic field slowly increased from 0.24 to 0.29 gauss) exhibited intensity maxima in the vicinity of 40 kev for L less than about 4; in the region $4 < L < 7$, the differential spectra decreased monotonically from 15 kev.

*Research sponsored by the Air Force Cambridge Research Laboratories, under contracts AF 19 (628) - 2392 and AF 19 (628) - 4207.

Introduction

Interest in electrons of 10's of kev energy has been stimulated by the observations of O'Brien, et al., from instrumentation on Injun I and III satellites [O'Brien and Laughlin, 1962; O'Brien,1962; O'Brien, 1964] , of extensive continuous precipitation of electrons of these energies into the Earth's atmosphere. O'Brien [1964] points out that if the solar wind is the source of these particles, then there must be an accelerating mechanism for converting about 1% of the total energy in the average solar wind into the 10's of kev energies of the precipitated particles and suggests that spectral studies of 15 to 100 kev electrons may provide information on the accelerating mechanism. We present some data on the intensities and differential energy spectra of such electrons that confirm their widespread spatial distribution and further show their spectral variations with the parameter L.

Instrumentation

The electrostatic analyzer used a quadrant of a spherical capacitor to whose plates a linear high voltage sweep was applied to accomplish spectral analysis. The transmitted electrons were post-accelerated and detected in a 0.1 cm thick x 2.0 cm diameter plastic scintillator (coated with 2000 Å of evaporated aluminum for light shielding) with a photomultiplier (PM). Electronics fed by the PM measured its current, which was linearly proportional (after subtracting dark current) to the rate of energy deposition in the plastic. Particle intensities were derived from this quantity and the electron energy.

The energy to which the flight analyzer was set at any time was found to depend linearly upon the voltages (of equal magnitude, positive

and negative) applied to the plates. An electron gun, variable from 5 to 20 kev, was used in this calibration. The plate voltage was measured by calibrated circuitry (the sweep monitor) whose output range was compatible with the spacecraft telemetry system. Energy-voltage linearity above 20 kev was assumed to derive the final calibration curve expressing particle energy as a function of sweep monitor signal. The flight instrument spanned the range 10 to 105 kev. The resolution was measured to be 15 percent full-width at half-maximum (FWHM) at 20 kev and was assumed constant over the full range; the resolution function dropped off very sharply beyond the half-width.

The PM current meter, which had a logarithmic response, was independently calibrated using a laboratory current source. The correspondence between rate of energy deposition and current meter output was determined originally by a one-point normalization which used an accurately assayed Po^{210} source on the unshielded scintillator. An electron energy of 0.50 Mev was taken to be equivalent in light output to the 5.30 Mev Po^{210} alpha particle; this relation holds for anthracene [Birks, 1954] and was consistent with laboratory measurements on the plastic used. Another electrostatic analyzer, identical to the flight instrument, was later calibrated using the 20 kev electron gun; results agreed with the Po^{210} calibration within the $\pm$ 6 percent RMS fluctuations expected for the flight instrument at the same counting rate level. The dynamic range of the flight instrument's current meter corresponded to 4×10^4 (equivalent to the PM dark current) to 10^{10} kev/sec. The accuracy of the electron intensity (particles/cm^2sec ster) derived from the current meter signal varied from a $\pm$ 30 percent RMS fluctuation at very low intensities (because of particle counting statistics) to a minimum of about $\pm$ 6 percent RMS fluctuations at higher intensities (because of telemetry limitations).

The angular aperture of the flight analyzer was measured to be $8\ 1/2^{\circ}$ by 80° (FWHM); these values are consistent with the theoretical values expected from the spherical plate geometry. The area of the entrance aperture, determined by a rectangular hole in a grounded plane, was 1.18 cm^2. The transmission of the spherical capacitor was measured to be 95 percent at normal incidence for a mono-energetic beam at the proper energy. The net geometrical factor of the instrument was calculated to be 0.198 cm^2 ster from these figures.

The electrons were post-accelerated by 10 kev. Thus the rate of energy deposition I (kev/sec) measured by the instrument at an energy E (kev) is related to the detected electron energy differential counting rate dR/dE (electrons/sec-kev) by the expression

$$I = \int_{0.925E}^{1.075E} (E' + 10)\ \frac{(dR)}{dE^1} \approx 0.15E\,(E + 10)\,\frac{dR}{dE}$$

dR/dE may be related to an average differential intensity $\langle dj/dE \rangle$ (electrons/cm^2 sec ster kev) by dividing by the geometrical factor of 0.198 cm^2 ster; the averaging is thus over the pitch angle range spanned by the fan-shaped angular field of view of the instrument. The resulting relation

$$\langle dj/dE \rangle = 33.7\ I\ [\ E\,(E + 10)\,]^{-1}$$

was used in the reduction of the data of this paper.

The electrostatic analyzer was one of six particle detection instruments carried aloft by Hitch-hiker I. The other instruments are described elsewhere [Paolini, Giacconi, Waters, Katz, and Smart; 1964] . Hitch-hiker I was launched from an Agena vehicle at 0850 PDT, 1 July 1963, into

an elliptical polar orbit of 82.14° inclination. The orbital period was 132.6 minutes. The satellite was spin stabilized at 68 revolutions per minute. The data presented here identified by "ϕ25", were obtained from orbit 25, of 4 July 1963. Apogee of 4133 km occurred at 17° S latitude, 119° W longitude, at 0011:30 Universal Time (UT); perigee of 340 km occurred at 17° N latitude, 45° E longitude, at 0118:00 UT. Data identified by "ϕ20" were obtained from orbit 20 of 3 July, with apogee at 19° S latitude, 81° E longitude, at 1057:00 UT; and perigee at 18° N latitude, 116° W longitude, at 1203:00 UT.

The logarithmic current meter signal was sampled at 0.133 second intervals over 1.33 seconds of a 2.00 second commutator period. The sweep monitor was sampled once per commutator period. The photomultiplier high voltage, post-acceleration voltage, and B+ voltages were also monitored to check proper instrument functioning.

Data and Discussion

The raw data obtained were reduced by a computer and printed out. Figure 1 is a typical plot of the rate of energy deposition as a function of Universal Time (UT) given in seconds of day, for ϕ25. The variation in the signal produced by the satellite spin is clearly evident. The most surprising feature about this spin modulation is that only one maximum occurs per satellite spin period. (The spin period measured from telemetry radiation patterns is indicated in Figure 1.) This implies, since the satellite spin precession was negligible, that the pitch angle distribution was asymmetric about 90° and that consequently electron precipitation into the atmosphere must have been occurring.

Figures 2 and 3 present energy spectra acquired from the night portion of $\phi 25$, over the time interval (approximately) 3340 to 4550 seconds of 4 July. Ephemeris information pertaining to each spectrum is given in Table I. Two successive energy sweeps were analyzed for each spectrum shown, covering a time interval of about 25 seconds. The data points shown as open (first sweep) and filled circles (second sweep) are the maximum values in $<dj/dE>$ that were observed in each satellite revolution (corresponding to the points marked M in Figure 1); no interpolation in $<dj/dE>$ was attempted.

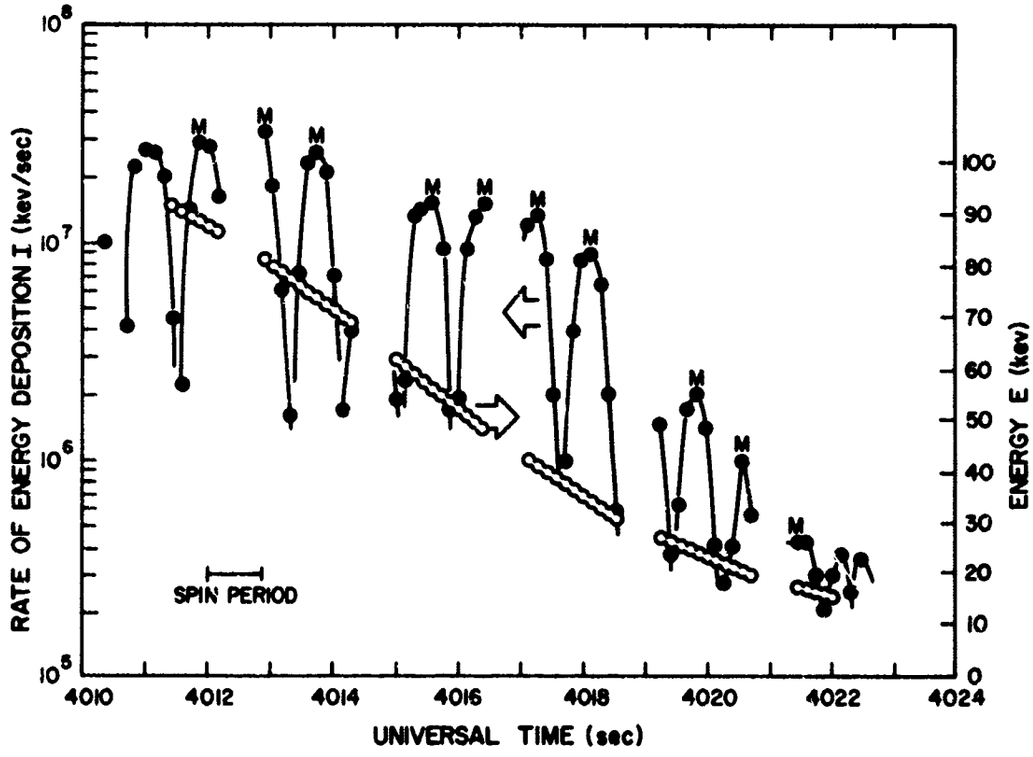

Fig. E1. Typical rate of energy deposition (kev/sec) in the electrostatic analyzer (filled circles) as a function of time. The points marked "M" are used to define a spectrum. Also shown (open circles) is the energy of the detected particles as a function of time.

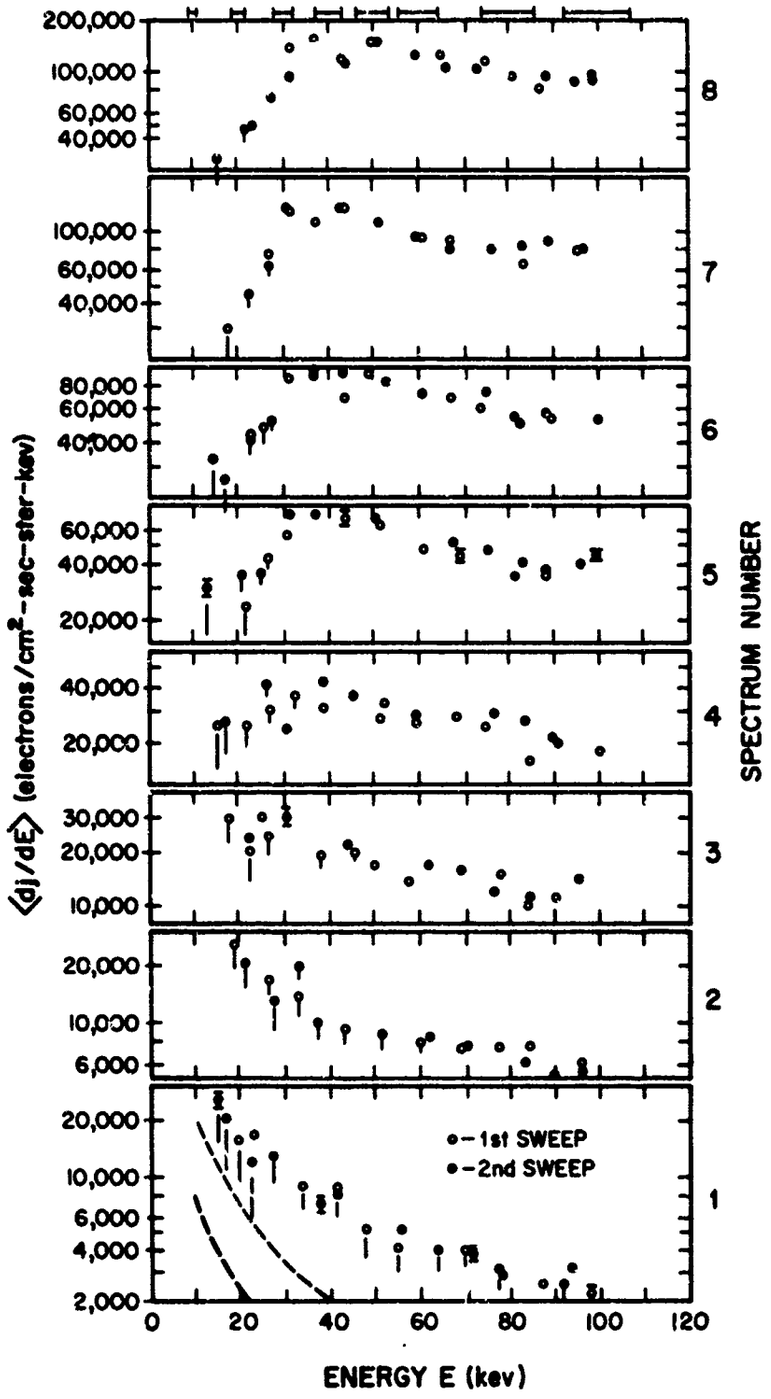

Fig. E2. Electron Spectra obtained over the UT interval (approx.) 3340 to 3940 seconds of day, 4 July 1963, ϕ 25. (B, L) coordinates vary from (0.235, 6.9) for Spectrum 1 to (0.250, 2.04) for Spectrum 8. The Spectrum Number refers to detailed ephemeris information given in Table I. The abscissa is electron energy (kev); the ordinates are peak values of the differential unidirectional flux <dj/dE> (electrons/cm^2-sec-ster-kev) observed during the satellite spin period. Two complete energy sweeps (about 25 seconds duration) were used to define each spectrum; points obtained from the earlier sweep are shown as open circles and those from the later sweep, as filled circles. For the explanation of other features in the figure, see the text.

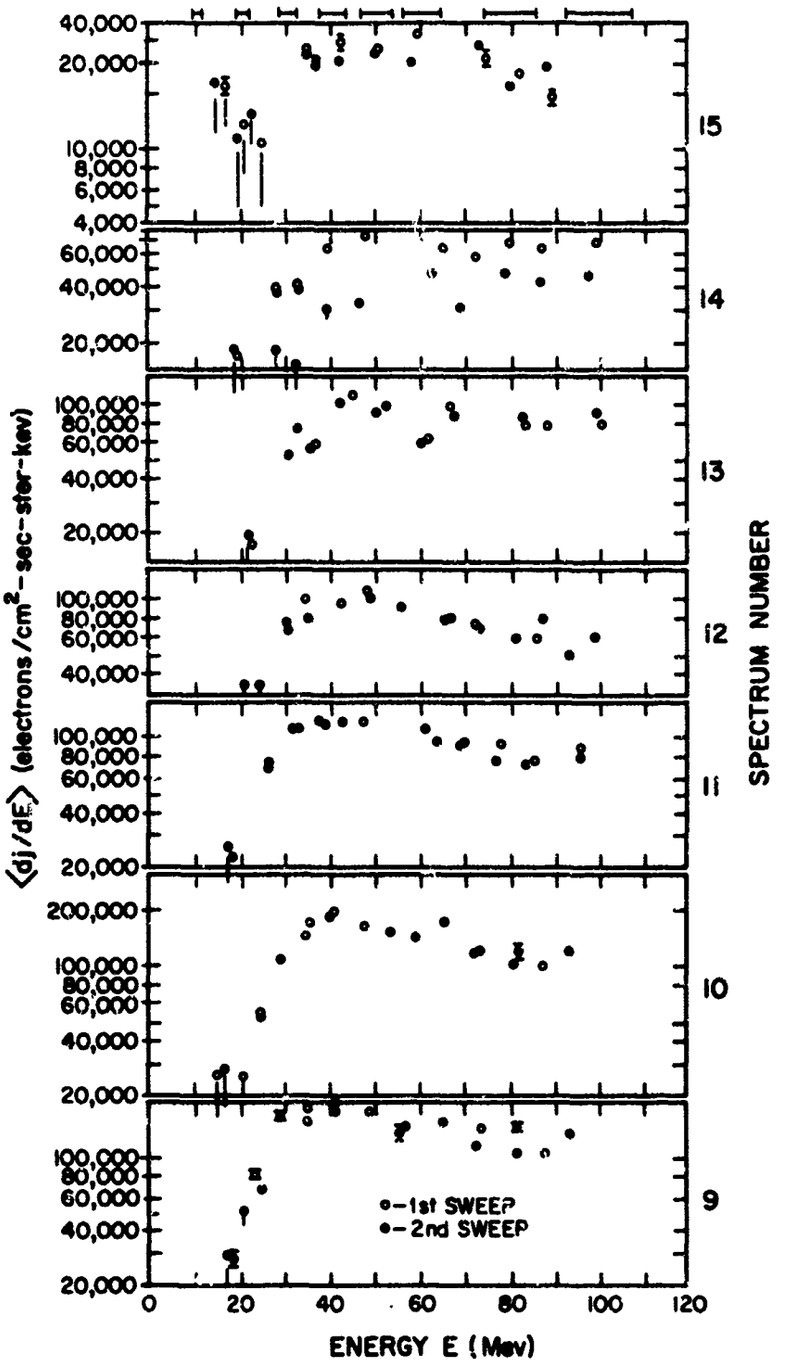

Fig. E3. Electron Spectra obtained over the UT interval (approx.) 4010 to 4540 seconds of day, 4 July 1963, ϕ 25. (B, L) coordinates vary from (0.255, 1.80) for Spectrum 9 to (0.293, 1.03) for Spectrum 15. Other features are as explained for Figure 2.

The heavy dashed curve in Figure 2 indicates the $<dj/dE>$ equivalent of the PM dark current measured prior to launch. The light dashed curve indicates the $<dj/dE>$ corresponding to the minimum current meter signal observed in the data analyzed; it therefore represents an upper limit to the PM dark current if one allows the possibility of its changing. The data points corrected for PM dark current are indicated in Figures 2 and 3 as vertical bars whose limits are the differences between the data points and the two dashed curves. The 15% FWHM energy resolution of the instrument is indicated by the horizontal bars on the upper abscissae. Data points were plotted versus linearly interpolated values of the energy E. Because of the method of data treatment, the scatter of the data points is often greater than the RMS fluctuations (indicated in the figures for sample points) expected a priori.

It is difficult to attach a precise physical significance to $<dj/dE>$ because of the fan-shaped segment of space viewed by the analyzer. If the pitch angle θ_o is defined with respect to a vector $\bar{n}$ in the center of the fan, and δ is the angle measured along the long dimension of the fan with respect to $\bar{n}$ ($-\delta_o \leq \delta \leq \delta_o$ where $\delta_o = 40^o$) then the analyzer views the range of pitch angles θ given by

$$\cos\theta = \cos\delta\cos\theta_o + \sin\delta\cos\gamma \quad (-\delta_o \leq \delta \leq \delta_o)$$

where γ is the angle between the magnetic field and the satellite spin axis. If the angular opening in the analyzer in the direction normal to the plane of δ is considered infinitesimal and dj/dE, the true unidirectional intensity, is a function of $\cos\theta$ only, then

$$<dj/dE> \approx [\ 2\sin\delta_o\ ]^{-1} \int_{-\delta_o}^{\delta_o} \frac{d}{dE}\left[\ j(\cos\delta\cos\theta_o + \sin\delta\cos\gamma)\right] d\sin\delta$$

expresses the approximate relationship between the plotted $<dj/dE>$ and dj/dE.

The angle γ (determined from a magnetometer) remained essentially constant throughout the time each spectrum was acquired and the maxima occurred at time intervals equal to the satellite spin period; the various $\langle dj/dE \rangle$ plotted therefore correspond to the same range of pitch angle. The energy dependence of dj/dE is thus investigated over an approximately constant range of pitch angles. It is not necessarily legitimate to compare spectra obtained from widely separated regions of space, however, since these will not all pertain to the same range of pitch angles. The following comments should be taken with reservations in view of these limitations.

The spectra of Figures 2 and 3 were obtained consecutively in time as the satellite cut through L shells at almost constant B (see Table I for precise information). Spectra 1, 2, and 3 show monotonic decreases in $\langle dj/dE \rangle$ with increasing energy E. Spectrum 4 shows $\langle dj/dE \rangle$ relatively flat with energy below about 40 kev. Spectrum 5 indicates a

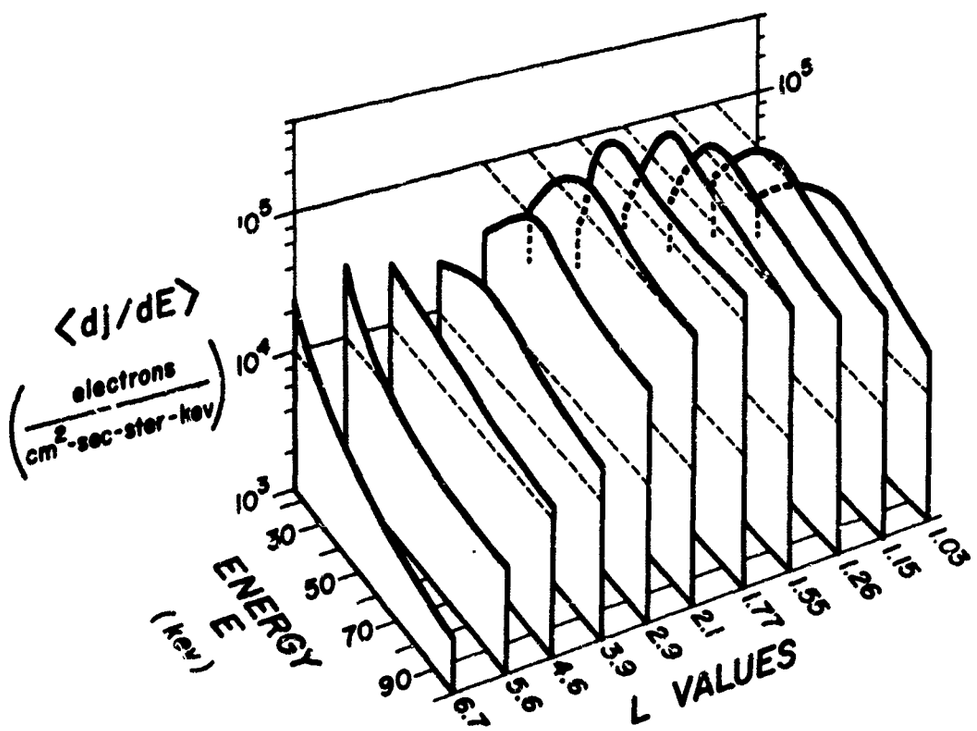

Fig. E4. Isometric representation of energy-differential unidirectional intensity $\langle dj/dE \rangle$ as a function of energy E and magnetic shell L. The smoothed curves were derived from selected spectra of Figures 2 and 3. The L-axis is not to scale. B increases slowly from 0.235 gauss at L ≈ 6.7 to 0.293 at L ≈ 1.03.

decrease in <dj/dE> below about 40 kev. The remaining spectra all exhibit this same characteristic. As L decreases from 6.86 (Spectrum 1) to 1.73 (Spectrum 9), the differential spectrum above 40 kev flattens, and the integral spectrum from 40 to 100 kev increases; there is no slot at these energies. As L decreases from 1.73 (Spectrum 9) to 1.14 (Spectrum 12), the 40 to 100 kev integral spectrum decreases. Spectrum 14 shows a very sudden change over the time of one energy sweep. The qualitative aspects of these spectra are perhaps more evident in Figure 4, which is an isometric representation of <dj/dE> as a function of both E and L.

Spectrum 15 shows an increase in <dj/dE> below about 20 kev, but this effect may not be real. Penetrating radiation (such as bremsstrahlung) which produces a constant rate of energy deposition (that is, independent of capacitor plate voltage) in the scintillator leads to an equivalent background spectrum of the same shape as the dashed curves in Figure 2. Such a background is most significant at low energies, and could cause the effect seen in Spectrum 15. If one extrapolates the electron energy spectrum (from the portion of Spectrum 15 above 40 kev) in order to calculate the rate of energy deposition from bremsstrahlung, a value as high as 6×10^5 kev/sec could be produced, assuming that all electrons were stopped in the satellite, and that the resulting bremsstrahlung was unattenuated. This number is about twice the rate of energy deposition observed at 20 kev in Spectrum 15. Bremsstrahlung background cannot therefore be ruled out as the cause of the apparent increase in <dj/dE> below about 20 kev. Other spectra, 5 and 6, may also have some bremsstrahlung contamination at low energies.

High energy electrons which penetrate the shielding around the analyzer's scintillator are not a likely cause of background. The minimum shielding is estimated to be about 5 g/cm^2 over 2 cm^2-ster.

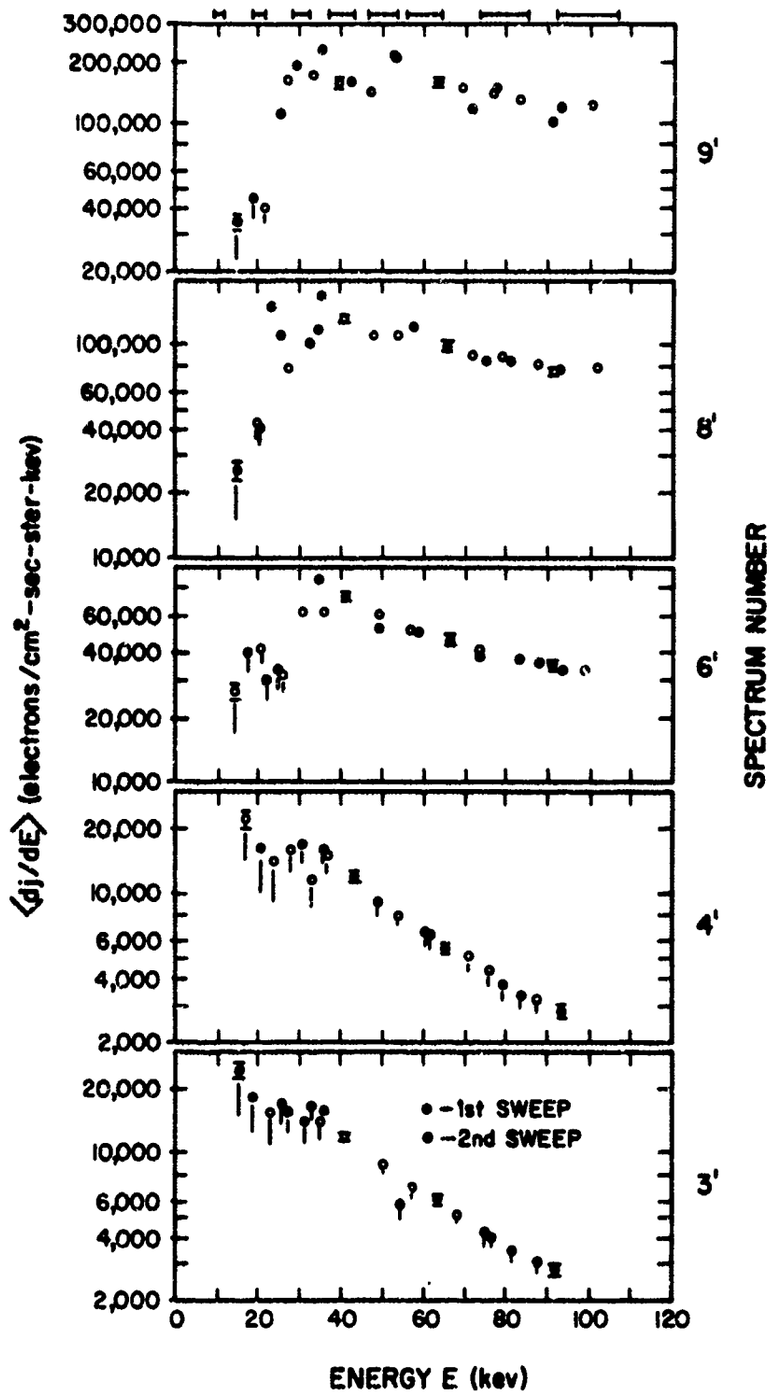

Fig. E5 Electron Spectra obtained over the UT interval (approx.) 42030 to 42500 seconds of day, 3 July 1963, ϕ 20. (B, L) coordinates vary from (0.280, 4.68) for Spectrum 3' to (0.285, 1.70) for Spectrum 9'. The numbers identifying the various spectra refer to detailed ephemeris information given in Table II. Other features are as explained for Figure 2.

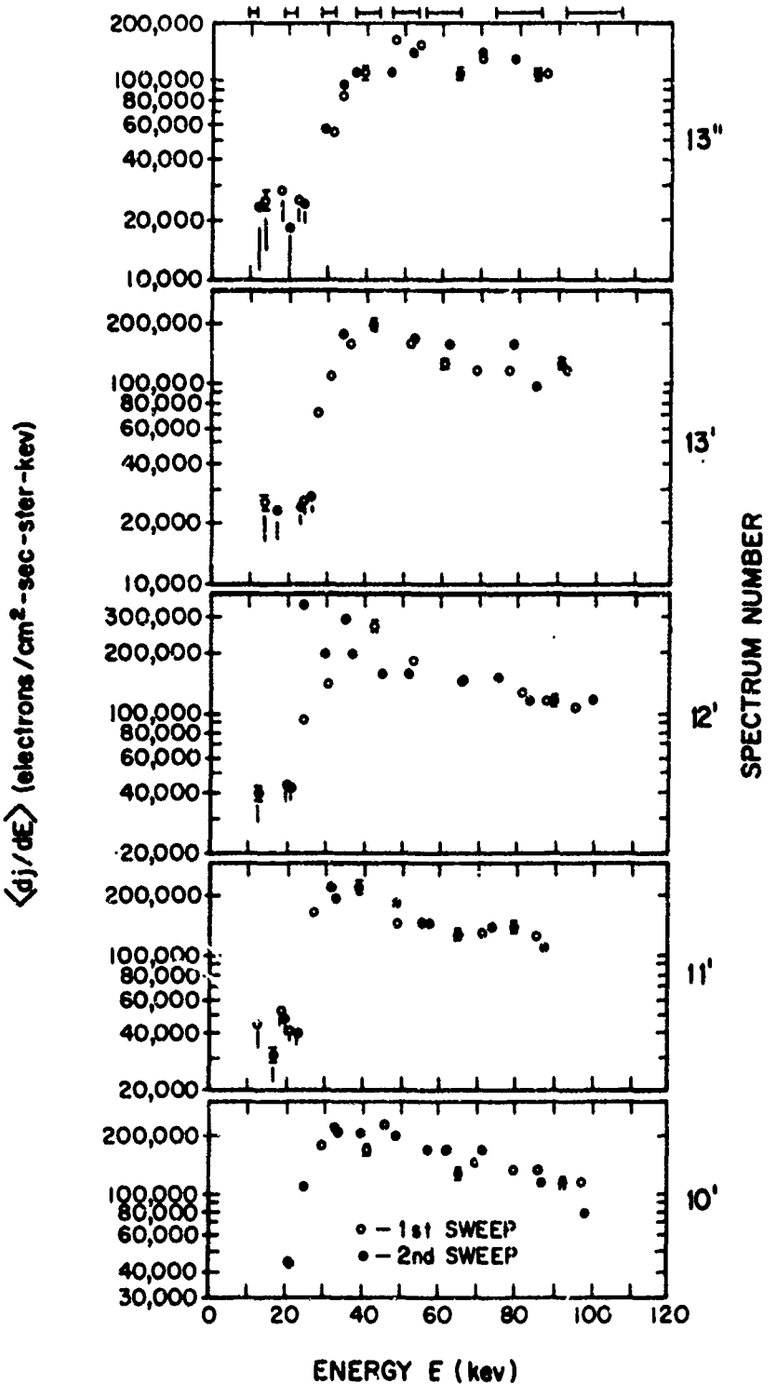

Fig. E6 Electron Spectra obtained over the UT interval (approx.) 42540 to 43250 seconds of day, 3 July 1963, ϕ 20. (B, L) coordinates vary from (0.283, 1.59) for Spectrum 10' to (0.302, 1.12) for Spectrum 13". Other features are as explained for Figure 5.

A unidirectional intensity of electrons (of energies exceeding 10 Mev) of the order of $7 \times 10^2/cm^2$-sec-ster would therefore be required to account for the observed effect. Such intensities at these energies have never been observed at $L \approx 1.04$, the shell in which Spectrum 15 was acquired.

Figures 5 and 6 present energy spectra acquired from the night portion of $\phi 20$, over the time interval (approximately) 42030 to 43250 seconds of 3 July. Precise ephemeris information pertaining to each spectrum is given in Table II. Data were treated in the same way as for $\phi 25$ data. Each spectrum of Figures 5 and 6 is identified by a number corresponding to the $\phi 25$ spectrum which is closest in L value. Corresponding spectra differ in B by as much as 16 percent, in altitude by as much as 30 percent, and in longitude by more than 160°. For these reasons, and for the reason mentioned earlier regarding the different ranges of pitch angle scanned by the fan-shaped field of view of the analyzer in different regions of space, corresponding spectra cannot be expected to agree in detail. In fact, 3' and the tail of 4' are steeper than 3 and 4, respectively; and maximum intensity of 6' is less than that of 6; and Spectra 10', 11', 12', 13', and 13" all exhibit maximum intensities greater than their counterparts by a factor of roughly 2. Nevertheless, the qualitative agreement between the two sets of spectra from orbits a half day apart is striking, and attests to the stability of the 15 to 100 kev radiation belt.

Comparison with Other Experiments

The State University of Iowa (SUI) group - Frank, Laughlin, O'Brien, Rosser and Van Allen, have previously made measurements [O'Brien and Laughlin, 1962; O'Brien, Van Allen, Laughlin and Frank, 1962; O'Brien, 1962; O'Brien, Laughlin, Van Allen and Frank, 1962; Rosser, O'Brien, Van Allen, Frank and Laughlin, 1962] from Injun I and Explorer XII

TABLE I

♦ 25 EPHEMERIS DATA: 15-100 KEV ELECTRON SPECTRA

	Initial Values						Final Values					
Spectrum	Time (sec)	Lat. (deg)	Long. (deg)	Alt. (km)	B (gauss)	L	Time (sec)	Lat. (deg)	Long. (deg)	Alt. (km)	B (gauss)	L
1	3346.35	-66.2	29.6	1681.6	0.235	6.9	3371.37	-65.0	30.5	1643.0	0.235	6.5
2	3426.49	-62.3	32.2	1558.4	0.236	5.8	3449.71	-61.1	32.9	1522.9	0.237	5.5
3.	3519.58	-57.5	34.5	1417.0	0.237	4.74	3543.06	-56.3	35.0	1381.7	0.238	4.51
4	3597.50	-53.4	36.0	1300.8	0.238	4.01	3623.00	-52.0	36.4	1263.3	0.239	3.81
5	3678.10	-48.9	37.2	1183.4	0.239	3.40	3703.10	-47.5	37.6	1147.8	0.240	3.23
6	3743.55	-45.2	38.1	1090.9	0.241	2.98	3769.11	-43.7	38.4	1055.5	0.241	2.84
7	3824.45	-40.4	39.0	980.7	0.243	2.54	3847.91	-39.0	39.2	949.7	0.244	2.43
8	3916.41	-34.9	39.8	862.2	0.248	2.14	3942.01	-33.3	40.0	830.6	0.250	2.04
9	4010.17	-29.0	40.5	750.2	0.255	1.80	4033.58	-27.5	40.7	723.9	0.257	1.73
10	4090.00	-23.8	41.1	663.2	0.262	1.58	4113.39	-22.2	41.2	639.3	0.264	1.52
11	4234.18	-14.1	42.0	528.4	0.272	1.28	4258.29	-12.5	42.1	509.0	0.274	1.24
12	4313.09	-8.7	42.4	468.5	0.276	1.17	4337.11	-7.0	42.6	452.3	0.278	1.14
13	4391.94	-3.1	42.9	419.5	0.280	1.093	4416.12	-1.4	43.0	406.6	0.282	1.078
14	4444.74	0.6	43.2	392.8	0.284	1.063	4469.02	2.4	43.3	382.3	0.286	1.052
15	4511.13	5.4	43.5	366.9	0.290	1.037	4535.57	7.1	43.7	359.5	0.293	1.030

Note: Longitude East is +

TABLE II

♦ 20 EPHEMERIS DATA: 15-100 KEV ELECTRON SPECTRA

	Initial Values						Final Values					
Spectrum	Time (sec)	Lat (deg)	Long (deg)	Alt. (km)	B (gauss)	L	Time (sec)	Lat (deg)	Long. (deg)	Alt. (km)	B (gauss)	L
3'	42031.70	-65.6	-130.3	1697.2	0.280	4.68	42055.14	-64.5	-129.5	1658.0	0.281	4.37
4'	42071.89	-63.7	-128.9	1632.3	0.282	4.17	42094.64	-62.6	-128.3	1597.3	0.284	3.91
6'	42204.51	-57.0	-125.6	1429.9	0.289	2.97	42230.12	-55.7	-125.1	1391.4	0.290	2.80
8'	42366.06	-48.3	-122.9	1191.3	0.290	2.12	42391.18	-46.9	-122.6	1155.4	0.290	2.03
9'	42473.42	42.1	-121.7	1040.6	0.287	1.76	42498.84	-40.6	-121.4	1006.2	0.285	1.70
10'	42541.32	-38.1	-121.0	949.7	0.283	1.59	42566.82	-36.6	-120.8	916.6	0.281	1.54
11'	42731.62	-26.2	-119.5	718.8	0.266	1.27	42755.04	-24.7	-119.3	693.2	0.264	1.24
12'	42824.25	-20.1	-118.9	621.9	0.258	1.17	42850.04	-18.4	-118.7	597.1	0.256	1.15
13'	43052.57	-4.5	-117.6	438.5	0.259	1.072	43076.08	-2.8	-117.4	424.7	0.262	1.072
13"	43225.47	7.8	-116.6	360.6	0.295	1.12	43248.99	9.5	-116.5	354.5	0.302	1.12

Note: Longitude East is +

satellites on electrons of energies above 40 kev. Using a two-channel magnetic spectrometer, covering about 40 to 60 kev in one channel, 80 to 110 in the other, they found [O'Brien and Laughlin, 1962; O'Brien, Van Allen, Laughlin and Frank, 1962] that outer belt omni-directional intensities, within 20° of the geomagnetic Equator, were at most 10^{8} particles/cm^{2}sec and generally of the order of 10^{7} particles/cm^{2}sec in these ranges. We can compare these numbers with calculations based on the data of Spectrum 4, which represents our closest approach to the Equator while still in the outer belt. Assuming an isotropic angular distribution, we obtain an upper limit to the omni-directional intensity of about 6×10^{6} particles/cm^{2}sec over the range 40 to 60 kev, and about the same value of the range 80 to 110 kev. The numbers are not inconsistent in view of the limitations previously pointed out. It is also interesting to note that the maximum intensities observed (Spectrum 9) lead to values of about 4×10^{7} particles/cm^{2}sec.

The SUI group also stated [O'Brien and Laughlin, 1962] that a wide spread in spectral slopes from 40 to 110 kev could be deduced from their data (assuming a power law spectrum) and pointed out that there was a tendency to a steeper slope as L increased. The data of this paper, although taken in different regions of the magnetosphere, support this statement. The SUI group [O'Brien and Laughlin, 1962; O'Brien, 1962] furthermore obtained angular distributions of electrons of energy above 40 kev which conclusively showed dumping: as mentioned, the spin modulation of the electrostatic analyzer signals implies that dumping must have been occurring during the acquisition of all spectra presented.

At 1000 km altitude, between magnetic latitudes 45° to 75°, the SUI magnetic spectrometer gave typical intensities of 10^{6} particles/cm^{2}

sec ster in the 40 to 60 kev [O'Brien, Laughlin, Van Allen and Frank, 1962] channel and about half this in the 80 to 110 kev channel with maxima of 2×10^6 and 8×10^5, respectively. Taking the data of Spectrum 6 (1090 km, magnetic latitude approximately 45° S), there results about 1.5×10^6 electrons/cm^{2}sec ster for each range. The values are consistent. We may make some comparison with the data of the 213 Geiger tube flown on Injun I [O'Brien, Laughlin, Van Allen and Frank, 1962] which gave typical intensities of 10^5 to 10^6 electrons/cm^{2}sec ster with a peak of 4×10^6, for electrons of energies exceeding 40 kev. Again using Spectrum 6, and fitting an exponential shape $\langle dj/dE \rangle \approx 1.3 \times 10^5 \exp(-0.01E)$ above 40 kev, we obtain about 9×10^6 electrons/cm^2 sec ster for $E \geq 40$ kev, not inconsistent with their Geiger tube results in view of the assumption regarding the spectrum shape.

Remarks

Our data give for the first time well-resolved electron spectra over the range 15 to 100 kev, and evidence of maxima in differential energy spectra in the vicinity of 40 kev. Furthermore, the spectra are stable in a time scale of the order of a day. The data on integral fluxes presented here are consistent with similar data obtained by other investigators.

The maxima observed may simply be representative of the higher scattering cross-sections for lower energy particles.

Further analysis will examine time variations in the spectra, especially those obtained in the auroral regions. Correlations with solar activity will be sought. A class 3 flare occurred on 28 June and a class 1+ on 4 July (after the data of this paper were acquired); data from orbits earlier than 20 and later than 25 may show significant changes.

REFERENCES

Birks, J. B., "Scintillation Counters", p. 82, Pergammon Press, Ltd., London (1954).

O'Brien, B. J., "Direct Observation of Dumping of Electrons at 1000 Kilometer Altitude and High Latitudes", J. Geophys. Research 67, 1227 (1962).

O'Brien, B. J., "High Latitude Geophysical Studies with Satellite Injun 3. 3. Precipitation of Electrons into the Atmosphere", J. Geophys. Research 69, 13 (1964).

O'Brien, B. J., Laughlin, C. D., "Electron Precipitation and the Outer Radiation Zone", Space Research III, p. 399 (Proceedings of the Third International Space Science Symposium, Washington, April 30 - May 9,1962), North Holland Publishing Company, Amsterdam (1963).

O'Brien, B. J., Laughlin, C. D., Van Allen, J. A., Frank, L. A., "Measurements of the Intensity and Spectrum of Electrons at 1000 Kilometer Altitude and High Latitudes", J. Geophys. Research 67, 1209 (1962).

O'Brien, B. J., Van Allen, J. A., Laughlin, C. D., Frank, L. A., "Absolute Electron Intensities in the Heart of the Earth's Outer Radiation Zone", J. Geophys. Research 67, 397 (1962).

Rosser, W. G. V., O'Brien, B. J., Van Allen, J. A., Frank, L. A., Laughlin, C. D., "Electrons in the Earth's Outer Radiation Zone", J. Geophys. Research 67, 4533 (1962).

Paolini, F. R., Giacconi, R., Waters, J. R., Katz, L., Smart, D., "Measurements in the Radiation Belts from Hitch-hiker I", Space Research V (Proceedings of the Fifth International Space Science Symposium, Florence, Italy, May 12 - 16, 1964) North Holland Publishing Company, Amsterdam (To be published 1964).

Unclassified
Security Classification

DOCUMENT CONTROL DATA - R&D

(Security classification of title, body of abstract and indexing annotation must be entered when the overall report is classified)

1. ORIGINATING ACTIVITY *(Corporate author)*
American Science and Engineering, Inc
11 Carleton Street, Cambridge, Mass 02142

2a. REPORT SECURITY CLASSIFICATION
Unclassified

2b. GROUP

3. REPORT TITLE
THE ENERGETIC CHARGED PARTICLE ENVIRONMENT OF THE EARTH (HITCH-HIKER I DATA ANALYSIS)

4. DESCRIPTIVE NOTES *(Type of report and inclusive dates)*
Final Scientific Report Period covered: 15 May 1964-14 August 1965

5. AUTHOR(S) *(Last name, first name, initial)*
Paolini, Frank R.; Theodoridis, George C.; Bate, Michael

6. REPORT DATE	7a. TOTAL NO. OF PAGES	7b. NO. OF REFS
13 September 1965	151	6

8a. CONTRACT OR GRANT NO.	9a. ORIGINATOR'S REPORT NUMBER(S)
AF19(628)-4207	
b. PROJECT AND TASK NO. 0000-24	ASE-1056
c. DOD ELEMENT 61430014	9b. OTHER REPORT NO(S) *(Any other numbers that may be assigned this report)*
d. DOD SUBELEMENT 6801/850F/0000	AFCRL-65-692

10. AVAILABILITY/LIMITATION NOTICES Qualified requestors may obtain copies of this report from DDC. Other persons or organizations should apply to the Clearinghouse for Federal Scientific and Technical Information (CFSTI), Sills Bldg., 5285 Port Royal Rd., Springfield, Virginia 22151.

11. SUPPLEMENTARY NOTES This research was supported by the Air Force In-House Laboratory Independent Research Fund.

12. SPONSORING MILITARY ACTIVITY
Hq. AFCRL, OAR (CRF)
United States Air Force
L. G. Hanscom Field, Bedford, Mass.

13. ABSTRACT

The results of the reduction and analysis of data obtained from instrumentation flown on the Air Force Satellite Hitch-hiker I (1963-25B) are presented. The instrumentation included two electrostatic analyzers (one for electrons, 15 to 100 kev, the other for protons, 15 to 100 kev); a scintillation spectrometer (for electrons, 0.7 to 4.0 Mev); a phoswich scintillation spectrometer (for protons 1. to 5. Mev and 7.5 to 120 Mev); and a Geiger counter (electrons greater than 4. Mev, protons greater than 40 Mev). Detailed data on integral energy spectra, pitch angle distributions, and perpendicular unidirectional intensities, as functions of B, L (or λ, L) and time are given in five papers appended to this report. No substantial intensities of protons, 15 to 100 kev, were observed. Electrons, 15 to 100 kev, were observed with intensities as great as $2 \times 10^5/cm^2$-sec-ster-kev, at 40 kev, but the anomalous angular distributions obtained cast doubt on the credibility of these data. Peak inner belt intensities for electrons above 1 Mev were about 5×10^6 electrons/cm^2sec ster at $L \approx 1.6$. Spectra were of the shape $\exp(-E/E_o)$, with $0.7 \leq E_o \leq 1.2$ Mev. Outer belt intensities fluctuated substantially, with severe depletions at times of magnetic and solar activity, and

DD FORM 1 JAN 64 1473

(continued on additional page)

Unclassified
Security Classification

subsequent recoveries in periods of a few to several days. Maximum observed intensities of electrons above 1 Mev at the horns of the outer belt at L ≈ 4.5 were about 10^5 electrons/cm^2 sec ster. Loss of outer belt electrons through dumping at high latitudes in the Anomaly was detected at rates up to 2×10^{11} ergs/sec. Outer belt spectra between 0.7 and 4 Mev were also approximately exponential, with $E_o = 0.4 \pm 0.1$ Mev. No drastic spectral shape changes were seen accompanying the observed intensity variations. The protons defined two belts, with hearts at L ~ 1.6 and L ~ 4.5, and a slot at L ~ 3.0. The integral spectra observed were all similar in shape, with approximately an exponential energy dependence. The spectra tended to be much steeper than electron spectra in the same energy range in the inner belt. Typical measured omnidirectional intensities for energy E > 2 Mev were $10^8/cm^2$ sec at $(L, \lambda) \approx (1.6, 8^o)$ and $2 \times 10^6/cm^2$sec at $(L, \lambda) \approx (4.5, 55^o)$, higher than values of other observers, for reasons which appear to be instrumental. All electron and proton pitch angle distributions observed with the scintillation spectrometers were peaked at 90° and had cutoffs consistent with theory. Data on electrons 0.7 to 4. Mev and protons 1.5 to 4. Mev are summarized in the main body as iso-intensity contours of perpendicular unidirectional intensities on rectangular B, L plots.

al

14. KEY WORDS	LINK A		LINK B		LINK C	
	ROLE	WT	ROLE	WT	ROLE	WT
trapped radiation Van Allen Belts Magnetospheric charged particle measurements Hitch-hiker I data						

INSTRUCTIONS

1. ORIGINATING ACTIVITY: Enter the name and address of the contractor, subcontractor, grantee, Department of Defense activity or other organization *(corporate author)* issuing the report.

2a. REPORT SECURITY CLASSIFICATION: Enter the overall security classification of the report. Indicate whether "Restricted Data" is included. Marking is to be in accordance with appropriate security regulations.

2b. GROUP: Automatic downgrading is specified in DoD Directive 5200.10 and Armed Forces Industrial Manual. Enter the group number. Also, when applicable, show that optional markings have been used for Group 3 and Group 4 as authorized.

3. REPORT TITLE: Enter the complete report title in all capital letters. Titles in all cases should be unclassified. If a meaningful title cannot be selected without classification, show title classification in all capitals in parenthesis immediately following the title.

4. DESCRIPTIVE NOTES: If appropriate, enter the type of report, e.g., interim, progress, summary, annual, or final. Give the inclusive dates when a specific reporting period is covered.

5. AUTHOR(S): Enter the name(s) of author(s) as shown on or in the report. Enter last name, first name, middle initial. If military, show rank and branch of service. The name of the principal author is an absolute minimum requirement.

6. REPORT DATE: Enter the date of the report as day, month, year, or month, year. If more than one date appears on the report, use date of publication.

7a. TOTAL NUMBER OF PAGES: The total page count should follow normal pagination procedures, i.e., enter the number of pages containing information.

7b. NUMBER OF REFERENCES: Enter the total number of references cited in the report.

8a. CONTRACT OR GRANT NUMBER: If appropriate, enter the applicable number of the contract or grant under which the report was written.

8b, 8c, & 8d. PROJECT NUMBER: Enter the appropriate military department identification, such as project number, subproject number, system numbers, task number, etc.

9a. ORIGINATOR'S REPORT NUMBER(S): Enter the official report number by which the document will be identified and controlled by the originating activity. This number must be unique to this report.

9b. OTHER REPORT NUMBER(S): If the report has been assigned any other report numbers *(either by the originator or by the sponsor)*, also enter this number(s).

10. AVAILABILITY/LIMITATION NOTICES: Enter any limitations on further dissemination of the report, other than those imposed by security classification, using standard statements such as:

(1) "Qualified requesters may obtain copies of this report from DDC."

(2) "Foreign announcement and dissemination of this report by DDC is not authorized."

(3) "U. S. Government agencies may obtain copies of this report directly from DDC. Other qualified DDC users shall request through _____."

(4) "U. S. military agencies may obtain copies of this report directly from DDC. Other qualified users shall request through _____."

(5) "All distribution of this report is controlled. Qualified DDC users shall request through _____."

If the report has been furnished to the Office of Technical Services, Department of Commerce, for sale to the public, indicate this fact and enter the price, if known.

11. SUPPLEMENTARY NOTES: Use for additional explanatory notes.

12. SPONSORING MILITARY ACTIVITY: Enter the name of the departmental project office or laboratory sponsoring *(paying for)* the research and development. Include address.

13. ABSTRACT: Enter an abstract giving a brief and factual summary of the document indicative of the report, even though it may also appear elsewhere in the body of the technical report. If additional space is required, a continuation sheet shall be attached.

It is highly desirable that the abstract of classified reports be unclassified. Each paragraph of the abstract shall end with an indication of the military security classification of the information in the paragraph, represented as *(TS), (S), (C), or (U).*

There is no limitation on the length of the abstract. However, the suggested length is from 150 to 225 words.

14. KEY WORDS: Key words are technically meaningful terms or short phrases that characterize a report and may be used as index entries for cataloging the report. Key words must be selected so that no security classification is required. Identifiers, such as equipment model designation, trade name, military project code name, geographic location, may be used as key words but will be followed by an indication of technical context. The assignment of links, rules, and weights is optional.